Electromyography and inertial sensor-based gesture detection and control

Rui Alberto Esteves Freixo

Supervisor at FEUP: Miguel Velhote Correia, PhD

Supervisor at Fraunhofer AICOS: Vânia Guimarães, MSc

Master in Bioengineering

June, 2015

Faculdade de Engenharia da Universidade do Porto

Electromyography and inertial sensor-based gesture detection and control

Rui Alberto Esteves Freixo

June, 2015

Abstract

With the advent of new technology the need of interacting with machines has increased. In order to improve this interaction it is necessary to create simple and intuitive interfaces which are accessible to everyone. Gestures are naturally used in the real world to interact with objects or transmit information. The ability to capture, recognize and interpret gestures may thus enable humans to communicate with machines and provide more natural ways of human-computer interaction (HCI).

This dissertation had as main objective the development of an algorithm that is able to perform gesture pattern recognition, using information from electromyography (EMG) and inertial measurement unit (IMU) sensors. The EMG provides information on muscular activity and the IMU allows the measurement of movement, for example, the velocity and orientation of body segments. Using the Myo gesture control armband, a device recently introduced in the market that incorporates seven EMG channels and one IMU, a comparison between the built system and a system in the market was possible.

The built system used, to acquire data, four EMG channels from BITalino device placed in the forearm, in combination with a smartwatch to acquire data from the IMU.

Twelve gestures were correctly identified, including hand contraction and extension, wrist extension and flexion, snap the fingers, among others.

For pattern recognition, using both systems, the twelve gestures were recorded, and data was pre-processed to enhance muscle activation and signal segmentation. Then, the best set of features, from both sensors, was chosen and finally, different classification techniques were applied.

In the end, all gestures were successfully recognized with no difference between the systems. The use of information from the two sensors proved to be essential.

The ability to recognize gestures enables the creation of new interaction techniques.

Keywords: EMG, IMU, Pattern Recognition, HCI, Wearable Devices

Resumo

Com o aparecimento das novas tecnologias o número de interações entre o Homem e a máquina aumentou. Para melhorar estas interações é necessário criar interfaces que sejam simples, intuitivas e acessíveis a todos.

Os gestos são uma maneira natural usada para interagir com objetos e transmitir informação. A habilidade de recolher, reconhecer e interpretar os gestos torna possível ao Homem comunicar com a máquina, possibilitando um meio de HCI mais natural.

Esta dissertação tem como principal objetivo desenvolver um algoritmo capaz de reconhecer padrões de gestos usando informação proveniente de sensores EMG e IMU. Através do EMG é possível saber informações ao nível anatómico, por exemplo, que músculos são utilizados num dados gesto. Por outro lado, o IMU, fornece informações físicas, por exemplo, a velocidade e a orientação de uma estrutura. Usando o Myo gesture control armband, um produto recentemente introduzido no mercado, foi possível comparar o sistema construído com um sistema já no mercado.

O sistema construído utilizou, para a aquisição de dados, quatro canais EMG, usando o BITalino como dispositivo, e um sensor IMU, utilizando um smartwatch como dispositivo.

Para o reconhecimento de padrões de gestos foram recolhidos, a partir dos dois sistemas, um conjunto de doze gestos, contendo a contração e a extensão da mão, a extensão e a flexão do punho, o estalar os dedos, entre outros. Após a recolha de dados, estes foram submetidos a técnicas de pré-processamento, realçando os momentos de ativação muscular em relação aos momentos de relaxamento. Em seguida, o melhor conjunto de características dos dois sensores foi escolhido e finalmente foram aplicados diferentes técnicas de classificação.

No final, os padrões de gestos foram reconhecidos com sucesso não havendo grande diferença entre os dois sistemas. A utilização de informação proveniente dos dois sensores demonstrou ser essencial.

A habilidade de reconhecer gestor, por parte das máquinas, possibilita a criação de novas técnicas de interação.

Keywords: EMG, IMU, HCI, Reconhecimento de padrões

Acknowledgments

Prof. Doctor Miguel Velhote Correia, my supervisor at FEUP, provided support and useful recommendations during the project.

Vânia Guimarães, my supervisor at Fraunhofer AICOS, provided prompt support in all phases of project, gave crucial recommendations and shared her characteristic enthusiasm, motivating during the entire project.

All my colleagues at Fraunhofer AICOS, who patiently participated in the test phases.

My family and close friends provided an important emotional support.

"The core of man's spirit comes from new experiences"

C. McCandless

Contents

List of Figures

List of Tables

List of Abbreviations

Acc	Accelerometer
ANN	Artificial neural network
DH	Down the hand
EMG	Electromyography
FEUP	Faculdade de Engenharia da Universidade do Porto
AICOS	Assistive information and communication solutions
FN	False negative
FP	False positive
Gyr	Gyroscope
HC	Hand contraction
HCI	Human-computer interaction
HE	Hand extension
IMU	Inertial measurement unit
k-NN	k-Nearest Neighborst
LDA	Linear discriminant analysis
MUAP	Motor unit action potential
NAP	Nerve action potentials
PCA	Principal components analysis
RMS	Root mean square
SBS	Sequential backward selection
sEMG	Surface electromyography
SFS	Sequential forward selection
snap	Snapping the fingers
TI	Thumb-Index
TM	Thumb-Middle
TN	True negative
TKEO	Teager-Kaiser energy operator
TP	True positive
UAF	Upper arm flexion
UALR	Upper arm lateral rotation
UH	Up the hand
WA	Wrist abduction

WE	Wrist extension
WF	Wrist flexion

Chapter 1

Introduction

This dissertation aims to study a new method of HCI based on gesture detection and control. To that purpose EMG and IMU are placed on the forearm enabling the detection and discrimination of a set of gestures. This set of gestures was chosen taken account their potential in HCI.

1.1 Context

The increase of computerized machines in our society led to increased needs, requirements and techniques to interact with technology, which led to advances in the field of HCI. Gestures are widely used in daily activities, so, gestures seem to be an effective and natural way to interact with technology, making it accessible for all.

Pattern recognition algorithms are now mature enough to allow us to get results with high accuracy and high precision. Pattern recognition techniques allow the machine to observe the environment, learn to distinguish the pattern of interest from the background and make a decision [1].

There are two approaches to recognize gestures in HCI, the non-biosignal approach and the biosignal approach [2]. The non-biosignal approach uses systems based on images and video for gesture recognition. These systems have many advantages, such as, the fact of not requiring the attachment of sensors on the body before and during its use, which makes them easily adaptable to serve specific needs of various disabilities [2]. However, there are several problems that can also be observed, due to the high volume of data required, such as, loss of communication, slow communication rate and high computation power that is needed. The biosignal approach uses the brain activity, through the electroencephalography, or muscle activity, through electromyography. The electroencephalography is a non-invasive technique, however its signal is extremely difficult to analyze since its part of interest is hidden by the noise. So it is advisable to use the EMG, which measures musle activity more directly near its source. This one is also a non-invasive technique, that allows the recognition of muscle contractions [3]. With this it is possible to know which muscles are active in a given gesture and so perform gesture pattern recognition.

EMG is used in many studies to recognize the execution of certain movements [4, 5, 6, 7]. However, the detected movements are few and of reduced complexity.

The IMU is an electronic device that uses three sensors - accelerometer (Acc), gyroscope (Gyr) and magnetometer - to measure different movement properties such as amplitude of movements and rotations. Using these data and combining it with EMG data, it is possible increase the number and complexity of gestures that can be recognized, maintaining the high accuracy [8, 9].

1.2 Motivation

Due to the advent of new technologies, there is on increasing need of studying new and intuitive ways of interacting with computerized machines. Thus, once the traditional means of interaction show to be limited, it is extremely important that interactive computing systems are made accessible for all people with intuitive and user-friendly interfaces.

Using the appropriate sensors and machine learning algorithms, it is now possible to perform gesture pattern recognition. Gestures are used naturally by people to manipulate objects or to transmit information, therefore using gestures may be a more natural and intuitive may to interact with machines.

Besides the possible applications in the field of HCI, gestures identification can have an important application in the area of medical rehabilitation, allowing, for example, a comparison between people without motor impairments and people with motor disabilities. As a consequence, the gesture recognition can provide the means for a more efficient rehabilitation.

1.3 Objectives

This dissertation has as principal objective the development of an algorithm, that fuses the information from EMG with IMU sensors data, capable of recognizing gestures that can be used in HCI.

1.4 Main contributions

This dissertation allowed the development of an algorithm to perform gesture pattern recognition, using data from IMU and EMG sensors. It was also possible to compare the performance of two systems - BITalino and LG G Watch system and Myo gesture control armband system.

1.5 Structure

This dissertation is divided into two main parts. In the first part is done a literature review with some background concepts. This part is composed of Chapter 2, describing the anatomical terms and by Chapter 3, which describes the methodology of pattern recognition. The second part describes all the work done. This part is composed of Chapter 4, describing the proposed work

and Chapter 5, which the results are described and analysed. At least, in Chapter 6, the conclusions related with this project are presented and some future work to potentially improve it is also identified.

Chapter 2

Anatomy of the Upper Limbs

Usually, for the description of gestures, anatomical structures or positions in the human body, it is strictly necessary to use specific terms of anatomy. This chapter helps to better understand the anatomical terms (Section 2.1), the skeletal system (Section 2.2), muscular system (Section 2.3), possible movements with the upper limbs (Section 2.4) and finally which of these movements can be used in HCI (Section 2.4.3).

2.1 Anatomical Terms

All the descriptions related with the structure or anatomic movement are based on the anatomical starting position (see Figure 2.1a). In this position, the body is in an erect stance with the head facing forward, arms at the side of the trunk with palms facing forward, and the legs together with the feet pointing forward.

The anatomical planes are imaginary planes that allow to describe the threedimensional location of the different structures. Three major planes are defined in human body (see Figure 2.1b) [10, 11]:

- the Sagital Plane is an Y-Z plane, perpendicular to the ground, that separates the body into medial and lateral parts. It is considered medial the part of the body which is nearest to the plane and lateral the furthest part of the plane;
- the Coronal Plane is an Y-X plane, perpendicular to the ground, that separates the body into anterior and posterior parts. It is considered anterior the part of the body in front of the plane and posterior the part on the back of the plane;
- the Transverse Plane is an X-Z plane, parallel to the ground, that separates the body into superior and inferior sections. It is considered superior the part at the top of the plane, and inferior the part at the bottom of the plane;

In the descriptions related with the limbs it is also common to use the terms distal and proximal, referring to the furthest part of the body and to the nearest part of the body, respectively (see Figure 2.1c) [11].

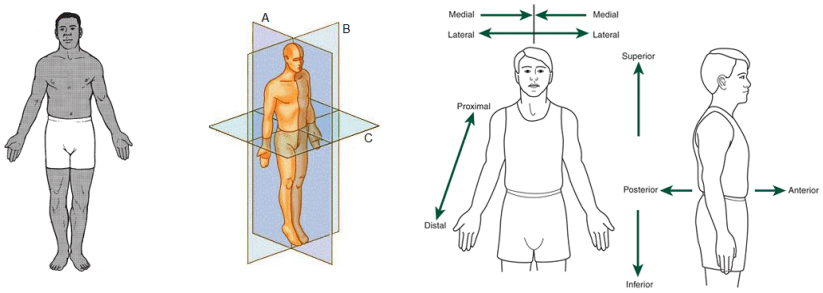

(a) (b) (c)

Figure 2.1: Representation of the anatomical references. (a)-anatomical starting position [11]; (b)-anatomical planes used to describe the location of the human body structures: A-Sagittal Plane, B-Coronal Plane and C-Transverse Plane [10]; and (c) -representation of the anatomical terms used to describe structures and movements [11].

2.2 Skeletal System

Composed by bones, the major functions of the human skeleton are support, movement, protection, production of blood cells, storage of ions and endocrine regulation [10]. It can be divided into axial skeleton, constituted by the skull, spine and rib cage, and the appendicular skeleton, constituted by shoulder girdle, pelvic girdle, and the bones of the upper and lower limbs.

The upper limbs are formed by four structures (see Figure 2.2). These structures are linked together through joints - areas where the bones are attached, allowing movements and mechanical support[10, 11] - and can be described as:

- Shoulder girdle - region composed of two bones, the clavicle and the scapula. While the proximal part links the upper limb to the axial skeleton using the sternoclavicular joint, the distal part is linked to the upper arm using the glenohumeral joint (also known as shoulder joint). This joint belongs to the ball-and-socket class (see Figure 2.3a), allowing movements around an indefinite number of axes.

- Upper arm - region between the shoulder joint and the elbow joint and it is solely composed by the humerus bone. The elbow joint is a complex of three joints - the humeroradial, humeroulnar, and superior radioulnar joints - and belongs to the hinge class (see Figure 2.3b) allowing movements in only one axis.

- Forearm - distal region between the elbow joint and the wrist, being composed of two bones (radius and ulna). It is at this region where most of the muscles that allow the movement of the hand are. The wrist belongs to the ellipsoid class (see Figure 2.3c) allowing movements in two axes.

- Hand - the most distal part of the upper limb. It has 27 bones wherein 14 are phalanges (proximal, intermediate and distal) of the fingers, 5 are metacarpals and 8 are carpal. This set of bones allows the manipulation of objects.

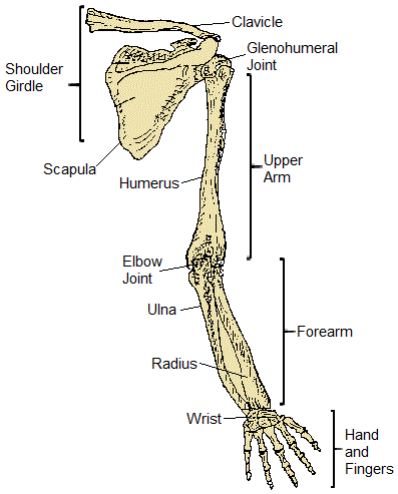

Figure 2.2: Representation of the location of the shoulder girdle, upper arm, forearm and hand and their main components

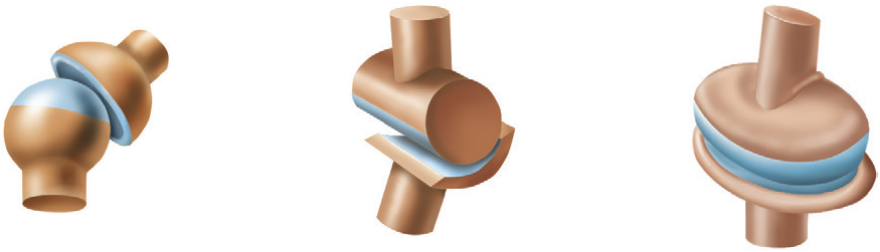

(a) (b) (c)

Figure 2.3: Representation of the three existing major joints in the upper limbs. (a)-Ball-and-socket Class representing the glenohumeral joint, (b)-Hinge Class representing the elbow joint and (c)-Ellipsoid Class representing the wrist [10].

2.3 Muscular System

The muscles are the tissues responsible for the human movements. With them it is possible to apply forces and perform precise movements, maintain a constant position, move a body structure or slow down/speed up a structure in movement.

The muscle tissue bind to the bones through tendons. In general it can be divided into three types: smooth muscle, cardiac muscle and skeletal muscle [10]. The first two allow involuntary movements like the heart beat, and are controlled by the autonomic nervous system, not being possible to the human beings control these tissues. On the other hand, the skeletal muscle can be voluntarily controlled. It has a wide variety of different functions, allowing the production of movement, maintaining postures and positions and stabilization of joints.

In its individual structure (see Figure 2.4), the skeletal muscle usually has a central thick portion, the belly of the muscle. Covering the outside of muscle there is a fibrous tissue, the epimysium [11]. This tissue has a fundamental role in muscle tension transfer to the bone. The epimysium transfers various tensions to the tendon causing the application of a soft force in the bone. In each muscle there may be thousands of carefully organized muscle fibers. The fibers bundles are called fascicle and may contain up to 200 muscle fibers. A fascicle is covered by perimysium whose main function is to protect the muscle fibers and provide pathways to the nerves and blood vessels [10, 11].

To control the muscle cells, the central nervous system uses motor neurons. Motor neurons are specialized nerve cells whose principal goal is to stimulate muscles fibers through synapses [12]. This kind of cells is originated in the cerebral cortex, its cell body is located in spinal cord and its axon prolong to skeletal muscle fibers [11]. Here the axon branches and each branch is projected towards the centre of one fibre (See Figure 2.5). Thus each motor neuron innervates more than one muscle fiber and each muscle fiber gets a branch of, at least, one axon. Most muscles are innervated by more than one motor neuron [10, 12].

The muscle fibers cells are electrical excitable and polarized. That means that the inside is more negatively charged when compared to the outside, which creates an electrical charge differ-

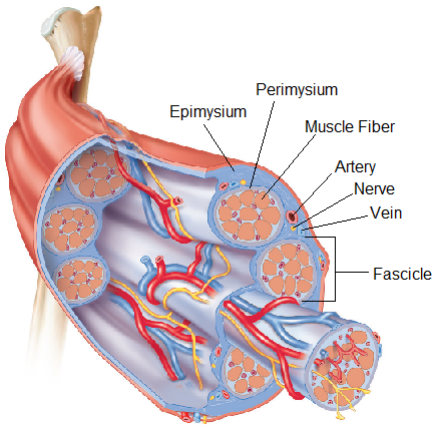

Figure 2.4: Representation of the anatomy of the skeletal muscle [10].

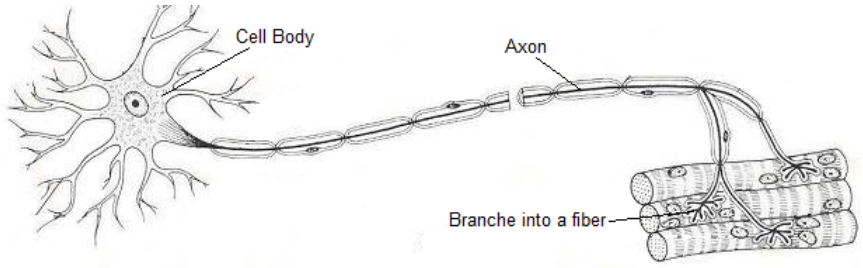

Figure 2.5: Representation of a motor neuron and and its binding to the fibers

ence across plasma membrane between 70 and 90 mV [13]. In order to control muscle contraction the nervous system sends electrical signals through motor neurons. These signals are called nerve action potentials (NAP). A NAP inverts the electrical charge in the membrane, turning the inside more positively charged than outside [11, 12]. This process has two phases, depolarization and repolarization. In depolarization the inside becomes less negative than a threshold, causing a brief contraction of muscle cells. In repolarization the membrane potential returns to a normal value. The action potential travels along the muscle fibers and can be detected on the surface of the muscle as a small electrical potential called motor unit action potential (MUAP) [12].

Each muscle has many motor units. A motor unit consists of a single motor neuron and all muscle fibers innervated by it [12]. All muscle fibers are stimulated simultaneously when the motor unit neuron fires. Thus a simple muscle contraction corresponds to a complex set of MUAPs. A well positioned electrode can record MUAP's. This sensing and recording is called EMG [13].

In relation to the upper limbs, multiple muscles enable the performance of a wide range of movements. The description of these movements and related muscles is presented hereinafter.

2.4 Movements of upper limbs

In the course of daily activities a person needs to perform a wide range of movements. The movements made by the upper limbs are some of the most important, allowing, for example, handling objects.

2.4.1 Type of Movements

There are several types of movements that the upper limbs can perform. The type of movement always depends on the type of joint - some joints limit the movements only in one direction, while other joints allow movements in several directions [11]. As noted above, the upper limbs have three major joints. Considering the characteristics of these joints, the movements at upper limbs can be basically divided into three types [10, 11]:

- Gliding movement - occurs between bones that meet at flat or nearly flat articular surfaces allowing only a slight movement. This is the type of movement observed, for example, between the carpal bones.

- Angular movements - occurs when one bone moves relative to another and, as a consequence, the angle between these two structures changes [11]. The most common angular movements are flexion, extension, abduction and adduction (see Figure 2.6a and 2.6b), wherein the pairs flexion-extension and abduction-adduction correspond to opposite movement directions:
  - Flexion - can be defined as the movement of bending that decreases the angle between a segment and its proximal segment.
  - Extension - can be defined as the movement that increases the angle between body parts.
  - Abduction - can be defined as a movement that pulls a structure away from the midline of the body.
  - Adduction - can be defined as a movement towards the midline.
- Circular movements - occurs when a structure rotates around an axis. The most common circular movements are rotation, pronation, supination and circumduction (see Figure 2.6c, 2.6d and 2.6e). The supination and pronation correspond to opposite movements and only occur in the forearm.
  - Rotation - corresponds to the turning of a structure around its long axis.
  - Pronation - enables the forearm rotation so that the palm of the hand turns posteriorly in relation to the anatomical position.
  - Supination - enables the forearm rotation so that the palm of the hand turns anteriorly in relation to the anatomical position.
  - Circumduction - corresponds to a combination of flexion, extension, abduction and adduction. It can only happen in very mobile joints like the shoulder joint.

The opposition and reposition are special movements that only occur between the thumb and the little finger (see Figure 2.6f). The opposition arises when these two fingers are brought toward each other. In reposition the fingers return to the anatomical position. The thumb can also oppose the other fingers, but, in this case, the fingers flex to touch in thumb.

Most gestures that we perform, like handling objects with hand or catching an object, are simple combinations of the movements described [10].

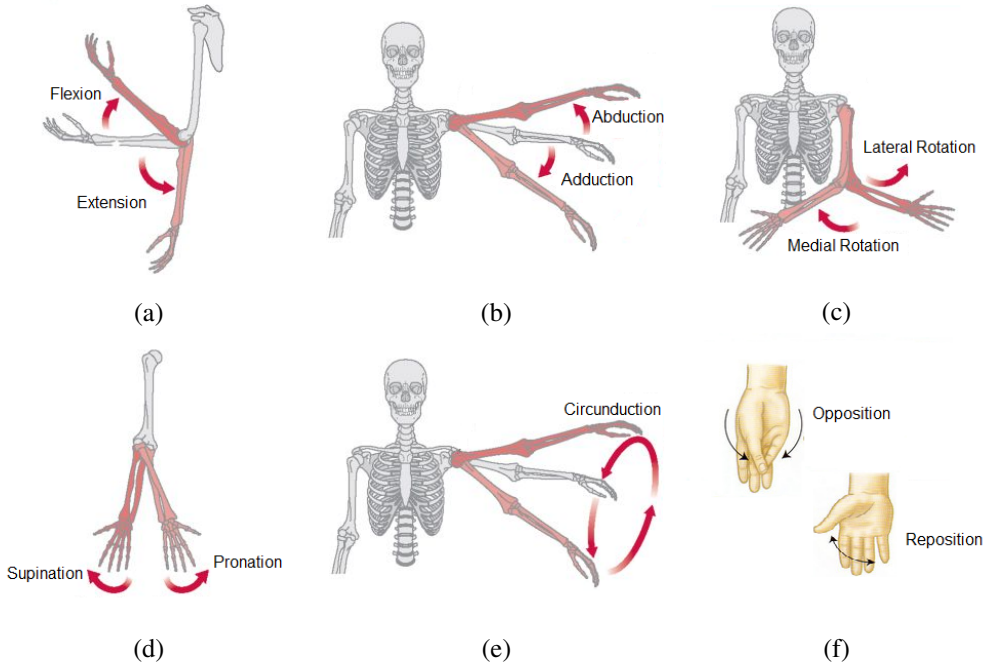

Figure 2.6: Representation of the different types of possible movements to perform with upper limbs. (a)-pair flexion-extension, (b)-pair abduction-adduction, (c)-pair medial rotation-lateral rotation, (d)-pair pronation-supination, (e)-circunduction and (f)-pair opposition-reposition

2.4.2 Movement structure and related muscles

Together, the three major joints and their surrounding muscles, allow the upper limbs to perform a large set of movements:

- The shoulder allows the arm to perform movements like, flexion, extension, abduction, adduction and medial and lateral rotations. The muscles involved in these movements are described in Table 2.1 and represented in Figure 2.7a and Figure 2.7b.
- The elbow allows the forearm to perform movements like, flexion, extension, supination and pronation. The muscles involved in these movements are described in Table 2.1 and represented in Figure 2.7c and Figure 2.7d.
- The wrist together with hand and fingers enable the execution of a wide range of movements. A complex combination of muscles is involved in these movements, which are described in Table 2.2.

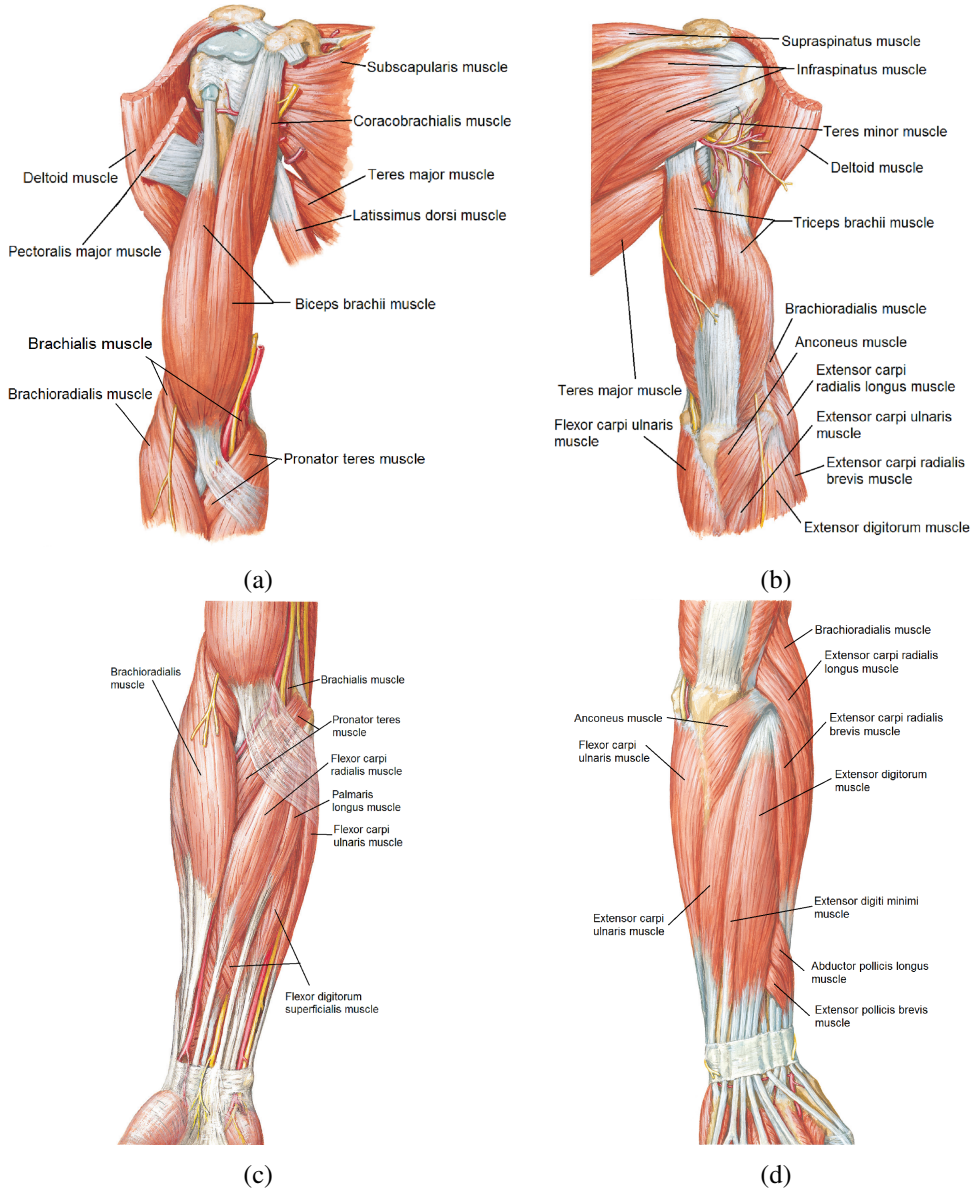

Figure 2.7: Main muscles on the superficial layer of the arm and forearm. (a)- anterior view of the arm muscles; (b)- posterior view of the arm muscles; (c)- anterior view of the forearm muscles; (d)- posterior view of the forearm muscles [14].

Table 2.1: Muscles acting on the movement of the shoulder, upper arm and forearm [10].

Body part	**Movement**	**Muscles**	**Movement**	**Muscles**
Shoulder and Upper Arm	Flexion	*Coracobrachialis* *Pectoralis major* *Deltoid*	Extension	*Deltoid* *Teres major* *Latissimus dorsi* *Pectoralis major* *Tríceps brachii*
	Abduction	*Deltoid* *Supraspinatus*	Adduction	*Pectoralis major* *Latissimus dorsi* *Teres major* *Teres minor* *Tríceps brachii* *Coracobrachialis*
	Medial Rotation	*Pectoralis Major* *Teres major* *Latissimus dorsi* *Deltoid* *Subscapularis*	Lateral Rotation	*Deltoid* *Infraspinatus* *Teres minor*
Forearm	Flexion	*Bíceps brachii* *Brachialis* *Brachioradialis*	Extension	*Tríceps brachii* *Anconeus*
	Supination	*Bíceps brachii* *Supinator*	Pronation	*Pronator quadratus* *Pronator teres*

2.4.3 Gestures for Human-Computer Interaction

In recent decades, the gestures have been widely studied due to its great potential to serve as means of HCI. Gestures are used naturally in the real world to interact not only with other people but also with real objects. Gesture recognition has application, for instance, in sign language recognition, gesture to speech, virtual environments, 3D modeling and human-machine dialogue [15].

Generalizing, we can perform four different kind of gestures that can be used as command in HCI [15]:

- Static simple gestures - the kind of gestures that are based on a single posture that is maintained for a certain amount of time (see Figure 2.8a).

- Static generalized gestures - the kind of gestures that are based on a sequence of a single postures that are maintained for a certain amount of time (see Figure 2.8b).

- Dynamic simple gestures - the kind of gestures in which the only information considered is the motion trajectory (see Figure 2.8c).

- Dynamic generalized gestures - the kind of gestures that combine motion trajectory with posture (see Figure 2.8d).

Table 2.2: Muscles acting on the movement of the wrist, hand and fingers. [10]

Body part	**Movement**	**Muscles**	**Movement**	**Muscles**
Wrist	Flexion	*Flexor carpi radialis* *Flexor carpi ulnaris* *Flexor digitorum profundus* *Flexor digitorum superficialis* *Palmaris longus*	Extension	*Extensor carpi radialis brevis* *Extensor carpi radialis longus* *Extensor carpi ulnaris* *Extensor digiti minimi* *Extensor digitorum* *Extensor indicis*
	Abduction	*Flexor carpi radialis* *Abductor pollicis longus* *Extensor carpi radialis brevis* *Extensor carpi radialis longus* *Extensor pollicis longus*	Adduction	*Flexor carpi ulnaris* *Extensor carpi ulnaris*
Thumb	Flexion	*Flexor digitorum profundus* *Flexor digitorum superficialis* *Flexor pollicis longus* *Flexor pollicis brevis*	Extension	*Abductor pollicis longus* *Extensor digitorum* *Extensor pollicis bravis* *Extensor pollicis longus*
	Abduction	*Abductor pollicis longus* *Extensor pollicis brevis* *Abductor pollicis brevis*	Adduction	*Adductor pollicis*
	Opposition	*Opponens pollicis*		
Index	Flexion	*Flexor digitorum profundus* *Flexor digitorum superficialis*	Extension	*Extensor digitorum* *Extensor indicis*
	Abduction	*Midpalmar muscles* *interossei dorsal*	Adduction	*Midoalmar muscles* *interossei palmar*
Middle	Flexion	*Flexor digitorum profundus* *Flexor digitorum superficialis*	Extension	*Extensor digitorum*
	Abduction	*Midpalmar muscles* *interossei dorsal*		
Ring	Flexion	*Flexor digitorum profundus* *Flexor digitorum superficialis*	Extension	*Extensor digitorum*
	Abduction	*Midpalmar muscles* *interossei dorsal*	Adduction	*Midpalmar muscles* *interossei palmar*
Pinky	Flexion	*Flexor digitorum profundus* *Flexor digitorum superficialis* *Abductor digiti minimi* *Flexor digiti minimi brevis*	Extension	*Extensor digitorum* *Extensor digiti minimi*
	Abduction	*Abductor digiti minimi*	Adduction	*Midpalmar muscles* *interossei palmar*
	Opposition	*Opponens digiti minimi*		
Fhalanges	Flexion	*Midpalmar muscles* *interossei lumbricals*	Extension	*Midpalmar muscles* *interossei*

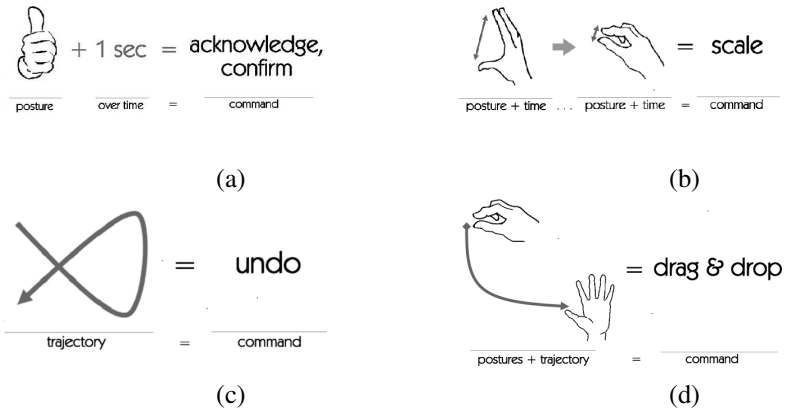

Figure 2.8: Different gestures that can be used in HCI. (a)-static simple gestures, (b)-static generalized gestures, (c)-dynamic simple gestures, (d)-dynamic generalized gestures [15].

In a deeper analysis, the gestures are divided into different forms within different domains, i.e., there are different form of gestures for different Input/Output devices. In a simple way, it is recommended a taxonomy with four categories to classify gestures [16] (see Figure 2.9): gesture style, application domain, enabling technology and system responses.

The gesture style can be a gesticulation, a manipulation, a semaphore, a deictic on a language gesture. Gesticulation is the most natural form of gesturing and is used in combination with conversational speech. The interfaces that use gesticulation are those which attempt to create a naturalistic, conversational style interaction without the need of electronic devices [16].These interfaces do not require the user to perform any poses or learn more gestures than those that are naturally used in everyday speech. The manipulative gestures are those that have the purpose to control some entity by a tight relationship between the actual movements of the gesturing hand/arm with the entity being manipulated [16]. The semaphoric gestures are any gesturing system that employs a dictionary of static or dynamic movement. These gestures are used as an universe of symbols that can be used to communicate with the machine. Deictic gestures are defined as gestures that involve pointing to establish the identity or spatial location of an object. They are used, for instance, when pointing to identify an object. Finally the language gestures are gestures used to communicate using sign language.

The gestures have multiple application domains. They can be used in desktops and tablets applications being an alternative to the mouse and keyboard, enabling a more natural interaction through the use of touchscreens, for example. It is possible to use the gestures in games as an input to control the movement and orientation of game objects. Moreover, they can be used with wearable devices that allow the user to interact within a smart room environment [16].

The gestures can be used as an input to enabling technology. Perceptual inputs are those that do not require any physical contact with an input device or object, allowing the user to communicate without having to wear, hold or manipulate any intermediate device. Instead, visual, audio or motion sensors are used. The non-perceptual inputs require the physical contact with devices or objects to transmit location, spatial or temporal information to the computer [16].

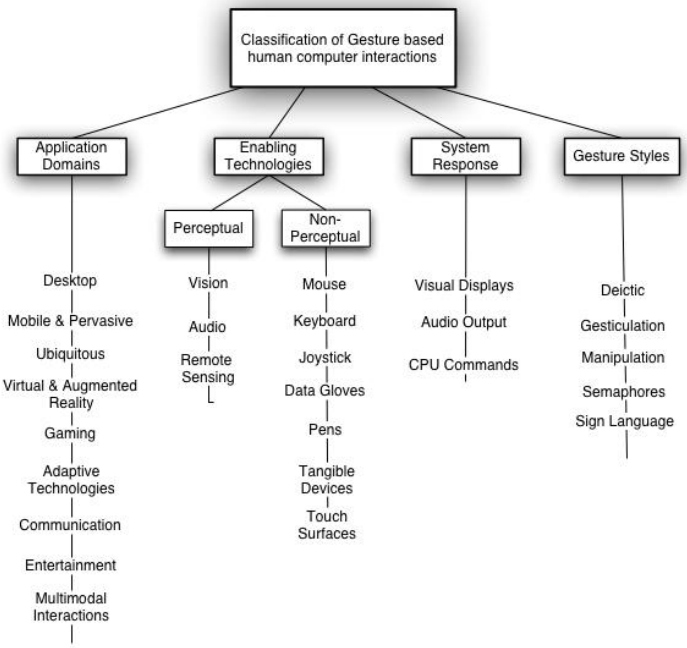

Figure 2.9: Taxonomy proposed [16]. The HCI gestures are split in four categories gesture style, application domain, enabling technology and system responses.

The system response refers to the output that a gesture interaction leads to. It can be separated into three different categories such as visual output, the most common, audio output, and command directed output. In visual output a user performs a gesture with the aim of interacting/-manipulating with the screen objects. In audio output a sound is made on the basis of the gesture that is performed, allowing uses to manipulate audio. In the last category, the command directed output is used to send commands to devices or applications.

Chapter 3

Pattern Recognition

The search for artificial intelligence, where the machines are capable of learning from data without being explicitly programmed, originated a subfield in computer science, i.e., the machine learning. Pattern recognition is a subfield of the machine learning and studies how machines can observe the environment, learn to distinguish patterns of interest from their background, and make sound and reasonable decisions about the categories of the patterns [1]. Table 3.1 describes some examples of pattern application recognition areas.

This chapter describes a traditional pattern recognition system, presenting pattern recognition methodologies (Section 3.1), the data acquisition step (Section 3.2), the preprocessing step (Section 3.3), feature extraction and selection step (Section 3.4), the classification step (Section 3.5) and finally the evaluation step (Section 3.6). In data acquisition and preprocessing it is given more emphasis to systems based on data from EMG and IMU sensors.

3.1 Pattern Recognition Methodologies

In pattern recognition there are four common approaches which can be used. Those approaches are summarized in Table 3.2. [1]:

- Template matching - it is the simplest approach. This approach determines the similarity between two entities of the same type. The pattern to be recognized is matched against the stored template, previously built using a training set. This approach, although effective in some specific application domains, has several disadvantages. For example, if the patterns have a large intraclass variation among this process will fail [1].

- Statistical - this approach represents each pattern in terms of d features. If different patterns have features that occupy a compact and disjoint region in d-dimensional feature space they are easily distinguished. The success is measured based on capability of dividing the features into the d-dimensional feature space. Using a training set it is possible to establish the decision boundaries which separate the patterns belonging to different classes. The decision boundaries are estimated using statistical methods [1].

Table 3.1: Examples of pattern recognition application areas [1].

Problem Domain	**Application**	**Input pattern**	**Pattern Classes**
Bioinformatics	Sequence analysis	DNA/Protein sequence	Known types of genes/patterns
Data mining	Searching for meaningful patterns	Points in multidimensional space	Compact and well-separated clusters
Document classification	Internet search	Text document	Semantic categories (e.g., business, sports,etc.)
Document image analysis	Reading machine for the blind	Document image	Alphanumeric characters, words
Industrial automation	Printed circuit board inspection	Intensity or range image	Defective/non-defective nature product
Multimedia database retrieval	Internet search	Video clip	Video genres
Biometric recognition	Personal identification	Face, iris, fingerprint	Authorized users for access control
Remote sensing	Forecasting crop yield	Multispectral image	Land use categories, growth patterns of crops
Speech recognition	Telephone directory enquiry without operator assistance	Speech waveform	Spoken words

- Syntactic - this approach is used with complex patterns being applied in a hierarhical perspective. In this case, a pattern is viewed as a composition of simpler subpatterns, in which the simplest subpatterns are called *primitives*. The organization of *primitives* in a pattern is made in accordance with rules/grammar. Using a training set it is possible to learn which rules can be applied to in each specific pattern and then perform pattern recognition [1].

- Neural networks - this approach uses organizational principles inspiring on human brain, being advisable for problems with several inputs/outputs. The basic design consists in an input layer, a hidden layer and an output layer. Each input neuron is connected with each hidden neuron and these ones are connected to the output neurons layer, These connections are known as weight. Although it is very complex, the great advantage of this approach is the ability to learn complex nonlinear input-output relationships, using sequential training procedures, and adapt themselves to the data [17].

To recognize patterns in EMG datasets or IMU datasets it is usual to use statistical approaches. The traditional design for this approach operates in two modes - training (learning) and testing (classification) and is constituted by the following steps: data acquisition, preprocessing, features extraction/features selection, classification and evaluation (see Figure 3.1). Generally, in the pre-

processing step, the most important information is exposed and emphasized, For example, for the EMG data, the preprocessing step will emphasize the active segments of the signals, distinguishing them from the background. After calculating a set of features from the input signals and when in the training mode, the feature extraction and selection step will find the features that better represent the input patterns, enabling then the creation of a classification model after the learning step, in which statistical approaches to separate patterns belonging to different classes are applied. In testing mode, the trained model assigns the input pattern to one of the pattern classes under consideration based on the measured features [1].

Table 3.2: Four approaches used in pattern recognition [1].

Approach	Representation	Recognition Function	Typical Criterion
Template matching	Samples, pixels, curves	Correlation, distance measure	Classification error
Statistical	Features	Discriminant function	Classification error
Syntactic	Primitives	Rules, grammar	Acceptance error
Neural networks	Samples, pixels, features	Network function	Mean square error

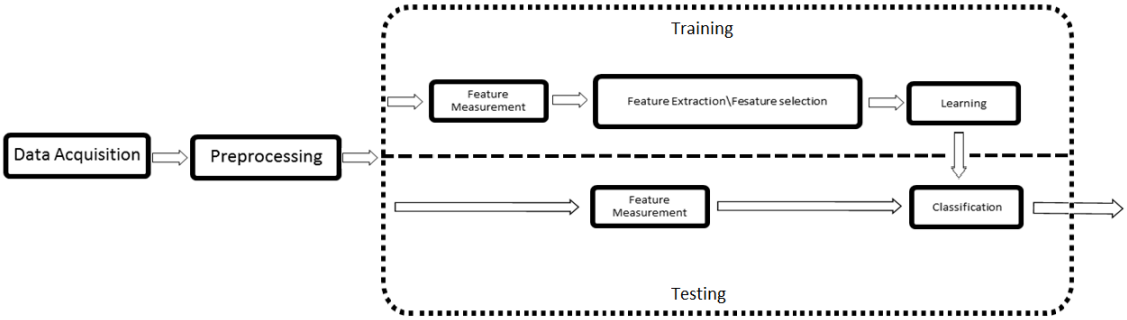

Figure 3.1: Representation of a traditional design for a classification algorithm [1].

3.2 Data Acquisition

The classification method starts with data acquisition. The recording of the data can be made considering two different perspectives, always depending on the final goal. In a user-specific perspective, the learning process is user-specific and the data are recorded from a specific individual. As example, this perspective is applied in medical area, where each patient has a specific treatment. On the other hand, in a user-independent perspective, the data are recorded from multiple individuals and the learning process is user-independent. For HCI this last perspective makes more sense since the objective is to make the interaction accessible for all.

In this step all data of interest will be recorded using the appropriate sensors. For this study it is necessary to record data from EMG and IMU sensors.

3.2.1 Electromyography

3.2.1.1 Signal Detection

A biomedical signal refers to a set of electrical signals acquired from any organ, representing a physical variable of interest. This kind of signal is normally a function of time and is described in terms of its amplitude, frequency and phase. The EMG is a biomedical signal that measures the electrical currents generated in muscles during their contraction, representing the neuromuscular activities [3]. Nowadays, it can be used in several areas being the main fields the medical applications and the HCI.

In order to obtain this biomedical signal two different methods [18], invasive or non-invasive can be used. The invasive method uses intramuscular sensors. A needle, containing one or more sensors, is inserted in the muscle. With this method it is possible to collect information about a voluntary motor activity, allowing to know if a group of muscles is active or not, as well as the insertional activity, allowing know the good condition of the muscle and its innervating nerve. The non-invasive method, called surface EMG (sEMG) uses sensors placed on the surface of the skin that enable, recording the MUAPs. The interface between the sensors and the skin is made by two electrodes and one reference. While the electrodes are placed over the muscles in action the reference is placed over a bone. This technique only allows to record data about the voluntary motor activity. Since it is be a non-invasive technique it has great advantages, being commonly used in HCI [6, 7, 8, 9].

The quality of the EMG signal is affected by many factors - extrinsic, intrinsic, intermediate and deterministic [4, 13]. The extrinsic factors are related with the structure and placement of electrodes, i.e, depends on area, shape, distance between electrodes, location and muscle orientation. The intrinsic factors are related with the human body characteristics, i.e., number of active motor units, muscle fibers composition, blood flow and distance between the muscle and the electrodes. Intermediate factors are related with the electrode electromagnetic proprieties, which are their ability in act like band-pass filter or integrators and their tendency to record cross-talk from other muscles. Lastly, the deterministic factors are related with the number of detected active motor units, the motor unit force, fiber interaction, firing rate, characteristics of action potential and recruitment characteristics. All these factors need to be taken into account when recording sEMG.

3.2.1.2 Number of Sensors and Placement

Nowadays, the increase need of information for the non-invasive analysis of muscle activity with medical and HCI applications led to an increase in the required number of EMG channels. As a major consequence, additional computing power is required to interpret the data. For HCI some studies indicate that the minimum number of channels, still maintaining a good accuracy, is two [6, 7, 8, 9].

Each gesture, when active, uses a specific group of muscles. To perform the gesture pattern recognition it is necessary to measure the MUAPs. To that purpose, sEMG sensors are placed on each active muscle.

The majority of the moves used in HCI are based on hand and wrist movements. The muscles which control these structures (see Table 2.2 and Figure 2.7) are located in the forearm. Thus, the forearm is the best structure to put the EMG sensors. In this structure the sensors can be placed in the most distal part, near the wrist, or the most proximal part, near the elbow (see Figure 3.2).

In the posterior side of the forearm, move a sensor from a distal position towards a proximal position, leads to results that are less sensitive to the extension of the thumb and index fingers and more sensitive to the extension of the middle and ring fingers [4, 5]. The sensors located in the medial part and the proximal part of the forearm have higher average recognition rates once they have better coverage of the forearm muscles [5]. Placing sensors along and around the forearm provides better information than placing the sensors on a circular configuration. This can be explained by the fact that a sensor not only records information about one muscle but also from the muscles nearby [4].

3.2.2 Inertial Measurement Unit

3.2.2.1 Definition

IMU is an electronic device that combines three sensors - accelerometer, gyroscope and magnetometer [19, 20]. Using an IMU it is possible measure velocity, orientation and gravitational forces. The accelerometer is a sensor that measures the linear acceleration caused by the movement and the earth gravitational acceleration [21]. The gyroscope is a sensor that measures the angular velocity. With it, it is possible to determinate how quickly a human structure rotates [22]. Lastly, a magnetometer is a sensor that measures the local earth magnetic field vector, proving additional information about orientation [20].

Applying sensor fusion algorithms it is possible to feasible get a better information about the orientation of the device relative to the geographic coordinates [20].

Using the data provided by IMU it is possible to estimate the posture or movement of the human body. These data have several applications in medical field [20, 23], e.g., comparing the movements between and pathological people, or in HCI where movements are used to control electronic devices [5].

(a) (b)

Figure 3.2: Representation of the electrode placement at the forearm. (a)-Near the wrist, (b)- Near the elbow.

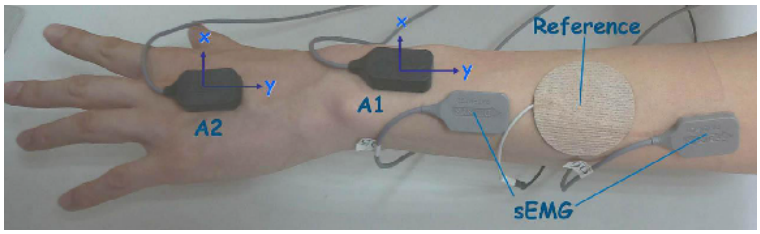

Figure 3.3: Representation of the IMU sensors placement [9]

Devices equipped with IMU provide a way to measure postures and movements and have the advantages of being portable, low-cost, low-power and with reduced size and weight when compared to other methods, such as those based on image analysis.

3.2.2.2 Number of Sensors and Placement

Similarly to the EMG, IMU data enables the evaluation of arm gestures for HCI in case the devices are placed at the appropriate place of the body, i.e. on the forearm. However using only IMU data it is impossible to recognize the fingers movements. When fused, the EMG and IMU data enables to achieve classification results of pattern recognition significantly higher [9].

When the IMU sensors are placed on the wrist or on the hand (see Figure 3.3) the performance of classifiers are identical, i.e., for classification, it is equal use the IMU on the wrist or on the hand [9]. Being the wrist a local that facilitates the placement of the sensors it is recommended to use this place.

3.3 Preprocessing

The main objective of the preprocessing step is to segment the patterns of interest from the background. For this, in most cases, it is necessary to remove the noise, normalize the patterns and perform other operations that will contribute to a better segmentation of data.

3.3.1 Noise reduction

In most of the cases we need to perform some noise reduction techniques in order to define a compact representation of the pattern, that will facilitate the segmentation task.

The EMG signal has lots of interference originated in different sources [3, 24]. One of these sources is the electronic equipment used to record the signal. All electronic equipments generate a type of noise which is impossible to avoid but, can still be reduced using better quality devices. The environment noise, caused by electromagnetic radiation, is one type which is impossible to avoid. Lastly, the electrode interface or electrode cables can give rise to motion artefacts. To smooth this type of noise analog or digital filters can be used [24, 25, 26].

The motion artefacts have a power density below 20 Hz. Using a high pass filter it is possible to attenuate this type of noise. In order to avoid loss of myoelectric signal power, the corner frequency of the high pass filter is frequently set at 10 Hz and generally should be set no higher

than 20 Hz [24]. Other possible way to attenuate the motion artefacts is to apply the average filter, estimating the motion artefacts, and then, subtract from the original signal the motion artefact estimated.

The power supply frequency (60 Hz in USA or 50 Hz in Europe) and its harmonics can result in a power line interference signal which can be much larger than EMG itself [24]. This type of noise can be reduced by shielding the recorder device or apply a notch filter centred at the fundamental frequency (50 or 60 Hz) [26].

Regarding the IMU signal most of the noise can be smoothed with analog or digital low-pass filters [27]. Using a low-pass filter an Acc signal can be divided into gravitational component and linear acceleration.

3.3.2 Active segments detection

Before starting with the process of extracting and selecting features, it is necessary distinguish the patterns that need to be recognized from the background.

With EMG signals it is usual to use methods based on thresholds to detect muscular activity, i.e., to segment the signal into segments where possible MUAPs occurred the active segments [6, 9]. This threshold (*th*) can be estimated based on mean (μ) and standard deviation (σ) of the baseline signal (see Equation 3.1) [28]. Using this approach, when the signal is higher than the *th* it is considered to be active, on the other hand, when the signal is lower than threshold it is considered to be non-active.

$$th = \mu + h\sigma \tag{3.1}$$

In order to turn the active signal segments more enhanced relative to non-active segments (see Figure 3.4) there are other techniques proposed, for example, techniques based on the root mean square (RMS)(see Equation 3.2) [7], the Teager–Kaiser energy operator (*TKEO*) (see Equation 3.3) [28] or the moving mean square (see Equation 3.4) [6, 9, 29]. In the equations, the x represents the value of the signal and the n and W represent the window size.

$$x_{\text{rms}} = \sqrt{\frac{1}{n}\left(x_1^2 + x_2^2 + \cdots + x_n^2\right)}. \tag{3.2}$$

$$TKEO = x^2(n) - x(n+1)x(n-1) \tag{3.3}$$

$$E_{MA}(t) = \frac{1}{W}\sum_{i=t-W+1}^{t}\left(EMG_{avg}^2(i)\right) \tag{3.4}$$

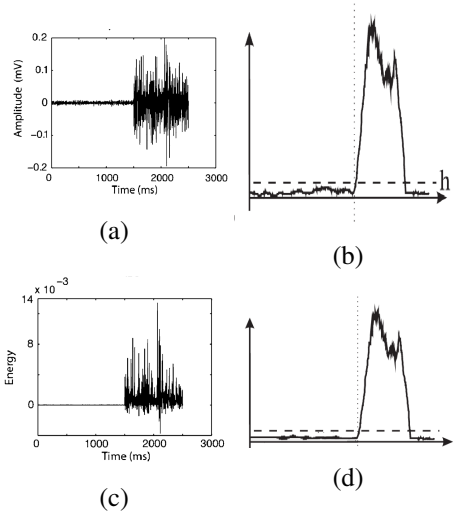

Figure 3.4: Difference between techniques to enhanced the active segments relative to non-active segments. (a)- original signal [28]; (b)- RMS [29]; (c)- TKEO [28]; (d)- moving average [29].

3.4 Features extraction and features selection

A pattern can be described in a set of descriptive characteristics, i.e. features. To better describe a pattern, the feature vector should incorporate features belonging to the time domain as well as to the frequency domain.

To perform pattern recognition using, the EMG signal, several features can be calculated from the signal (see Table 3.3) [4]. Features like first order autoregressive coefficient, amplitude histogram, wilson amplitude, variance of the central frequency, mean absolute difference value, mean frequency and zero crossing have shown to have a great discriminant power [4] in the context of gestures recognition for HCI gestures.

Taking into account the IMU signal features like mean, standard deviation, maximum, minimum, mean absolute difference value, fundamental frequency and spectral energy have a good ability in the differentiation of classes.

The number of features are limited by the number of training samples. Some studies demonstrated that, with a small dataset, a big number of features can degrade the performance of the classifier [1]. However, a small number of features can not be enough for a great result. Thus it is advisable to use algorithms for feature selection to discard the features less discriminating or use feature extraction techniques to build new features subspaces in different domains.

There are two big reasons for reduce the number of features, the power cost needed to process all data and the increase of the classifier accuracy [1]. With a reduced feature vector only the representative features are used and consequently the classifier will be faster and will require the use of less computational power and memory.

To better understand the dimensionality reduction it is important to hightlight the differences between feature selection and feature extraction. While feature selection algorithms will select the best subset of input features, the feature extraction methods will create new features based

Table 3.3: Features that can be extracted from the sEMG signal [4].

Acronym	Name	Formula
MAV	Mean Absolute Value	$MAV = \frac{1}{N}\sum_{i=1}^{N}\|x_{i\|}$
LogDet	Log Detector	$LogDet = \exp(\frac{1}{N}\sum_{i=1}^{N} log_e(\|x_i\|))$
MedAV	Median Absolute Value	$MedAV = median_i\|x_i\|$
VAR	Variance	$VAR = \frac{1}{N-1}\sum_{i=1}^{N} x_i^2$
MADV	Mean Absolute Difference Value	$MADV = \frac{1}{N-1}\sum_{i=1}^{N-1}\Delta_i$
ZC	Zero Crossing	$ZC = \sum_{i=1}^{N-1}\phi(\Delta_i)$. Where $\phi(\Delta_i) = \begin{cases} 1 & x_i.x_{i+1} < 0, \phi(\Delta_i) > \varepsilon_Z \\ 0 & \text{otherwise} \end{cases}$
NT	Number of Turns	Number of times that the slope of the waveform changes in sign and the difference in amplitude with adjacent slope changes is at least ε_N
WAMP	Wilson Amplitude	$WAMP = \sum_{i=1}^{N-1}\Psi(\Delta_i)$.Where$\Psi(\Delta_i) = 1$ if $\Delta_i > \varepsilon_W$; and 0 otherwise
Fmean	Mean Frequency	$Fmean = (\sum_{b=1}^{M} f_b P_b)/(\sum_{b=1}^{M} P_b)$
PKF	Peak Frequency	$PFK = argmax_{fb}P_b$
VCF	Variance of the Central Frequency	$VCF = \frac{1}{F_{mean}}\sum_{b=1}^{M}(P_b - f_c)^2$
Ahist$_j$	Amplitude Histogram	The amplitude range is subdivided into N bins. Each AhistJ, with 1≤J≤N, represents the frequency with which the absolute value of the EMG signal falls in the J bin.
Fhist$_j$	Frequency Histogram	The frequency spectrum is divided into N equal-size segments. The feature FhistJ , with 1≤J≤N, represents the percentage of power in the J segment
Ar$_r$	Auto-regressive Coefficients	$x_i = \sum_{r=1}^{4} AR_r x_{i-r} + \varepsilon_i$
CC$_r$	Cepstral Coeffiients	The cepstrum of a signal is the Inverse Fourier Transform of the logarithm of the signal's spectrum. It can be obtained from the AR coefficients $CC_r = -AR_r - \sum_{n=1}^{r-1}(1-\frac{n}{r})AR_n CC_{r-n}$
Q_j	Quantiles	The Q_j, with J=10, 20,...,90, is the frequency that marks the upper boundary of the lower J% of the spectrum's power
EnWC_j	Energy of the Wavelet Coefficients	The signal is decomposed by the discrete wavelet transform into 7 levels. The % of energy of each band is used as a feature.
ZCWC_j	ZC of the Energy Wavelet Coefficients	The ZC of each band is used as a feature.
MAVWC_j	MAV of the Energy Wavelet Coefficients	The MAV of each band is used as a feature.
EnWP_j	Energy of the Wavelet Packet Coefficient	The signal is decomposed by the discrete wavelet packet transform into 3 levels. The % of energy of each band is used as a feature.

on transformations and combinations of the original features vector. The choise of using one technique or the other always depends on the final goal. By using feature selection it is possible to save power cost while maintaining the original physical interpretation of the selected features. On the other hand, feature extraction enable to get a more discriminant subset of features, however, the new features may not have a clear physical meaning.

In Table 3.4 are described some algorithms that can be used in feature extraction and in feature selection.

3.5 Classifiers

After reducing the number of features to be used the data is ready to be classified. So, it is necessary to choose the classifier algorithm to use. This choice proves to be difficult but, in the end, it is possible to identify the class of the input pattern, i.e., discriminate the gesture performed.

In Ahsan et.al.2009 [2] an overview of the results obtained by the most common classifiers in EMG pattern recognition was made. This overview is resumed in Table 3.5.

In this dissertation, an highlight is given to five different classifiers which demonstrated to have great results in EMG and IMU pattern recognition [6, 7, 30], i.e., the Decision Tree, k-Nearest Neighbours (k-NN), linear discriminant analysis(LDA), naïve Bayes and artificial neural network (ANN).

- Decision tree - following the analogy with a tree, the leaves represent the class labels (i.e. the gestures) and the branches represent the set of features necessary to choose to achieve the leaves. In a branch the decision is made taking into account some statistical terms [31].

- k-NN - having a new pattern to recognize, the principle of this method is to find a predefined number of training samples closest in distance to this new sample. The standard Euclidean distance is the most common metric used to evaluate distance between features.

- LDA - the principle of this method is to find a linear combination between features. This method uses the training set to find that combination. The new pattern will be classifier taking account the combination founded.

- naïve Bayes - it is a simple method that uses the probability distribution of the training set to construct a model and then, predict a class to a input pattern. In a simple way this method uses the probability of each feature to belong to a particular class.

- ANN - are models inspired in biological neural networks, composed of a input layer, hidden layer and output layer. All layers are connected. Using a training set it is possible know the path used to the output, for each class. According to the used path, a new pattern will be classified.

Table 3.4: Methods for feature extraction and feature selection [1].

	Method	Property	Comments
Features Extraction	Principal Component Analysis (PCA)	Linear map; fast; eigenvector-based.	Traditional, eigenvector based vector, also know as Karhunen-Loève expansion; good for Gaussian data.
	Linear Discriminant Analysis	Supervised linear map; fast; eigenvector-based.	Better than PCA for classification; limited to (c-1) components with non-zero eigenvalues.
	Projection Pursuit	Linear map; iterative, non-Gaussian.	Mainly used for interactive exploratory data-analysis.
	Independent Component Analysis	Linear map, iterative, non-Gaussian	Blind source separation, used for de-mixing non-Gaussian distributed features
	Kernel PCA	Nonlinear map; eigenvector-based.	PCA-based method, using a kernel to replace inner products of pattern vectors.
	PCA Network	Linear map; iterative	Auto-associative neural network with linear transfer functions and just one hidden layer.
	Nonlinear PCA	Linear map; non.Gaussian criterion; usually iterative	Neural network approach, possibly used for ICA
	Nonlinear auto-associative network	Nonlinear map; non-Gaussian criterion; iterative.	Bottleneck network with several hidden layers; the nonlinear map is optimized by a nonlinear reconstruction; input is used as target.
	Multidimensional scaling, and Sammon's projection	Nonlinear map; iterative	Often poor generalization; sample size limited; noise sensitive; mainly used for 2-dimensional visualization.
	Self-Organizing Map	Nonlinear, iterative	Based on a grid of neurons in the feature space; suitable for extracting spaces of low dimensionality
Features Selection	Exhaustive Search	Evaluate all $\binom{d}{m}$ possible subset	Guaranteed to find the optimal subset; not feasible foe even moderately large values of m and d
	Branch-and-Bound Search	Uses the well-know branch-and-bound search method; only a fraction of all possible feature subsets need to be enumerated to find the optimal subset	Guaranteed to find the optimal subset provided the criterion function satisfies the monotonicity property; the worst-case complexity of this algorithm is exponential.
	Best Individual Features	Evaluate all the m features individually; select the bes m individual features	Computationally simple; not likely to lead to an optimal subset.
	Sequential Forward Selection (SFS)	Select the best single features and then add one feature at a time which in combination with the selected features maximizes the criterion function	Once a feature is retained, it cannot be discarded; computationally attractive since to select a subset of size 2, it examines only (d-1) possible subsets
	Sequential Backward Selection (SBS)	Start with all the d features and successively delete one feature at a time	Once a feature is deleted, it cannot be brought back into the optimal subset; requires more computation than SFS.
	"Plus l-take away r" Selection	First enlarge the feature subset by l features using forward selection and then delete$r$ features using backward selection.	Avoids the problem of feature subset "nesting" encountered in SFS and SBS methods; need to select values of l and r.
	Sequential Forward Floating Search and Sequential Backward Floating Search	A generalization of "plus-l take away-r" method; the values of l and r are determined automatically and updated dynamically.	Provides close to optimal solution at an affordable computational cost.

Table 3.5: Summary of major classifiers used with EMG signals [2].

Classifier Used	**Researcher**	**Description**
Artificial Neural Network	Putnam et. al. (1993)	·A_r model parameters based feature vector for Neural Network · 95% accuracy in classification was achieved · More robust classifier required for persons with disabilities
	Rosenberg (1998)	· Performance of 94% according to Fitt's law · More sophisticated neural network and better training methods required for future improvement
	Tsenov et. al (2006)	· Both time and frequency domain features used · Classification accuracy can be 98% using 4-channel data set, but computational time becomes double · It is hard to determine complete set of relevant discrimination features
	Kyung Kwon Jung et. al (2007)	·Yule-Walker algorithm based A_r model for spectral estimation 4th order A_r model parameters as input ·Classifier success rate is about 78% ·There is no mechanism in a strictly competitive layer design depending on input vector classes
Back-propagation Neural Network	Itou et. al. (2001)	· 70% recognition rate ·Not applicable for long term use ·Limited to 4 directions and drag action absent
	Naik et. al. (2007, 2008), Eman M. El-Daydamony et.al. (2008)	·RMS value of each signal used to form feature vector as input to neural network ·Combination of the mixing matrix and network weights to classify the sEMG recordings in almost real-time ·Number of hand gesture identification was restricted to three and six
Log-Linearized Gaussian Mixture Network	Tsuji et. al. (1995) Fukuda et. al. (1999)	·LLGMN for creating LLGM model through learning and calculating the posteriori probability of pointer movement in each base direction · Higher discrimination performance can be achieved than other neural network · The direction of pointer movement is achieved by output of neural network · The accuracy of pointer movement depends on number of learning data and the accuracy of estimated direction depends on number of base directions
Recurrent LLGMN	Tsuji et. al. (2003) Fukuda et al. (2004)	·Finite base direction assumed which leads to avoid heavy learning calculation and huge network structure ·Higher accuracy for the discrimination of time sequence of signal ·Direction errors improved remarkably
LLGMN based Probalistic Neural Network	Nan Bu et. al. (2004)	·Classification rate of hardware is 97.9%, more than software ·Shortage of memory for hardware language ·Processing speed needs to improve

Fuzzy Mean Max Neural Network	Jong-Sung Kim et. al. (2004)	·Stochastic values such as integral absolute value were used as features ·Six distinctive wrist motions can be classified well ·Difference Absolute Mean Value extracted from the EMG signals is used as the input vectors in learning and classifying the patterns ·Pattern recognition rate of each wrist motions is above 90%, whereas average recognition rate yield 97% ·4 channel raw EMG signal used ·It is important to extract appropriate feature vector for the classifier
Radial Basis Function Neuro Network	Farid Mobasser et al. (2006)	·Moving Window Least Squares estimation method used to identify limited number of operating points ·RBFNN is trained using limited points and is utilized for interpolation /extrapolation for online estimation of arm dynamic parameters ·Parameters error found because of stochastic nature of EMG signals
Hidden Markov Model	Wheeler (2003), Chan et al. (2005)	·Moving average selected for feature space as it is best and simplest HMM has inherent ability to deal with spurious misclassification ·During classifier training, HMM provides large computational savings ·Reported that the used methodology does not vary adaptively ·Further improvement would required in model correcting adaptation and calibration stage
Bayes Network	Alsayegh, Xiang Chen et. al (2007), Jonghwa Kim et al. (2008)	·Reported that structured type movements have higher classification success rate than pointing movements · Common time domain and frequency domain features extracted ·K-Nearest Neighbour (k-NN) classifier added with Bayes to obtain good result ·Addition of accelerator meter with EMG sensors can increase the classification rate 5-10% ·Feature selection is important for better classification and increasing number of features does not always produce good result ·Average classification rate reported was over 94%

3.6 Evaluation

After applying a classifier, each pattern is assigned to a label. To evaluate the performance of the classifier, some techniques that allow measuring some evaluation metrics are applied. The most common evaluation method is based on a confusion matrix. In this matrix, while columns represent the predicted classes, the rows represent the actual class (see Figure 3.5). With this matrix it is possible to observe, true positive (TP), true negative (TN), false positive (FP) and false negative (FN) samples. The TP are classes classified as positives that are really positives. The TN are classes classified as negatives that really are negatives. The FP are classes classified as positives that, in really, are negatives. The FN are classes classified as negatives that, in really are positives. Using these variables it is possible to measure a new set of metrics:

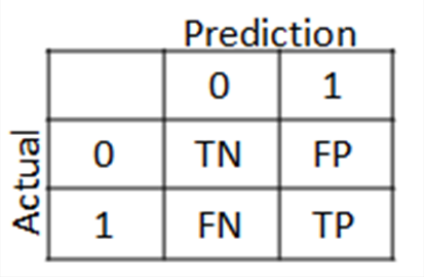

Figure 3.5: Representation of an example of a matrix confusion. The TN, TP, FP and FN are represented for classes 0 and 1.

- Sensitivity - also known as true positive rate, measures the proportion of positives that really are positives (see Equation 3.5).
- Specificity - also known as true negative rate, measures the proportion of negatives that are really true negatives (see Equation 3.6).
- Precision - also known as positive predictive value, measures the proportion of supposed positives that are true positives (see Equation 3.7)
- Negative predictive values - measures the proportion of supposed negatives that are true negatives (see Equation 3.8).
- Accuracy - measures the capacity of the algorithm to correctly detect classes (see Equation 3.9).
- F1 scope - combines precision and sensitivity by using their harmonic mean (see Equation 3.10).

$$Sensitivity = \frac{TP}{TP+FN} \tag{3.5}$$

$$Specificity = \frac{TN}{TN+FP} \tag{3.6}$$

$$Precision = \frac{TP}{TP+FP} \tag{3.7}$$

$$Negativepredictivevalues = \frac{TN}{TN+FN} \tag{3.8}$$

$$Accuracy = \frac{TP+TN}{TP+FP+TN+FN} \tag{3.9}$$

$$F1score = \frac{2 \times TP}{2 \times TP+FP+FN} \tag{3.10}$$

Chapter 4

Proposed Work

This dissertation aims to develop an algorithm capable of recognizing a set of gestures, using sEMG and IMU data. The method used is described in this chapter. It is divided into two main parts. The first part includes Section 4.1 and Section 4.2, where the set of chosen gestures are nominated and characterized and the methods for recording data reported. The second part includes the Sections 4.3, 4.4, 4.5 and 4.6. In these sections, the methods applied to preprocessing, features generation, classification and evaluation are described.

4.1 Set of gestures

This work starts with the identification of the gestures that have an interest in being recognized (see Figure 4.2). The gestures were chosen based on their potential in the field of HCI which may be used to select menus, sweep the interface, among others.

All gestures start in the same position - upper limb forming 90^{o} with the vertical, forearm in extension and pronation and with the hand in a relaxed state - and then perform a characteristic change:

- Hand contraction ("HC") - flexion and adduction of all fingers (see Figure 4.2a).
- Hand extension ("HE") - extension and abduction of all fingers(see Figure 4.2b).
- Wrist extension ("WE") - forearm in neutral position and extension of the wrist and fingers(see Figure 4.2c).
- Wrist flexion ("WF") - forearm in neutral position, flexion of the wrist and extension of the fingers(see Figure 4.2d).
- Upper arm flexion ("UAF") - flexion of the upper arm, extension of the wrist and fingers abduction and extension (see Figure 4.2e).
- Thumb-Index ("TI") - wrist flexion and opponency of the thumb with the index (see Figure 4.2f).

- Thumb-Middle ("TM") - wrist flexion and opponency of the thumb with the middle(see Figure 4.2g).
- Up the hand ("UH") - wrist extension and abduction of the thumb (see Figure 4.2h).
- Down the hand ("DH") - wrist flexion and abduction of the thumb(see Figure 4.2i).
- Snapping the fingers ("snap") - forearm in neutral position, flexion of the ring and pinky and wide opponency of thumb and middle until extension of the thumb and flexion of the middle (see Figure 4.2j).
- Wrist abduction ("WA") - forearm in neutral position, flexion and adduction of the middle, ring and pinky, extension of the thumb and index and abduction of the wrist(see Figure 4.2k).
- Upper arm lateral rotation ("UALR") - forearm in neutral position and wide lateral rotation of the upper arm (see Figure 4.2l).

4.2 Dataset

4.2.1 Sensors and devices

To collect data from EMG and IMU sensors two different systems were used, one composed by two devices, BITalino (EMG data) and LG G Watch (IMU data) (see Figures 4.1a and 4.1b) and other composed by solely Myo gesture control armband (see Figure 4.1c).

BITalino is a low-cost toolkit made explicitly to applications using body signals. This device has 8 channels - 6 analogical and 2 digital - and support several different types of sensors. The EMG sensors record at a sampling frequency of 1000 HZ and a bandwidth between 20 and 400 Hz.

LG G Watch is a device belonging to the family of the smartwatch. This one has incorporated an IMU sensor that allows recording at a sampling frequency of around 100 Hz. The directions of the axes of this sensor are represented in Figure 4.3.

Myo gesture control armband is a device recently introduced on the market that is preprogrammed to recognize four different gestures. This device has incorporated two different sensors

(a) (b) (c)

Figure 4.1: Devices used in data recording. (a)- BITalino; (b)- LG G Watch; (c)- Myo Gesture Control Armband;

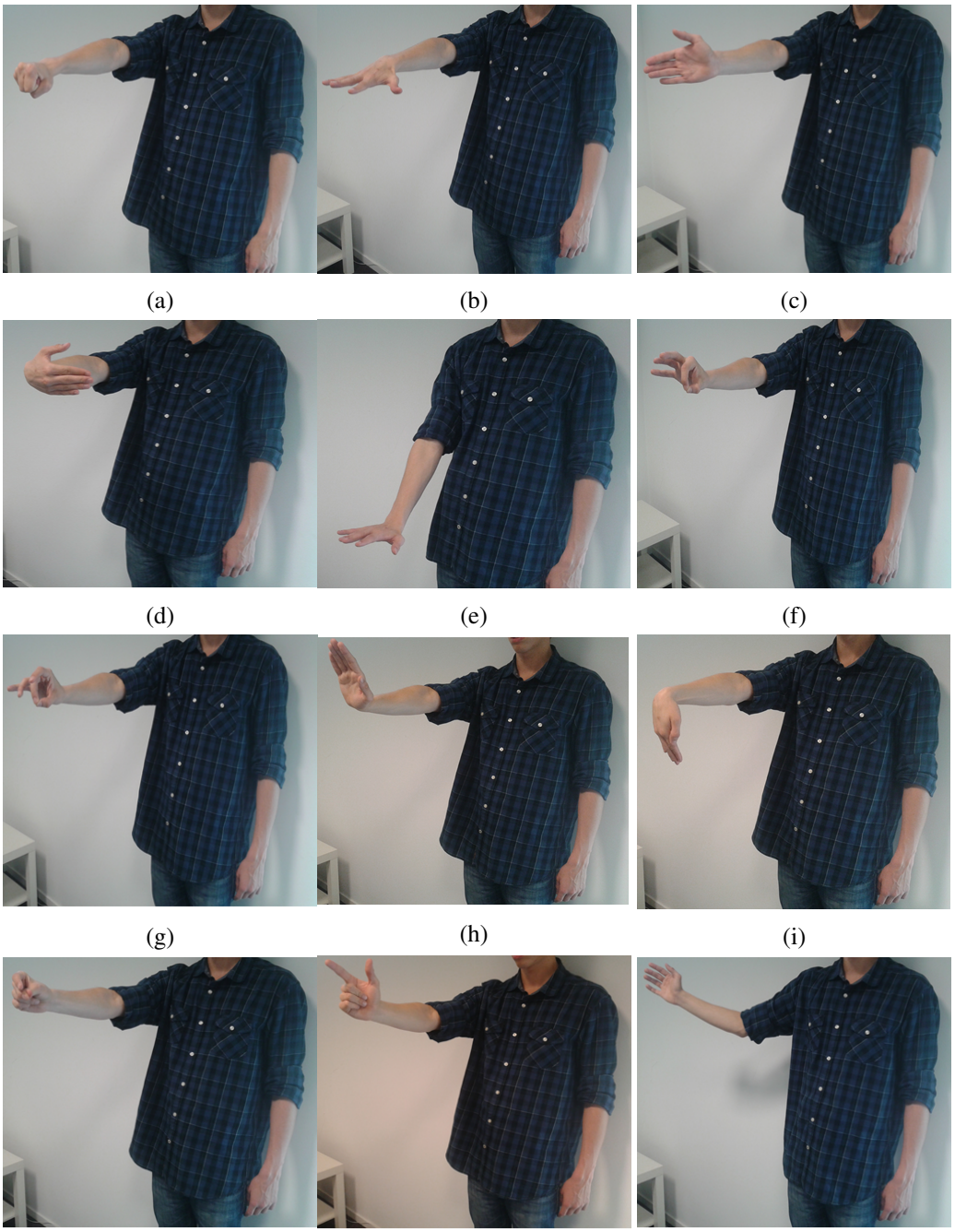

Figure 4.2: Representing the set of gestures that will be recognized. (a)-"HC"; (b)-"HE"; (c)-"WE"; (d)-"WF"; (e)-"UAF"; (f)-"TI"; (g)-"TM"; (h)-"UH"; (i)-"DH"; (j)-"snap"; (k)-"WA"; (l)-"UALR"

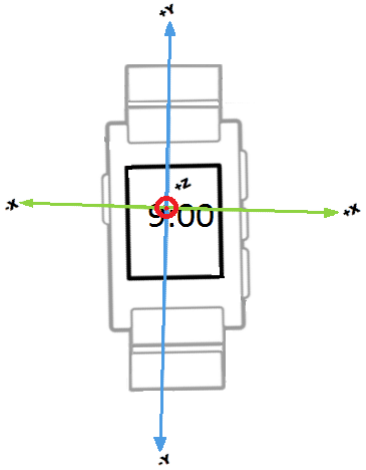

Figure 4.3: Representation of IMU coordinate system.

- 7 EMG channels and 1 IMU sensor - distributed by cells around the forearm. With him it is possible record data at a sampling frequency of 1000 Hz.

All the devices were connected via Bluetooth to a recording application developed at Fraunhofer AICOS, which was running on a laptop. Data was recorded in text files using a comma-separated format with the identification of the source of the values, as well as their timestamp. Only accelerometer and gyroscope data were recorded from IMU since the information provided by the magnet would not be relevant in the context of gesture pattern recognition. Changes in orientation on the horizontal earth plane are already provided by the gyroscope, not being fundamental the detection of the absolute orientation relative to the north.

4.2.2 Sensors placement

The EMG data was collected from 4 different channels of BITalino. The interface between the sensors and the skin was made by pre-gelled electrodes with a conductive and adhesive hydrogel, allowing a greater electrical conduction (see Figure 4.4). These electrodes have 24 mm in diameter and 1 mm in thickness, allowing the measurement of a biomedical signal from a specific muscle, not being too big or too small. The electrodes were placed over the muscles that are active when the chosen gestures are performed. The IMU sensor was placed on the wrist as shown in Figures 4.5 and Figure 4.6a and Figure 4.6b:

- Channel 1 - was placed on the *flexor carpi radialis* muscle.
- Channel 2 - was placed on the *flexor digitorum superficialis* muscle.
- Channel 3 - was placed on the *flexor carpi ulnaris* muscle.
- Channel 4 - was placed on the *extensor carpi ulnaris* muscle.

The Myo gesture control armband has a bracelet format, and was developed to be placed around the proximal part of the forearm (see Figures 4.6c and 4.6d).

4.2.3 Dataset recording

The dataset was collected from nine different people - six males and three females - with an average age equal to 23 years. Data was recorded both from the left (five people) and right arms (four people). To record the data, the following steps were considered for each system:

- BITalino + LG G Watch system:
  - In order to clean dead cells and possible dirt, which interferes with signal quality, clean the forearm was cleaned with ethanol.
  - All sensors were put in the correct place (see Section 4.2.2).
  - The following steps were performed and recorded:
    1. Start with the upper limb along the body.
    2. Put the upper limb at 90º with the forearm in extension and pronation and the wrist and hand in a neutral position.
    3. Perform the gesture a few times (between ten and twenty).
    4. Return the upper limb to the initial position along the body.
    5. Repeat these four steps for all gestures indicated in Section 4.1.
  - Remove all devices.
- Myo gesture control armband system:
  - In order to clean dead cells and possible dirt, which interferes with signal quality, the forearm was cleaned with ethanol.
  - The myo device was placed on the forearm in the correct place (see Section 4.2.2).
  - The following steps were followed to record gestures data:
    1. Start with the upper limb along the body.
    2. Put the upper limb at 90º with the forearm in extension and pronation and the wrist and hand in a neutral position.
    3. Perform the gesture a few times (between ten and twenty).
    4. Return the upper limb to the initial position.
    5. Repeat these four steps for all gestures indicated in Section 4.1.
  - Remove all devices.

Figure 4.4: Pre-gelled electrodes.

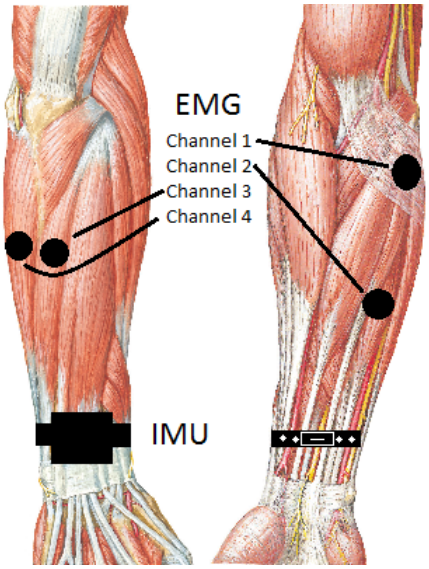

Figure 4.5: Representation of the electrodes placement on the forearm for the BITalino + LG G Watch system. On the left side it is represented the posterior view with the channels 3 and 4 and on the right side is represented the anterior view with the channels 1 and 2. The IMU sensor is represented on the wrist.

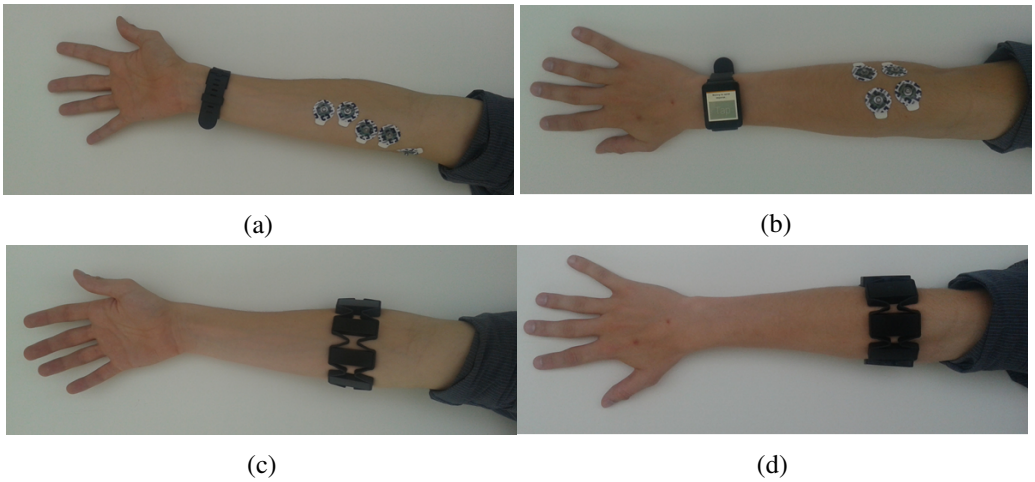

Figure 4.6: Placement of the sensors. (a)- System BITalino + LG G Watch anterior view; (b)- System BITalino + LG G Watch posterior view; (c)- Myo gesture control armband anterior view; (d)- Myo gesture control armband posterior view;

4.3 Preprocessing

With the objective of distinguishing the active from the non-active signal segments a set of methodologies were applied and are described in this section. These methods were implemented in Python, a free and open-source software being a high-level programming language. As integrated development environment was used Pycharm.

In this dissertation the preprocessing step is divided in two parts. First, some filters were applied with the objective of reducing the noise. Then, after apply some algorithms, that contributed to a better segmentation, the active segments were identified. In this case, the moment when the person interacts with the computer was distinguished from the moment when the person not performing any interaction.

4.3.1 Filters

Two different filters were applied to all EMG channels, to attenuate signal noise. Firstly a 3^{rd} order digital bandpass butterworth filter with a bandwidth between 20 and 400 Hz was applied, followed by a notch filter with a cutoff frequency equal to 50 Hz.

Acceleration data was decomposed into linear acceleration and gravity, using a 3^{rd} order digital lowpass Butterworth filter with a cutoff frequency of 2 Hz, that enabled to create an approximation of the gravity signal containing the small fluctuations. This signal, was subtracted from de original acceleration data, creating the second signal containing the linear acceleration. With the high fluctuations.

To the Gyr data was applied a 3^{rd} order digital lowpass butterworth filter with a cutoff frequency equal to 50 Hz to eliminate high frequency noise.

4.3.2 Active segments segmentation

Once all gestures are present in EMG signals, the segmentation was made focusing on this signal. With the objective of enhance the active segments the following algorithm was applied. This algorithm was conceived empirically, joining the best different methods:

- The good state of the recorded data was checked, having as criterion of choice the visual detection of the active segments.
- The offset of each channel was removed. This way the baseline stabilized on zero.
- All channels were added. With this, the active segments were enhanced.
- Using the added channels the TKEO was calculated (see Equation 3.3)
- The RMS was applied.
- Using half of the mean, the threshold value was found (see Equation 4.1).

- Segments with higher valuer than the threshold were considered as active segments and were extracted. Segments with lower value than the threshold were considered as non-active segments.
- In order to reduce the FP, the extracted segments were compared in length and magnitude. Segments with a length less than half the average or the magnitude less than two thirds of the average were ignored.

$$threshold = \frac{1}{2n}\sum_{i=1}^{n} x_i \tag{4.1}$$

4.4 Features

A pattern can be described as a set of features. This set must contain time domain features as well as frequency domain features. This part of the work is made in two steps. First, a set of features is generated to an input pattern. Then, this set of features is reduced in size, by applying algorithms for feature selection or feature extraction.

To describe the input pattern in a set of features the Python language was used. To perform the feature extraction and selection the RapidMiner was used. RapidMiner is a software platform specifically developed for applications in machine learning.

4.4.1 Features generation

For each input pattern the following features were calculated [4]:

- For each EMG channel:
  - Auto-regressive coefficient 1^{st} order
  - Auto-regressive coefficient 2^{nd} order
  - Auto-regressive coefficient 3^{rd} order
  - Auto-regressive coefficient 4^{th} order
  - Mean absolute value (mV)
  - Mean frequency (Hz)
  - Variance of central frequency
  - Mean absolute difference value (mV)
  - Zero crossing
  - Duration (samples)
- For the three axes of the Gravity signal (generated with lowpass):
  - Mean (m/s^2)

  - Standard deviation (m/s^2)
  - Maximum value (m/s^2)
  - Minimum value (m/s^2)
  - Zero crossing
  - Mean absolute difference value (m/s^2)
  - Fundamental frequency (Hz)
  - Spectral energy

- For the three axes of the Linear Acceleration signal (generated with the highpass):
  - Mean (m/s^2)
  - Standard deviation (m/s^2)
  - Maximum value (m/s^2)
  - Minimum value (m/s^2)
  - Zero crossing
  - Mean absolute difference value (m/s^2)
  - Fundamental frequency (Hz)
  - Spectral energy

- For the three axes of Gyr signal filtered with the lowpass:
  - Mean (radians/s)
  - Standard deviation (radians/s)
  - Maximum value (radians/s)
  - Minimum value (radians/s)
  - Zero crossing
  - Mean absolute difference value (radians/s)
  - Fundamental frequency (Hz)
  - Spectral energy

These features are calculated on all signals from both systems giving, for the system BITalino + LG G Watch a total of 109 features and for the Myo gesture control armband system a total of 136 features. This difference is related to the different number of EMG channels.

4.4.2 Feature extraction and feature selection

In order to reduce the dimension of the features vector two different algorithm were tested. PCA, a feature extraction algorithm, and SFS, a feature selection algorithm.

"PCA decomposes the covariance structure of the dependent variables into orthogonal components by calculating the eigenvalues and eigenvectors of the data covariance matrix. Eigenvalues assist in making decisions about the number of orthogonal components that will be used in further analyses, while eigenvectors assist in determining the relationship between the original variables and these new components. Eigenvalues and eigenvectors transform the original variable space into a 'new' set of variables, called principal components" [32].

SFS select the best feature and then add one features at time. The selected feature is the one that maximizes the criterion function [1].

Thus, in this work feature selection and feature extraction algorithms were tested. The PCA was chosen because it is recommended in literature as a good method for feature extraction in EMG [32, 33]. On the other hand, the SFS was chosen because it is a simple method and because it uses less computational power when compared with other algorithms of the same type.

4.5 Classifiers

After reducing the dimension, the set of features can be applied in a classification algorithm. In this dissertation five different classifiers were tested , i.e., Decision Tree, k-nn, LDA, naïve Bayes and ANN.

To improve the performance, firstly, all data were normalized to values between 0 and 1 [1].

All used methods need to perform the training and then test phases. To do this the dataset need to be divided in two - training set and test set. In training phase the algorithms uses the training set, whose class is known to learn how to classifier a unknown pattern. In test phase, the algorithm use the means learned in training phase and for each unknown patterns is assigned a class.

To avoid overfit [1] cross validation methods were used. In this work was chose the kfolds method with k equal to 10. In this methodology the dataset were divided in ten different times ensuring that a pattern in the training set does not enter in the testing set.

4.6 Evaluation

In order to evaluate the results of the classifier in correctly identifying gestures the metrics listed in Section 3.6 were used.

After obtaining the confusion matrix the number of TP, TN, FP and FN were calculated, as well as the sensitivity, specificity, precision negative predictive values, accuracy and F1 scope. These metrics were compared and the best classifier was chosen.

Chapter 5

Results and Discussion

In this Chapter will be presented all the results obtained through the steps described on Chapter 4. The results are divided in two parts. On the first part will be presented the results related with data recording and preprocessing (Section 5.1 and 5.2) and them it will be presented the results of features measurement and reduction (Section 5.3) and classification step 5.4).

5.1 Dataset Recording

The work started with data collection, as stated in Section 4.2.3, this collection was made at 9 subjects - 6 males and 3 females. During the collection were used both, right (four cases) and left upper limb (five cases).

In Figure 5.1 and Figure 5.2 are represented an example of all signals collected from each system. The last six graphics represent the IMU signals and the others represent all EMG channels. In each graph are represented the twelve gestures that will be identify (see Section 4.1).

Analysing the gestures, it is possible to observe that in antagonistic pairs - HC-HE, WE-WF and UH-DH - there is a big difference between signals. For example, observing the EMG signal collected from channel 1 (Figure 5.1) it is possible to found that gestures with greater flexion of the structures, have a signal with higher magnitude. On the other hand, observing the EMG signal collected from channel 4 (Figure 5.1) it is possible to found the opposite, i.e., the gestures with a greater extension of the structures, have a higher magnitude. The reason why this happen is because the electrodes are placed on flexors and extensors muscles, respectively. So, having account the others gestures we can see that, the UAF, being a gesture that require a extension of wrist and fingers, have a higher magnitude in channels with electrodes placed on extensors muscles. The set of gestures composed of snap, WA and UALR, contains gestures with a higher complex degree, wherein, visually, are distinguished better through IMU signals. Lastly, the pair TI-TM contains very similar gestures, being difficult its distinction at a visual level.

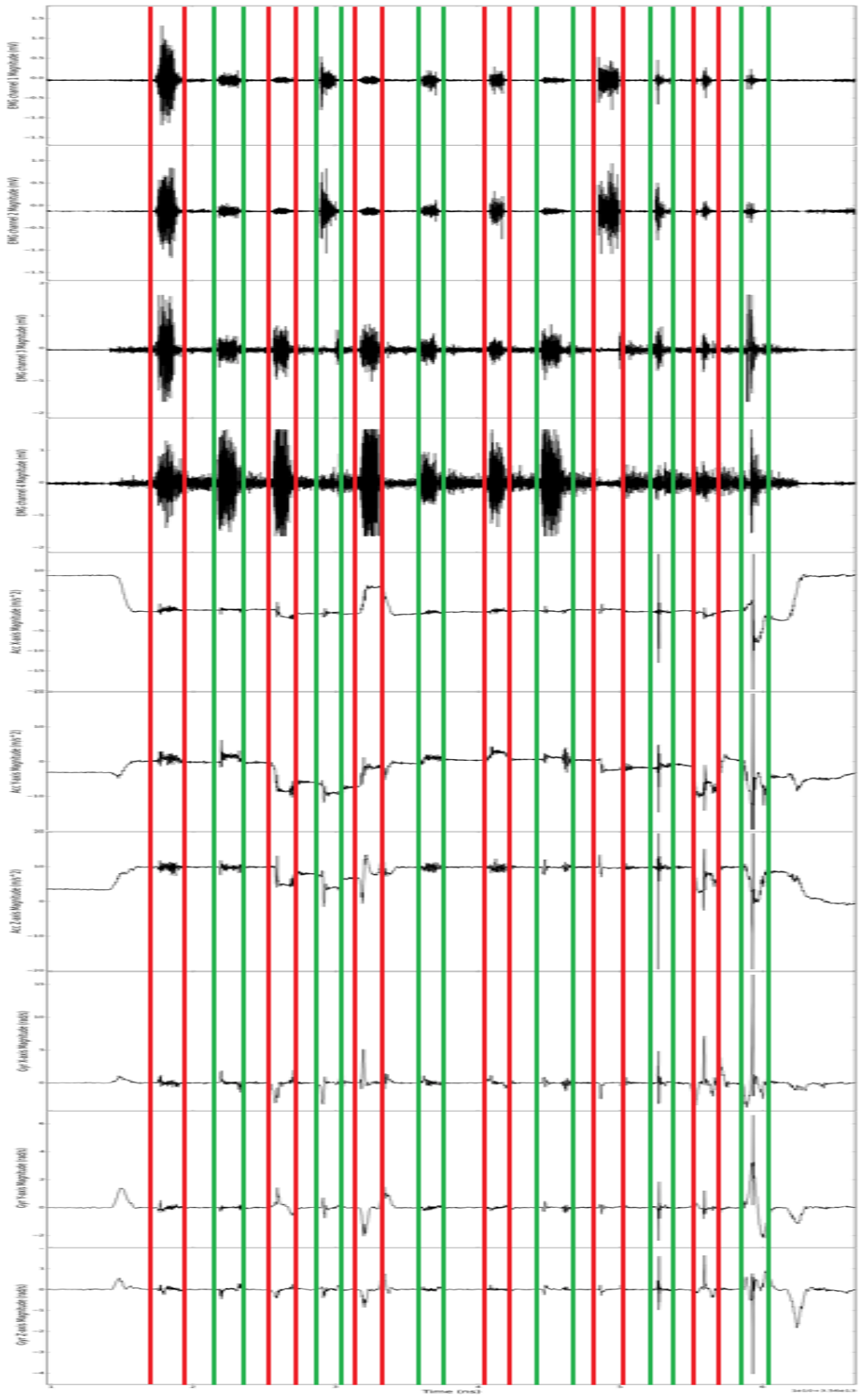

Figure 5.1: Representation of the shape of the signal for every gesture. From left to right: HC, HE, WE, WF, UAF, TI, TM, UH, DH, snap, WA and UALR. From top to bottom: EMG data from channel 1, EMG data from channel 2, EMG data from channel 3, EMG data from channel 4, Acc X-axis, Acc Y-axis, Acc Z-axis, Gyr X-axis, Gyr Y-axis and Gyr Z-axis.

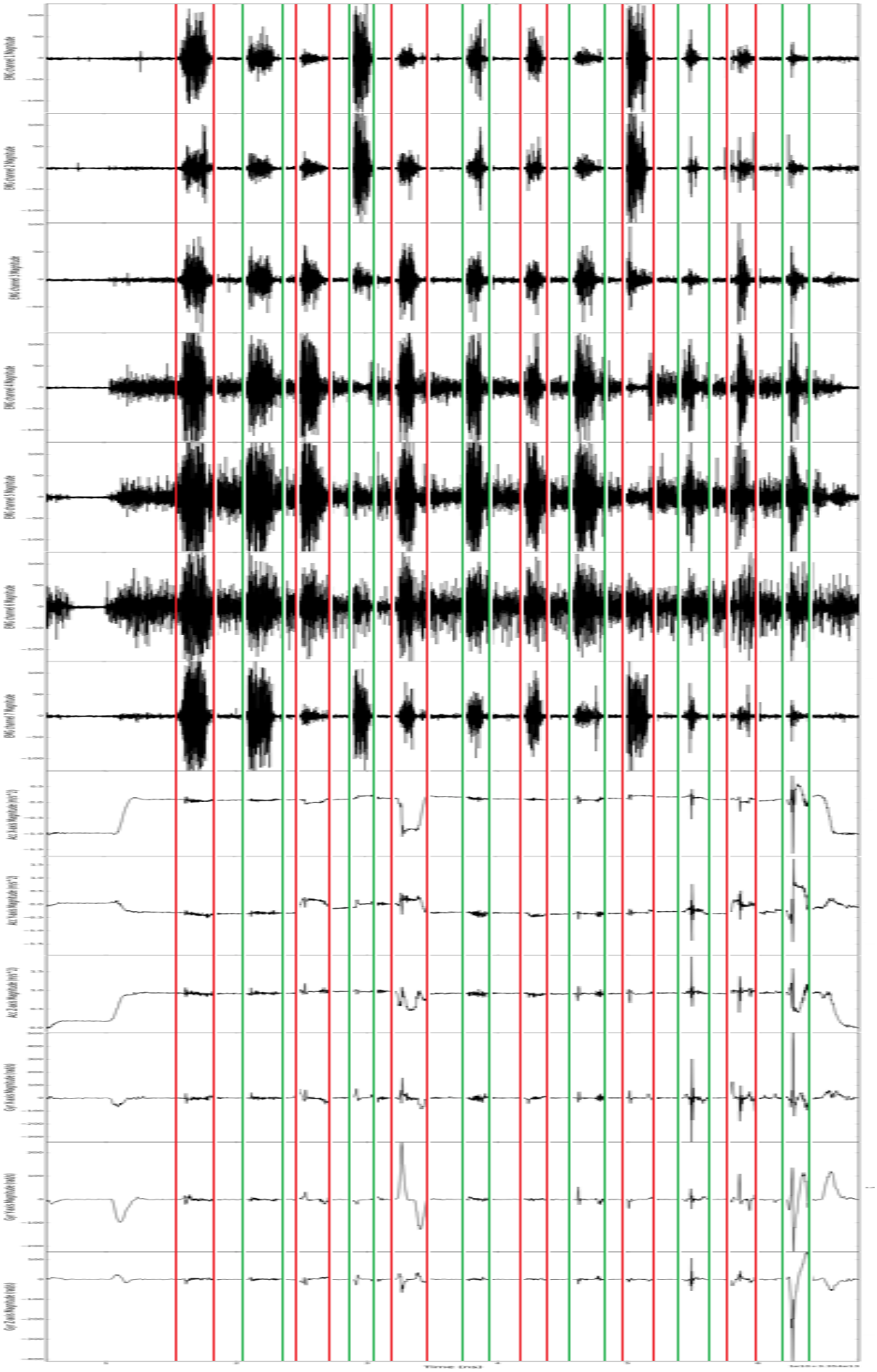

Figure 5.2: Representation of the shape of the signal for every gesture. From left to right: HC, HE, WE, WF, UAF, TI, TM, UH, DH, snap, WA and UALR. From top to bottom: EMG data from channel 1, EMG data from channel 2, EMG data from channel 3, EMG data from channel 4, EMG data from channel 5, EMG data from channel 6, EMG data from channel 7, Acc X-axis, Acc Y-axis, Acc Z-axis, Gyr X-axis, Gyr Y-axis and Gyr Z-axis.

5.2 Preprocessing

With the intent of a good extraction of the active segments, to the original data, from both systems, was applied techniques, that aims to reduce the noise and enhance the active segments. In this part of the work it will be presented the used filters to reduce the noise as well as the used algorithm to extract the active segments.

5.2.1 Filters

To recorded signals, from both systems, were applied digital filters. A comparative example of a filtered signal and non-filtered signal, collected from BITalino + LG G Watch system, can be seen in Figure 5.3. In this Figure are represented the results of the filters applied to the three different signals - EMG collected from channel 1, Acc X-axis and Gyr X-axis collected from IMU.

To all EMG channels was applied two filters - 3^{rd} order bandpass Butterworth filter, with bandwidth between 20 and 400 Hz, and a notch filter with a cutoff frequency equal to 50 Hz. As shown in the two upper graphs of Figure 5.3a, the bandpass filter allowed smoothing the signal, that will eliminate the noise caused by lifting and lowering the upper limb. The notch filter allowed eliminate the noise caused by power supply frequency. Observing the two bottom graphs of Figure 5.3a is possible verify the effect of the applied filters.

The signals from Acc were decomposed into gravity, containing the small fluctuations, and linear acceleration, containing the big fluctuations. Later, due to this decomposition, it was possible measure features with gravity information and linear acceleration information separately. The gravity signal was created by applying a 3^{rd} order lowpass butterworth filter with cutoff frequency equal to 2 Hz. The effects of this filter can be observed in Figure 5.3b. Observing the power frequency spectrum, present in this figure, it is possible to compare the filtered signal, on the right, with the non-filtered signal, on the left. In the filtered signal, the high frequencies was smoothed staying the low frequencies. On the other hand, the linear acceleration signal was created by subtracting the gravity signal to the original signal. A comparison between a filtered signal and a non-filtered signal can be seen in Figure 5.3c. As expected, the low frequencies disappeared staying the high frequencies.

Lastly, to the signals from Gyr was only applied a 3^{rd} order lowpass Butterworth filter with cutoff frequency equal to 50 Hz. With this, it was possible eliminate the noise associated with high frequencies. In the power frequency spectrum (see Figure 5.3d) it is possible to see the effect's that the filter had on the signal.

5.2.2 Active segments segmentation

After filtering the signal, eliminating the noise, the active segments were extracted. The detection of the active segments was made based on EMG data. To do this it was necessary apply techniques to enhance the active segments regarding the non-active segments.

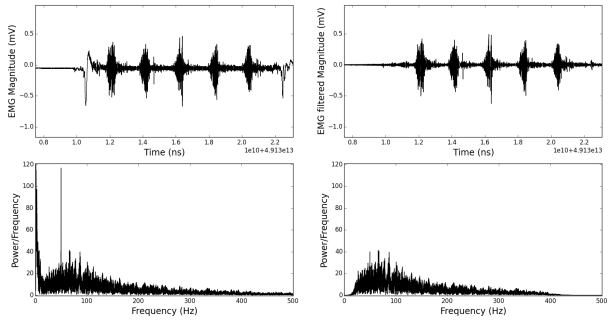

(a)

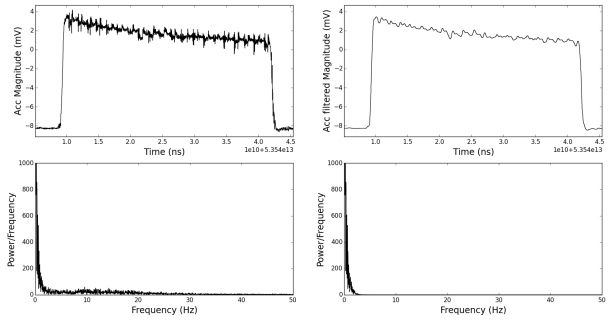

(b)

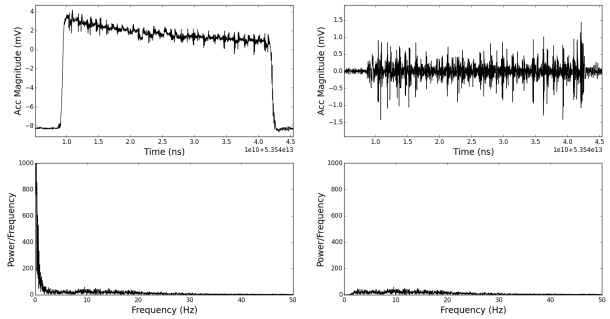

(c)

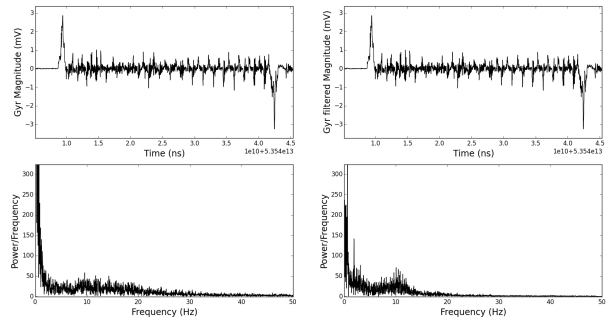

(d)

Figure 5.3: Comparison between the original signal and the filtered signal. Top left: original signal; Top right: filtered data; Bottom left: power spectrum of original data; Bottom right: power spectrum of filtered data; (a)- EMG data from channel 1, was applied a bandpass filter with bandwidth between 20 and 400 Hz as well as a Notch filter with cutoff frequency equal to 50 Hz;(b)- Acc data from X-axis, was applied a lowpass filter with cutoff frequency equal to 2 Hz;(c)- Acc data from X-axis, was applied a highpass filter with cutoff frequency equal to 2 Hz; (d)- Gyr data from X-axis, was applied a lowpass filter with cutoff frequency equal to 50 Hz;

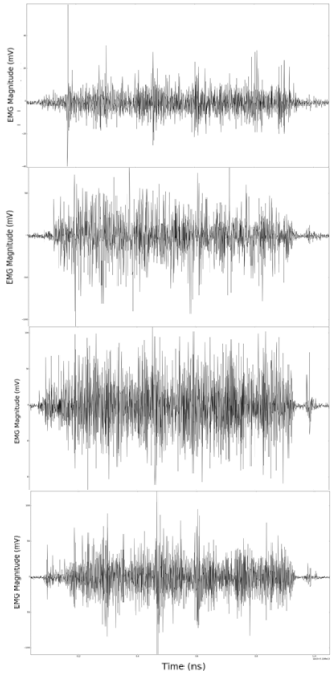

Figure 5.4: Representation of a EMG signal with too much noise. From top to bottom: channel 1, channel 2, channel 3 and channel 4. In Y-axis is represented the magnitude in millivolts and in X-axis is represented the time in nanoseconds.

Firstly, the signals that demonstrate having too much noise, not being possible to, visually, distinguish the active segments from non-active segments, were eliminated. In Figure 5.4 is represented one signal with too much noise. Observing this Figure it is possible to note that, in all channels, the active segments are confused with the non-active segments. This happens, in BITalino + LG G Watch, because, the electrodes are pré-gelled and well fixed to the skin, the electric circuit is not sufficiently well insulated, creating noise. Other possible cause is the bad connection between the tree devices - laptop, BITalino and LG G Watch - and the recording application, having, sometimes, significant losses. In Myo gesture control armband, although the electric circuit is well protect, the electrodes are not fixed to skin causing instability and noise. On the other hand, Myo placement is made of a somewhat subjective way. The channels can not be placed, exactly, on the same place. All signals with this noise were not considered.

In collected signals correctly was applied a RMS filter with window of 30 samples (see Equation 3.2. As result, while the non-active segments were with lower magnitude, the active segments were represented by a envelope with positive value. In Figure 5.5 is represented the gesture HC through the EMG signal collected by channel 1, in grey, as well the filtered signal with RMS, in black color.

The next step was sum all EMG channels. With this, it was possible enhance the active segments relative to non-active segments. The result of this operation is represented in Figure 5.6. As can be seen, the active segments have a positive envelope with magnitude higher than magnitude of non-active segments. Comparing the filtered signal with the original it is possible to verify that the envelope of filtered signal match with muscle activations.

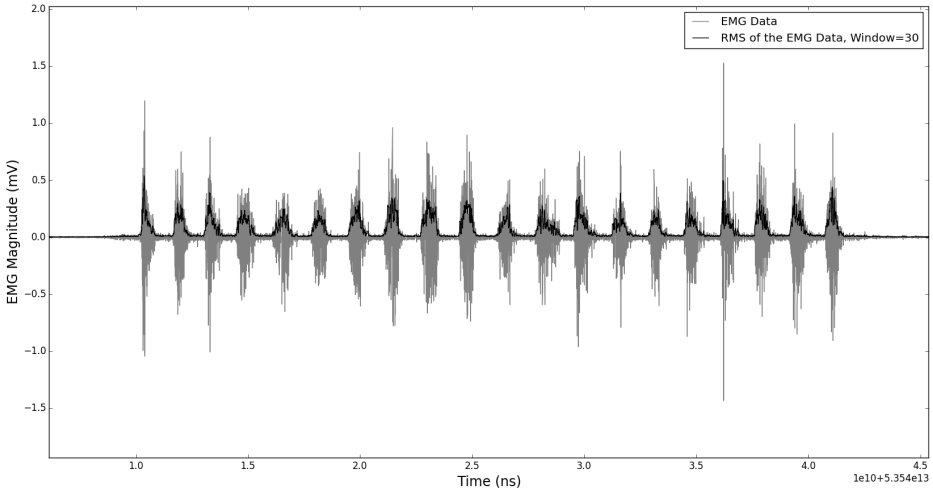

Figure 5.5: Comparison between a EMG signal recorded from channel 1 and the same signal after having applied the filter RMS. In grey is represented the original data and in black the filtered data. In Y-axis is represented the magnitude in millivolts and in X-axis is represented the time in nanoseconds.

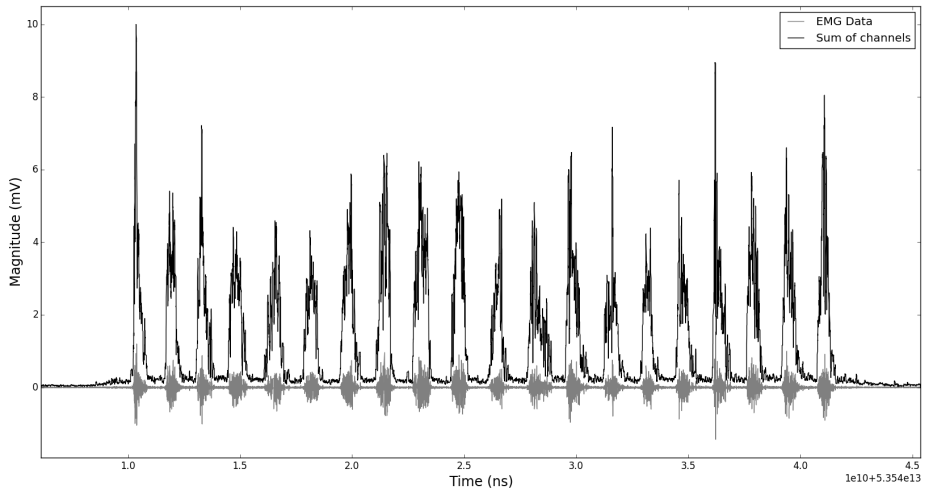

Figure 5.6: Representation of the sum of all channels of EMG data. In grey is represented the original data and in black the filtered data. In Y-axis is represented the magnitude in millivolts and in X-axis is represented the time in nanoseconds.

In order to reduce the magnitude of non-active segments, increasing the magnitude of active segments, TKEO was measured (Equation 3.3). Next, to obtain only the envelope was applied a new RMS with windows of 100 samples. In Figure 5.7 is represented an example of the result of calculation of TKEO. In TKEO signal, represented by black, the difference between active segment magnitude and non-active segment magnitude is high. The application of RMS can be seen in Figure 5.8. The envelope signal match with muscular activations present in original signal, represented by grey color.

Lastly, using half of average of the signal, was calculated a threshold value. The signal parts with values higher than threshold were considered as active segments and the signal parts with value lower than threshold were considered as non-active segments. In Figure 5.9 are represent the enhanced signal, in black, the original signal, in grey, and the threshold value, in red. Observing this Figure it is possible note that, using the measured threshold is possible to perform a good segmentation of the active segments. In some cases, using only the threshold value, a few FP are detected. So in order to eliminate these FP, were performed two different tests. The first test was compared the length of each detected segments with the half of average of all detected segments. If the segment length was lower this segment was eliminated. Next, it was compared the magnitude value of each segment with two thirds of the magnitude average of all the segmented signals. If the magnitude of a single segment was lower this segment was ignored. In Figure 5.10 is represented the results of these tests. While the Figure 5.10a represents the success of this segmentation, the Figure 5.10b represents a case where some TP are eliminated. Observing the Figure regarding to successful cases, it is possible to verify that, from the graphic above to the center, two FN were eliminated. This happen because their length is too small. Comparing the graph of the center with the graph below it is possible note that the other FN is eliminated because has a very low

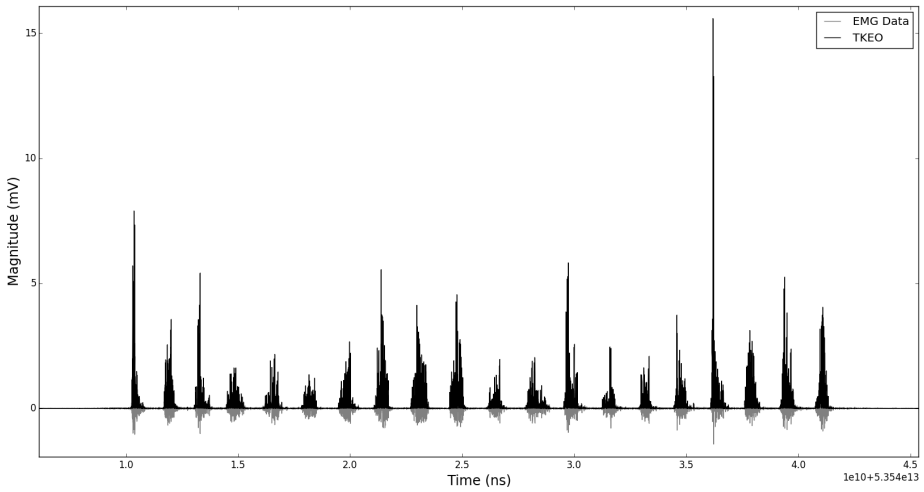

Figure 5.7: Representation of the TKEO of the sum of EMG channels. In black is represented the TKEO and in grey is represented the original data. In Y-axis is represented the magnitude in millivolts and in X-axis is represented the time in nanoseconds.

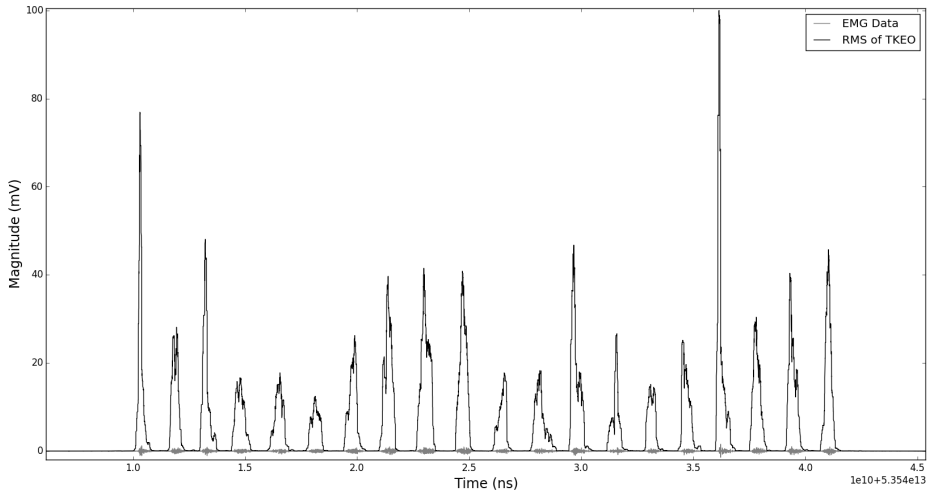

Figure 5.8: Result of RMS of the TKEO signal. In black is represented the filtered signal and in grey is represented the original data. In Y-axis is represented the magnitude in millivolts and in X-axis is represented the time in nanoseconds.

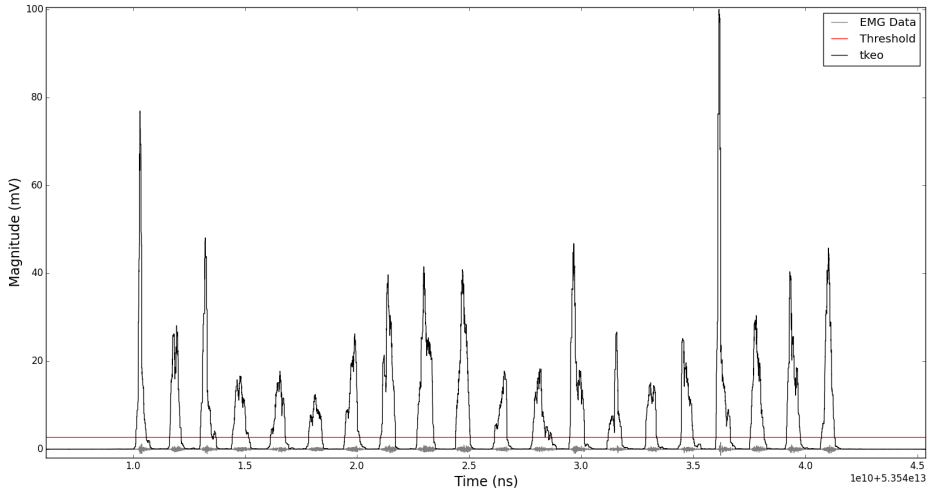

Figure 5.9: Representation of the threshold value calculated, being possible distinguish the active segments from non-active segments. In black is represented the envelope of the TKEO, in grey is represented the original data and in red the threshold value. In Y-axis is represented the magnitude in millivolts and in X-axis is represented the time in nanoseconds.

magnitude. Paying attention to the Figure relative to cases where TP are eliminated it is possible to note that this happen because the active segment is divided in two - part of the segment is lower than the threshold. These two segments detected have a length and a magnitude too lower and they are eliminated. Once it is preferable to lose some TP instead of extracting FP, this approach was maintained.

In Figure 5.11 is represented the extracted segments, in red, in comparison with the originals signals, in black. Figure 5.11a represents a case which all segments were extracted with success while Figure 5.11b represents a case which some TP were eliminated. In any case FP were extracted.

In Table 5.1 are represented, to both systems, the number of gestures recorded for each gesture, as well as, the number of extracted segments with success. It is possible to observe the number of recorded gestures varies from class to class. This happens because the number of gestures performed by each person has not always been the same and because, as already indicated, some gestures had to be eliminated due to their poor record. Having a percentage of 97,72% and 89,11% for the BITalino + LG G Watch system and Myo gesture control armband respectively is it possible consider that the segmentation algorithm extract the active segments with success. The difference between the systems is due to the fact that Myo gesture control armband has more EMG channels which, in step of sum the channels, sometimes, adds noise in the signal, worsening the segmentation.

Table 5.1: Relationship between active segments performed and extracted for both systems

System	**Active Segment**	**HC**	**HE**	**WE**	**WF**	**UAF**	**TI**	**TM**	**UH**	**DH**	**snap**	**WA**	**UALR**	**Total**	
BITalino + LG G Watch	performed	168	168	165	145	133	145	144	170	150	145	146	159	1838	
	segmented	168	163	164	140	132	144	143	169	146	140	144	143	1796	
															97.72%
Myo gesture control armband	performed	165	170	170	170	169	120	104	170	165	115	170	150	1838	
	segmented	165	146	167	120	169	110	95	161	111	86	155	153	1638	
															89.11%

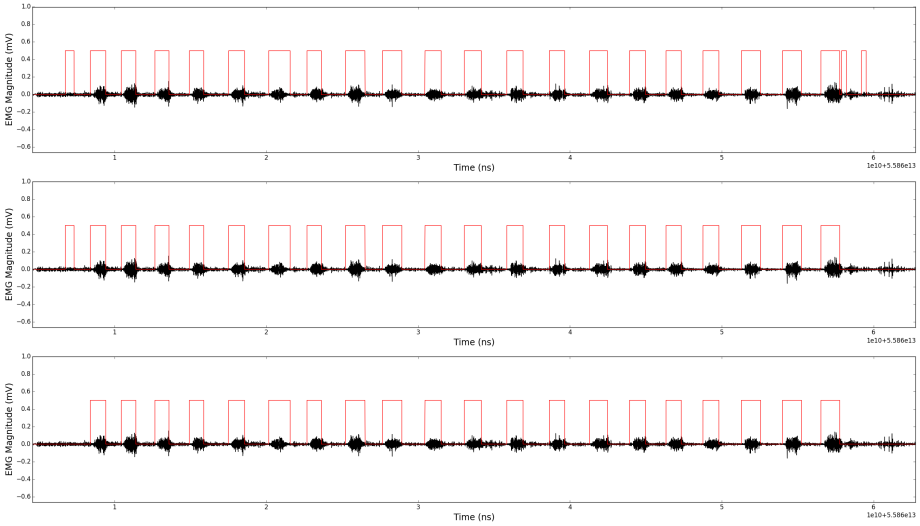

(a)

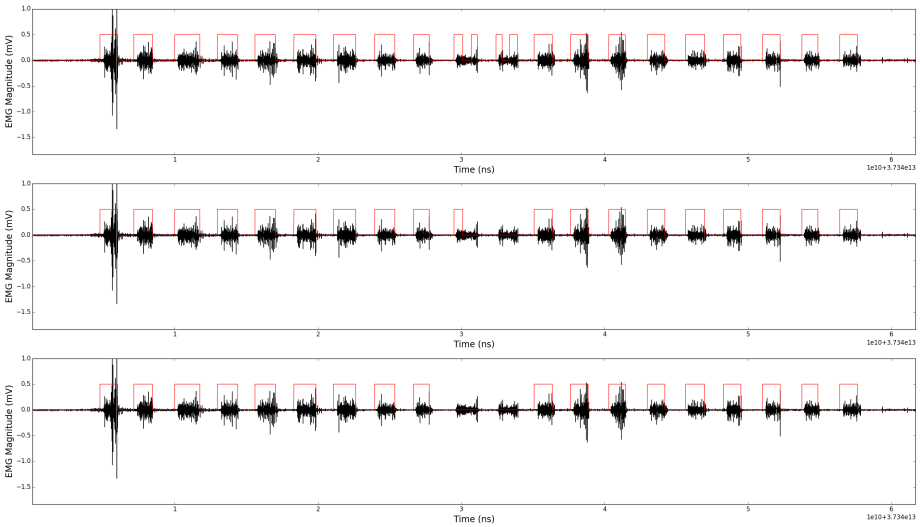

(b)

Figure 5.10: Representation of the detection phases of active segments, as well as, the tests conducted in order to eliminate FP in BITalino + LG G Watch system. (a)- case with success in segmentation; (b)- case which some TP are eliminated; In each Figure the graph above represents the segmentation with threshold, the graph of the center represents the elimination of FP by the length test and the graph below represents the elimination of FP by the magnitude test.

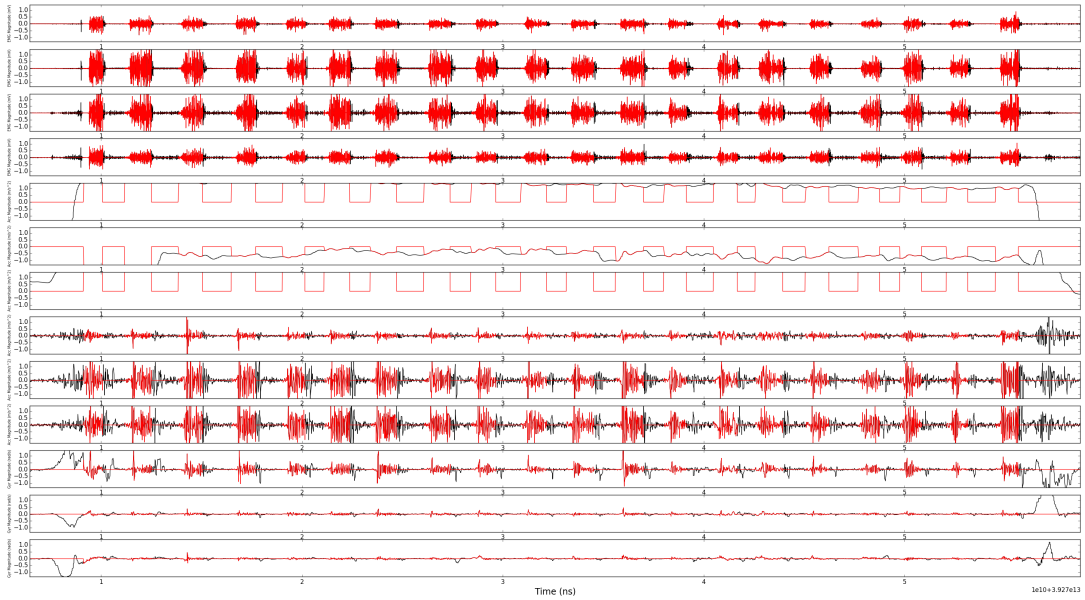

(a)

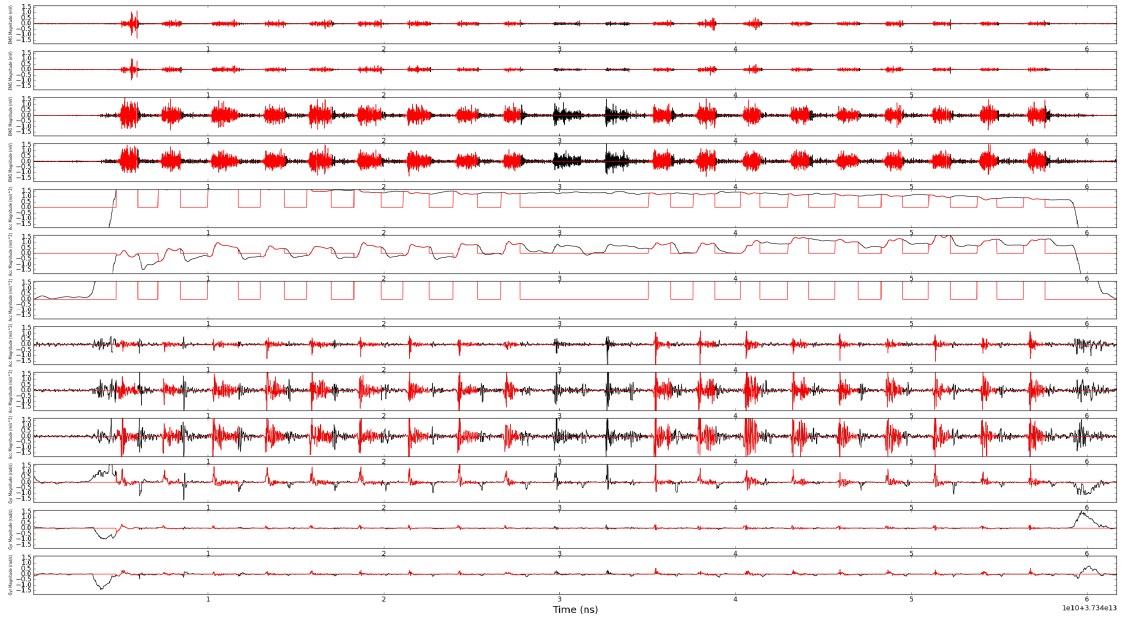

(b)

Figure 5.11: Representation of the extraction of active segments for each recorded signal in BITalino + LG G Watch system. (a)- case with success in segmentation; (b)- case which some TP are eliminated; From top to bottom: EMG channel 1, EMG channel 2, EMG channel 3, EMG channel 4, Gravity X-axis, Gravity Y-axis, Gravity Z-axis, Linear acceleration X-axis, Linear acceleration Y-axis, Linear acceleration Z-axis, Gyr X-axis, Gyr Y-axis and Gyr Z-axis.

5.3 Features

A pattern can be defined as a set of features. In this part of the work it will be shown the chosen features for each system as well the results of the feature selection and feature extraction algorithms used.

5.3.1 Features measurement

For each pattern were measured a total of 109 features for the BITalino + LG G Watch system and a total of 136 features for the Myo gesture control armband system. These set of features incorporate features of time domain and frequency domain. Due to the applied filters to the Acc signal it was still possible differentiate features regarding with gravity and linear acceleration.

In Table A.1 and Table A.2 are represented the mean and standard deviation of each feature measured for each recorded signal of the BITalino + LG G Watch system and Myo gesture control armband, respectively.

5.3.2 Features extraction and features selection

After measuring the feature vector, it was performed the reduction of dimension of this vector. For such were tested two methods, i.e., one feature extraction method - PCA - and one feature selection method - SFS.

PCA is a reduction of attributes process used to reduce redundancy, trying to reduce the number of attributes to the smaller number of principal components possible. After apply this algorithm the features vector was reduced to 20 and 34 principal components (see Table 5.2), to BITalino + LG G Watch and Myo gesture control armband systems, respectively. Once the extraction methods rarely keep the original physical interpretation [1] it is not possible discriminate the chosen features. The results of using this features reduction method along with other algorithms in test will be presented later.

SBS begins with choosing the best feature which alone, allows the classification with higher score. Then the method will adding, in each round, the feature that, jointly with the already selected, will allow a better classification. The adding feature is done until the classification performance does not improve. As a criterion function was used a classifier k-NN with k equal to three. After apply this algorithm the features vector, in both systems, was reduced to 16 features (see Table 5.2). To the BITalino + LG G Watch system were chosen the follow features:

Table 5.2: Number of features found, for each system, by a method of feature selection and by a method of feature extraction.

System	**PCA**	**SFS**
BITalino + LG G Watch	20	16
Myo gesture control armband	34	16

- Maximum value of X-axis of the gravity signal.
- Mean absolute difference value of channel 1 of EMG signal.
- Mean absolute difference value of channel 4 of EMG signal.
- Minimum value of Z-axis of gravity signal.
- Mean absolute difference value of channel 3 of EMG signal.
- Mean absolute difference value of Z-axis of linear acceleration signal.
- Mean absolute difference value channel 2 of EMG signal.
- Auto-regressive coefficient 1^{st} order of channel 1 of EMG signal.
- Mean frequency of channel 4 of EMG signal.
- Auto-regressive coefficient 3^{rd} order of channel 3 of EMG signal.
- Mean absolute difference value of Z-axis of gravity signal.
- Zero crossing of X-axis of Gyr signal.
- Mean of Z-axis of linear acceleration signal.
- Maximum value of Z-axis of linear acceleration signal.
- Mean absolute difference value Y-axis of Gyr signal.
- Mean absolute difference value of channel 1 of EMG signal.

To the Myo gesture control armband system were chosen the follow features:

- Mean of Y-axis of Gyr signal.
- Mean of Y-axis of gravity signal.
- Standard deviation of Y-axis of Gyr signal.
- Mean of X-axis of gravity signal.
- Mean absolute difference value of channel 1 of EMG signal.
- Mean absolute difference value of channel 2 of EMG signal.
- Mean absolute difference value of channel 7 of EMG signal.
- Maximum value of Z-axis of Gyr signal.
- Variance of central frequency of channel 5 of EMG channel.

- Mean absolute difference value of channel 4 of EMG signal.
- Minimum value of Y-axis of gravity signal.
- Mean absolute difference value of Z-axis of Gyr signal.
- Zero-crossing of Y-axis of linear acceleration signal.
- Mean absolute difference value of Y-axis of Gyr signal.
- Maximum value of Y-axis of gravity signal.
- Minimum value of Z-axis of linear acceleration signal.

As can be observed, in both systems, were chosen features from EMG and IMU sensors.

While in BITalino + LG G Watch system were chosen eight features from EMG signals and eight features from IMU signals, in Myo gesture control armband system were chosen five features from EMG signals and eleven features from IMU signals. Comparing the two systems, the fact of Myo gesture control armband system has more features from IMU sensor it may be due to the different position of this sensor - on wrist in BITalino + LG G Watch system and on forearm in myo gesture control armband. It is also important highlight that, in BITalino + LG G Watch system the selected features are, in the vast majority , the mean absolute difference value. Demonstrating that, the velocity of a gesture is an important feature to obtain a great performance.

5.4 Classifiers and evaluation

After the reduction of the features vector dimension we applied five different classifiers - Decision Tree, k-NN, LDA, Naïve Bayes and ANN.

In Table 5.3 are represented the measured metrics for each used algorithm. Comparing the different methods of features reduction it is possible to see that the algorithm of feature selection - SFS - had better results than the algorithm of feature extraction - PCA - then it is preferable to use SFS instead of PCA. Comparing the results between the different classifiers it is possible to find out that, generally, the k-NN and the ANN obtained the best metrics. Paying attention to classifiers that act after the SFS method is possible to observe that, while in BITalino + LG G Watch system, there is no big difference between k-NN and ANN, in Myo gesture control armband the k-NN is clearly the best choice. The classifiers with best performances have a sensitivity, specificity, precision, negative predictive value, accuracy and F1 scope superior to 95%. In both systems, Decision Tree and LDA were the classifiers with worse results, always getting the lowest metric.

In Tables at Appendix B are represented the confusion matrices for each used algorithm and the TP, TN, FP and FN values calculated, as well as, the metrics measures for each gesture. Observing the tables relating to classifiers with better performances, i.e., k-NN and ANN with SFS as feature reduction algorithm, is possible see that some gestures are often confused with others:

- HE by TI and UF

- WE by WA
- WF by DH
- TI by HE and TM
- TM by TI
- UH by WE, WF and WA
- DH by HC, snap
- snap by DH
- WA by WE and UALR
- UALR by WA

This exchange happen because different gestures uses some common muscles. For example, the gestures WA and WE perform an extension of the wrist and so it is common to exchange them. The set of gestures TI and TM are very similar, only changing a finger, and thus may be confused.

Comparing the two systems metrics it is possible observe that BITalino + LG G Watch system classifies with more success. This difference may happen due to fact that Myo gesture control armband not contain fixed electrodes to the skin, slightly varying its position in each test. Despite this difference, both systems can successfully recognize gestures in more than 95% of the cases.

To apply gesture pattern recognition in HCI the classifier that should be used is the k-NN. Although the ANN also obtained good results the k-NN is simpler and requires less computational power. As feature reduction method must be used the SFS, since achieved better metrics, although in some studies the PCA has also obtained good results [33]. Between systems there is no big difference. If necessary perform gesture recognition with a very small error should be used the BITalino + LG G Watch system. On the other hand, if a slightly large error is acceptable it can be used the Myo gesture control armband. This system takes advantage by being intuitive, easy to use and requires no wires that can affect the movements.

Table 5.3: Results of each classifier for each algorithm of feature selection and extraction and for each system.

System	Feature Selection/ Extraction	Classifier	Sensitivity (%)	Specificity (%)	Precision (%)	Negative predictive value (%)	Accuracy (%)	F1 scope (%)
BITalino + LG G Watch	PCA	Decision Tree	40,73	91,16	43,99	88,79	82,42	39,04
		KNN	87,31	98,69	88,10	98,69	97,63	87,60
		LDA	82,04	98,03	83,25	98,02	96,44	82,22
		Naive Bayes	85,10	98,40	85,45	98,39	97,10	85,05
		ANN	96,55	99,67	96,56	99,67	99,40	96,54
	SFS	Decision Tree	80,19	97,90	84,26	97,95	96,20	79,02
		KNN	98,72	99,88	98,76	99,88	99,78	98,74
		LDA	78,84	97,61	81,30	97,60	95,68	78,97
		Naive Bayes	88,46	98,81	89,42	98,82	97,83	88,14
		ANN	96,22	99,64	96,30	99,65	99,35	96,23
Myo gesture control armband	PCA	Decision Tree	29,58	91,80	49,80	86,29	79,93	26,22
		KNN	82,99	98,40	84,11	98,41	97,10	83,37
		LDA	74,23	97,28	75,51	97,27	95,10	74,57
		Naive Bayes	71,29	96,64	71,25	96,62	93,97	70,95
		ANN	88,84	98,98	89,04	98,99	98,15	88,91
	SFS	Decision Tree	50,55	93,48	59,24	93,03	88,11	49,52
		k-NN	96,11	99,69	96,49	99,69	99,43	96,27
		LDA	66,94	96,13	68,21	96,10	93,10	67,42
		Naive Bayes	69,37	96,38	69,82	96,42	93,55	68,84
		ANN	88,72	98,97	89,09	98,98	98,12	88,75

5.5 Gesture Pattern Recognition Algorithm

In Figure 5.12 is represented a flowchart. This one represents the algorithm developed. The algorithm starts with training the classifier. Them, the data are acquire as described in Section 4.2.3, preprocessed (Section 4.3) and the features indicated in Section 5.3 are measured. Finally the classification is made using the trained classifier.

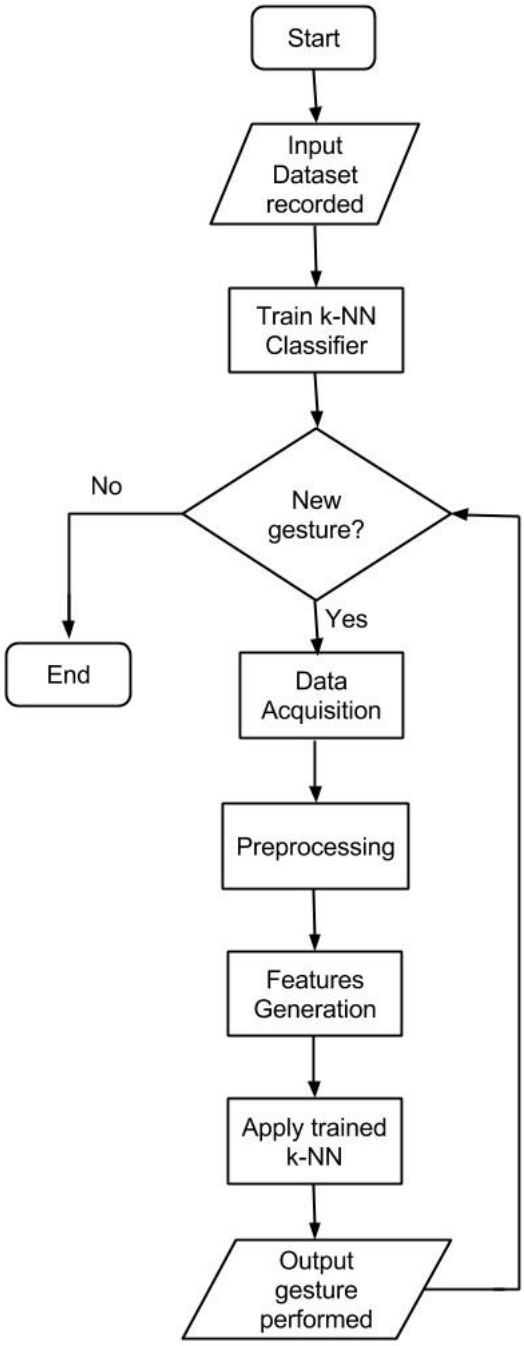

Figure 5.12: Representation of the developed algorithm.

Chapter 6

Conclusions and Future Work

With the advent of new technologies the number of interactions between man and machine increased. In order to improve this interaction it is necessary to create simple and intuitive interfaces which are accessible to anyone. The gestures are naturally used in the real world to interact with objects or transmit informations. The ability to capture, recognize and interpret gestures may thus enable humans to communicate with machines and provide more natural ways of human-computer interaction.

This dissertation had as main objective the development of an algorithm that is able to perform the gestures pattern recognition, using information from EMG and IMU sensors. As a secondary objective has been possible to compare the two systems. A system composed of two devices - BITalino and LG G Watch - and another constituted of a product, already on the market - Myo gesture control armband.

The first big challenge of this work was the extraction of the active segments of the collected EMG signal. To this end, were applied some techniques that enhance areas of interest. The extraction was performed with a success of 97,72% at BIT + LG G Watch system and 96.11% at Myo gesture control armband system. The second major challenge of this work was the classification of the active segments. To this, were extracted features from both systems and applied five different classifiers

After the features extracted, and performed the dimension reduction methods, it is important to state that, the final sets of features, contained information from both sensors, proving that the fusion of information from the two sensors was important in gestures pattern recognition.

Applied the classifiers, is notorious claim that the k-NN was the classifier with best performances in both systems, with metrics exceeding 95%. It is also important claim that in some cases others classifiers obtained good performances, but being the k-NN a simple algorithm that consumes less computational power, this should be used in HCI applications.

Both systems obtained very similar results and, for HCI applications, either one or the other can be successfully used.

Using information from EMG and IMU it is possible perform successfully the gesture pattern recognition and may, in the future, be created interfaces intuitive, easy to use and accessible for

all.

6.1 Future work

Given the results of this work, some future wotk was identified as having potential for improvement:

- Improve the extraction of active segments - in HCI applications is important that all performed actions are detected. So it is important to develop a simpler and more effective method to extract the active segments.
- Evaluate which actions are most important in HCI - This evaluation would allow find out which gestures are more intuitive and more used in HCI. And then, would possible to direct the detection algorithms to such gestures.
- Distinguish the gestures that not belong to the chosen set - It would be interesting turn the algorithm capable of distinguish the gestures that not belong to the chosen set. Thus, if someone perform a gesture that not belong to the chosen set this would not be considered.
- Apply this technique to biomedical areas, for example:
  - HCI - This technique can be used to helping people with Parkinson's disease.
  - Rehabilitation - This technique can provide a way of compare normal movements with disabled movements.

Bibliography

[1] A. K. Jain, R. P. W. Duin, and J. Mao, "Statistical pattern recognition: A review," *Pattern Analysis and Machine Intelligence, IEEE Transactions on*, vol. 22, no. 1, pp. 4–37, 2000.

[2] M. R. Ahsan, M. I. Ibrahimy, and O. O. Khalifa, "Emg signal classification for human computer interaction: a review," *European Journal of Scientific Research*, vol. 33, no. 3, pp. 480–501, 2009.

[3] M. Reaz, M. Hussain, and F. Mohd-Yasin, "Techniques of emg signal analysis: detection, processing, classification and applications," *Biological procedures online*, vol. 8, no. 1, pp. 11–35, 2006.

[4] I. Mesa, A. Rubio, I. Tubia, J. De No, and J. Diaz, "Channel and feature selection for a surface electromyographic pattern recognition task," *Expert Systems with Applications*, vol. 41, no. 11, pp. 5190–5200, 2014.

[5] X. Zhang, X. Chen, Z.-y. Zhao, Y.-q. Tu, J.-h. Yang, V. Lantz, and K.-q. Wang, "Research on gesture definition and electrode placement in pattern recognition of hand gesture action semg," in *Medical Biometrics*. Springer, 2007, pp. 33–40.

[6] X. Chen, X. Zhang, Z.-Y. Zhao, J.-H. Yang, V. Lantz, and K.-Q. Wang, "Multiple hand gesture recognition based on surface emg signal," in *Bioinformatics and Biomedical Engineering, 2007. ICBBE 2007. The 1st International Conference on*. IEEE, 2007, pp. 506–509.

[7] J. Kim, S. Mastnik, and E. André, "Emg-based hand gesture recognition for realtime biosignal interfacing," in *Proceedings of the 13th international conference on Intelligent user interfaces*. ACM, 2008, pp. 30–39.

[8] X. Chen, X. Zhang, Z.-Y. Zhao, J.-H. Yang, V. Lantz, and K.-Q. Wang, "Hand gesture recognition research based on surface emg sensors and 2d-accelerometers," in *Wearable Computers, 2007 11th IEEE International Symposium on*. IEEE, 2007, pp. 11–14.

[9] X. Zhang, X. Chen, W.-h. Wang, J.-h. Yang, V. Lantz, and K.-q. Wang, "Hand gesture recognition and virtual game control based on 3d accelerometer and emg sensors," in *Proceedings of the 14th international conference on Intelligent user interfaces*. ACM, 2009, pp. 401–406.

[10] C. L. VanPutte, J. Regan, and A. Russo, *Seeley's Anatomy & Physiology*. McGraw-Hill, 2014.

[11] J. Hamill and K. M. Knutzen, *Biomechanical basis of human movement*. Lippincott Williams & Wilkins, 2006.

[12] T. Moritani, D. Stegeman, and R. Merletti, "Basic physiology and biophysics of emg signal generation," *Electromyography Physiology Engineering and Noninvasive Applications*, pp. 1–20, 2004.

[13] M. Wehner, "Man to machine, applications in electromyography," *EMG Methods for Evaluating Muscle and Nerve Function. Intech Publishing, retrieved January*, vol. 22, p. 2012, 2012.

[14] F. H. Netter and S. Colacino, *Atlas of human anatomy*. Ciba-Geigy Corporation, 1989.

[15] R. D. Vatavu and S. G. Pentiuc, "Multi-level representation of gesture as command for human computer interaction," *Computing and Informatics*, vol. 27, no. 6, pp. 837–851, 2012.

[16] M. Karam *et al.*, "A taxonomy of gestures in human computer interactions," 2005.

[17] S.-C. Wang, "Artificial neural network," in *Interdisciplinary Computing in Java Programming*. Springer, 2003, pp. 81–100.

[18] L. J. Hargrove, K. Englehart, and B. Hudgins, "A comparison of surface and intramuscular myoelectric signal classification," *Biomedical Engineering, IEEE Transactions on*, vol. 54, no. 5, pp. 847–853, 2007.

[19] J. Yang, E.-S. Choi, W. Chang, W.-C. Bang, S.-J. Cho, J.-K. Oh, J.-K. Cho, and D.-Y. Kim, "A novel hand gesture input device based on inertial sensing technique," in *Industrial Electronics Society, 2004. IECON 2004. 30th Annual Conference of IEEE*, vol. 3. IEEE, 2004, pp. 2786–2791.

[20] H. J. Luinge, P. H. Veltink, and C. T. Baten, "Ambulatory measurement of arm orientation," *Journal of biomechanics*, vol. 40, no. 1, pp. 78–85, 2007.

[21] L. Salhuana, "Tilt sensing using linear accelerometers," *Appl. note AN3461*, 2012.

[22] S. Nasiri, S.-H. Lin, D. Sachs, and J. Jiang, "Motion processing: the next breakthrough function in handsets," *InvenSense Inc., July 2009*, 2010.

[23] W. Y. Wong, M. S. Wong, and K. H. Lo, "Clinical applications of sensors for human posture and movement analysis: a review," *Prosthetics and orthotics international*, vol. 31, no. 1, pp. 62–75, 2007.

[24] E. Clancy, E. L. Morin, and R. Merletti, "Sampling, noise-reduction and amplitude estimation issues in surface electromyography," *Journal of Electromyography and Kinesiology*, vol. 12, no. 1, pp. 1–16, 2002.

[25] S. Conforto, T. D'Alessio, and S. Pignatelli, "Optimal rejection of movement artefacts from myoelectric signals by means of a wavelet filtering procedure," *Journal of Electromyography and Kinesiology*, vol. 9, no. 1, pp. 47–57, 1999.

[26] J.-U. Chu, I. Moon, Y.-J. Lee, S.-K. Kim, and M.-S. Mun, "A supervised feature-projection-based real-time emg pattern recognition for multifunction myoelectric hand control," *Mechatronics, IEEE/ASME Transactions on*, vol. 12, no. 3, pp. 282–290, 2007.

[27] D. Figo, P. C. Diniz, D. R. Ferreira, and J. M. Cardoso, "Preprocessing techniques for context recognition from accelerometer data," *Personal and Ubiquitous Computing*, vol. 14, no. 7, pp. 645–662, 2010.

[28] S. Solnik, P. Rider, K. Steinweg, P. DeVita, and T. Hortobágyi, "Teager–kaiser energy operator signal conditioning improves emg onset detection," *European journal of applied physiology*, vol. 110, no. 3, pp. 489–498, 2010.

[29] G. Staude and W. Wolf, "Objective motor response onset detection in surface myoelectric signals," *Medical Engineering & Physics*, vol. 21, no. 6, pp. 449–467, 1999.

[30] F. Riillo, L. Quitadamo, F. Cavrini, E. Gruppioni, C. Pinto, N. C. Pastò, L. Sbernini, L. Albero, and G. Saggio, "Optimization of emg-based hand gesture recognition: Supervised vs. unsupervised data preprocessing on healthy subjects and transradial amputees," *Biomedical Signal Processing and Control*, vol. 14, pp. 117–125, 2014.

[31] S. R. Safavian and D. Landgrebe, "A survey of decision tree classifier methodology," *IEEE transactions on systems, man, and cybernetics*, vol. 21, no. 3, pp. 660–674, 1991.

[32] N. F. Güler and S. Koçer, "Classification of emg signals using pca and fft," *Journal of Medical Systems*, vol. 29, no. 3, pp. 241–250, 2005.

[33] D. Zhang, A. Xiong, X. Zhao, and J. Han, "Pca and lda for emg-based control of bionic mechanical hand," in *Information and Automation (ICIA), 2012 International Conference on*. IEEE, 2012, pp. 960–965.

Appendix A

Measuring Features

Table A.1: Mean and standard deviation of each feature measured for each recorded signal of the BITalino + LG G Watch system.

		EMG signal		
Feature	CH1	CH2	CH3	Ch4
Auto-regressive coefficient 1^{st} order	0.687 ± 0.136	0.675 ± 0.130	0.704 ± 0.11	0.689 ± 0.105
Auto-regressive coefficient 2^{nd} order	0.586 ± 0.179	0.439 ± 0.164	0.651 ± 0.166	0.616 ± 0.138
Auto-regressive coefficient 3^{rd} order	0.558 ± 0.179	0.428 ± 0.180	0.612 ± 0.164	0.595 ± 0.142
Auto-regressive coefficient 4^{th} order	0.544 ± 0.176	0.397 ± 0.176	0.589 ± 0.161	0.597 ± 0.143
Mean absolute value	0.512 ± 0.036	0.377 ± 0.037	0.532 ± 0.064	0.531 ± 0.081
Mean frequency	0.487 ± 0.175	0.643 ± 0.150	0.362 ± 0.165	0.421 ± 0.130
Variance of central frequency	0.240 ± 0.146	0.282 ± 0.162	0.317 ± 0.178	0.278 ± 0.155
Mean absolute difference value	0.130 ± 0.152	0.080 ± 0.135	0.175 ± 0.189	0.239 ± 0.177
Zero crossing	0.351 ± 0.172	0.293 ± 0.140	0.239 ± 0.118	0.252 ± 0.132
Duration		0.298 ± 0.152		
		Gravity signal		
Feature	X-axis	Y-axis	Z-axis	
Mean	0.001 ± 0.024	0.999 ± 0.024	0.782 ± 0.236	
Standard deviation	0.001 ± 0.024	0.001 ± 0.024	0.089 ± 0.124	
Maximum value	0.001 ± 0.024	0.001 ± 0.024	0.567 ± 0.197	
Minimum value	0.999 ± 0.024	0.999 ± 0.024	0.800 ± 0.208	
Zero crossing	0.041 ± 0.106	0.044 ± 0.106	0.048 ± 0.153	
Mean absolute difference value	0.001 ± 0.024	0.001 ± 0.024	0.079 ± 0.110	
Fundamental frequency	0 ± 0	0 ± 0	0 ± 0	
Spectral energy	0.001 ± 0.024	0.001 ± 0.024	0.021 ± 0.061	
		Linear acceleration signal		
Feature	X-axis	Y-axis	Z-axis	
Mean	0.999 ± 0.024	0.001 ± 0.024	0.454 ± 0.053	
Standard deviation	0.001 ± 0.024	0.001 ± 0.024	0.134 ± 0.157	
Maximum value	0.001 ± 0.024	0.001 ± 0.024	0.144 ± 0.172	
Minimum value	0.999 ± 0.024	0.999 ± 0.024	0.872 ± 0.188	
Zero crossing	0.362 ± 0.180	0.333 ± 0.168	0.259 ± 0.166	
Mean absolute difference value	0.001 ± 0.024	0.001 ± 0.024	0.096 ± 0.116	
Fundamental frequency	0.351 ± 0.301	0.327 ± 0.300	0.311 ± 0.298	
Spectral energy	0.001 ± 0.024	0.001 ± 0.024	0.042 ± 0.088	
		Gyr signal		
Feature	X-axis	Y-axis	Z-axis	
Mean	0.997 ± 0.024	0.028 ± 0.023	0.999 ± 0.024	
Standard deviation	0.001 ± 0.024	0.001 ± 0.024	0.001 ± 0.024	
Maximum value	0.001 ± 0.024	0.001 ± 0.024	0.001 ± 0.024	
Minimum value	0.999 ± 0.024	0.999 ± 0.024	0.999 ± 0.024	
Zero crossing	0.065 ± 0.070	0.091 ± 0.083	0.054 ± 0.073	
Mean absolute difference value	0.001 ± 0.024	0.001 ± 0.024	0.001 ± 0.024	
Fundamental frequency	0.217 ± 0.288	0.265 ± 0.276	0.267 ± 0.272	
Spectral energy	0.001 ± 0.024	0.001 ± 0.024	0.001 ± 0.024	

Table A.2: Mean and standard deviation of each feature measured for each recorded signal of the Myo gesture control armband system.

EMG signal							
feature	CH1	CH2	CH3	Ch4	Ch5	Ch6	Ch7
Auto-regressive coefficient 1^{st} order	0.483 ± 0.124	0.472 ± 0.130	0.469 ± 0.126	0.432 ± 0.142	0.467 ± 0.152	0.351 ± 0.116	0.482 ± 0.143
Auto-regressive coefficient 2^{nd} order	0.472 ± 0.112	0.492 ± 0.119	0.492 ± 0.115	0.458 ± 0.146	0.457 ± 0.133	0.342 ± 0.108	0.474 ± 0.129
Auto-regressive coefficient 3^{rd} order	0.418 ± 0.100	0.519 ± 0.123	0.516 ± 0.111	0.364 ± 0.126	0.428 ± 0.121	0.351 ± 0.107	0.411 ± 0.116
Auto-regressive coefficient 4^{th} order	0.403 ± 0.098	0.551 ± 0.130	0.503 ± 0.102	0.362 ± 0.118	0.424 ± 0.118	0.358 ± 0.113	0.413 ± 0.116
Mean absolute value	0.524 ± 0.081	0.345 ± 0.057	0.436 ± 0.091	0.514 ± 0.070	0.467 ± 0.084	0.490 ± 0.067	0.590 ± 0.061
Mean frequency	0.484 ± 0.099	0.446 ± 0.111	0.479 ± 0.105	0.560 ± 0.132	0.520 ± 0.130	0.689 ± 0.098	0.503 ± 0.124
Variance of central frequency	0.055 ± 0.117	0.079 ± 0.122	0.102 ± 0.155	0.099 ± 0.125	0.095 ± 0.148	0.085 ± 0.122	0.033 ± 0.068
Mean absolute difference value	0.211 ± 0.182	0.283 ± 0.207	0.344 ± 0.245	0.401 ± 0.199	0.448 ± 0.225	0.438 ± 0.189	0.409 ± 0.167
Zero crossing	0.295 ± 0.140	0.272 ± 0.135	0.297 ± 0.130	0.279 ± 0.139	0.272 ± 0.129	0.295 ± 0.138	0.296 ± 0.135
Duration	0.276 ± 0.135						

Gravity signal			
Feature	X-axis	Y-axis	Z-axis
Mean	0.528 ± 0.171	0.474 ± 0.199	0.775 ± 0.169
Standard deviation	0.106 ± 0.167	0.066 ± 0.110	0.086 ± 0.149
Maximum value	0.528 ± 0.168	0.473 ± 0.199	0.781 ± 0.164
Minimum value	0.553 ± 0.169	0.474 ± 0.200	0.774 ± 0.176
Zero crossing	0.296 ± 0.135	0.056 ± 0.230	0.007 ± 0.082
Mean absolute difference value	0.409 ± 0.167	0.128 ± 0.201	0.085 ± 0.137
Fundamental frequency	0 ± 0	0 ± 0	0 ± 0
Spectral energy	0.026 ± 0.080	0.014 ± 0.064	0.020 ± 0.071

Linear aceleration signal			
Feature	X-axis	Y-axis	Z-axis
Mean	0.603 ± 0.086	0.391 ± 0.081	0.537 ± 0.082
Standard deviation	0.128 ± 0.168	0.136 ± 0.146	0.078 ± 0.098
Maximum value	0.332 ± 0.108	0.169 ± 0.134	0.139 ± 0.124
Minimum value	0.852 ± 0.090	0.872 ± 0.113	0.858 ± 0.100
Zero crossing	0 ± 0	0.148 ± 0.158	0.195 ± 0.140
Mean absolute difference value	0.107 ± 0.183	0.080 ± 0.099	0.147 ± 0.132
Fundamental frequency	0.134 ± 0.254	0.134 ± 0.266	0.126 ± 0.247
Spectral energy	0.063 ± 0.139	0.054 ± 0.115	0.019 ± 0.057

Gyr Signal			
Feature	X-axis	Y-axis	Z-axis
Mean	0.480 ± 0.091	0.570 ± 0.090	0.422 ± 0.085
Standard deviation	0.087 ± 0.098	0.110 ± 0.163	0.079 ± 0.149
Maximum value	0.169 ± 0.133	0.210 ± 0.156	0.087 ± 0.115
Minimum value	0.841 ± 0.119	0.903 ± 0.139	0.929 ± 0.118
Zero crossing	0.196 ± 0.163	0.348 ± 0.186	0.350 ± 0.191
Mean absolute difference value	0.089 ± 0.095	0.096 ± 0.114	0.094 ± 0.135
Fundamental frequency	0.001 ± 0.025	0 ± 0	0.001 ± 0.025
Spectral energy	0.277 ± 0.151	0.277 ± 0.151	0.277 ± 0.151

Appendix B

Metrics and confusion matrix

PCA and Decision Tree for BITalino + LG G Watch system

Table B.1: Confusion matrix for PCA and Decision Tree for BITalino + LG G Watch system.

		Class predicted											
		HC	HE	WE	WF	UAF	TI	TM	UH	DH	snap	WA	UALR
Class real	HC	68	31	20	7	11	27	28	34	28	6	24	4
	HE	0	0	0	0	0	0	0	1	0	0	0	0
	WE	0	0	67	3	5	0	0	0	0	0	5	9
	WF	1	2	2	107	1	0	1	0	1	2	1	1
	UAF	3	0	9	1	73	0	0	3	1	2	2	9
	TI	0	0	0	0	0	0	1	0	0	0	0	0
	TM	2	0	0	0	0	2	0	0	0	0	0	0
	UH	92	127	31	13	30	112	111	128	56	17	55	1
	DH	2	0	14	6	1	2	0	2	60	0	36	4
	snap	0	1	1	3	1	0	2	0	0	107	3	1
	WA	0	2	2	0	2	1	0	0	0	2	11	7
	UALR	0	0	18	0	8	0	0	1	0	4	7	107

Table B.2: Calculated metrics for PCA and Decision Tree for BITalino + LG G Watch system.

		Gesture												
		HC	HE	WE	WF	UAF	TI	TM	UH	DH	snap	WA	UALR	Mean
Metrics	TP	68	0	67	107	73	0	0	128	60	107	11	107	
	TN	660	728	661	621	655	728	728	600	668	621	717	621	
	FP	220	1	22	12	30	1	4	645	67	12	16	38	
	FN	100	163	97	33	59	144	143	41	86	33	133	36	
	Sensitivity	40,48%	0,00%	40,85%	76,43%	55,30%	0,00%	0,00%	75,74%	41,10%	76,43%	7,64%	74,83%	40,73%
	Specificity	75,00%	99,86%	96,78%	98,10%	95,62%	99,86%	99,45%	48,19%	90,88%	98,10%	97,82%	94,23%	91,16%
	Precision	23,61%	0,00%	75,28%	89,92%	70,87%	0,00%	0,00%	16,56%	47,24%	89,92%	40,74%	73,79%	43,99%
	Negative predictive value	86,84%	81,71%	87,20%	94,95%	91,74%	83,49%	83,58%	93,60%	88,59%	94,95%	84,35%	94,52%	88,79%
	accuracy	69,47%	81,61%	85,95%	94,18%	89,11%	83,39%	83,20%	51,49%	82,63%	94,18%	83,01%	90,77%	82,42%
	F1 scope	29,82%	0,00%	52,96%	82,63%	62,13%	0,00%	0,00%	27,18%	43,96%	82,63%	12,87%	74,31%	39,04%

PCA and k-NN for BITalino + LG G Watch system

Table B.3: Confusion matrix for PCA and k-NN for BITalino + LG G Watch system

		Class predicted											
		HC	HE	WE	WF	UAF	TI	TM	UH	DH	snap	WA	UALR
Class real	HC	145	7	0	0	0	13	13	4	7	4	1	0
	HE	6	129	2	0	8	21	3	16	1	0	0	0
	WE	0	0	155	1	0	0	0	4	0	0	7	4
	WF	0	0	0	134	0	0	0	0	0	0	0	0
	UAF	0	1	0	0	121	1	0	5	0	0	0	3
	TI	6	12	0	0	0	99	9	3	1	0	3	0
	TM	11	3	0	0	0	4	116	0	0	1	2	0
	UH	0	11	4	0	3	3	2	136	1	0	1	0
	DH	0	0	0	1	0	2	0	0	134	0	0	0
	snap	0	0	0	0	0	0	0	0	0	134	0	0
	WA	0	0	3	3	0	1	0	1	2	1	129	3
	UALR	0	0	0	1	0	0	0	0	0	0	1	133

Table B.4: Calculated metrics for PCA and k-NN for BITalino + LG G Watch system.

		Gesture												
		HC	HE	WE	WF	UAF	TI	TM	UH	DH	snap	WA	UALR	Mean
Metrics	TP	145	129	155	134	121	99	116	136	134	134	129	133	
	TN	1420	1436	1410	1431	1444	1466	1449	1429	1431	1431	1436	1432	
	FP	49	57	16	0	10	34	21	25	3	0	14	2	
	FN	23	34	9	6	11	45	27	33	12	6	15	10	
	Sensitivity	86,31%	79,14%	94,51%	95,71%	91,67%	68,75%	81,12%	80,47%	91,78%	95,71%	89,58%	93,01%	87,31%
	Specificity	96,66%	96,18%	98,88%	100,00%	99,31%	97,73%	98,57%	98,28%	99,79%	100,00%	99,03%	99,86%	98,69%
	Precision	74,74%	69,35%	90,64%	100,00%	92,37%	74,44%	84,67%	84,47%	97,81%	100,00%	90,21%	98,52%	88,10%
	Negative predictive value	98,41%	97,69%	99,37%	99,58%	99,24%	97,02%	98,17%	97,74%	99,17%	99,58%	98,97%	99,31%	98,69%
	accuracy	95,60%	94,50%	98,43%	99,62%	98,68%	95,19%	97,02%	96,43%	99,05%	99,62%	98,18%	99,24%	97,63%
	F1 scope	80,11%	73,93%	92,54%	97,81%	92,02%	71,48%	82,86%	82,42%	94,70%	97,81%	89,90%	95,68%	87,60%

PCA and LDA for BITalino + LG G Watch system

Table B.5: Confusion matrix for PCA and LDA for BITalino + LG G Watch system

		Class predicted											
		HC	HE	WE	WF	UAF	TI	TM	UH	DH	snap	WA	UALR
Class real	HC	110	1	0	1	0	5	1	0	10	9	0	0
	HE	13	120	5	0	8	11	0	22	0	0	0	2
	WE	0	0	142	3	0	0	0	0	0	0	4	8
	WF	0	0	0	123	0	0	0	0	0	0	5	1
	UAF	1	0	0	0	111	0	0	2	0	0	1	4
	TI	10	18	0	0	1	110	5	7	0	0	4	0
	TM	27	8	0	0	0	12	135	1	2	7	3	0
	UH	6	16	5	0	6	1	1	136	0	0	1	0
	DH	0	0	0	2	0	0	0	1	133	0	0	0
	snap	0	0	0	0	0	0	0	0	0	117	0	7
	WA	1	0	10	10	0	5	1	0	1	7	123	13
	UALR	0	0	2	1	6	0	0	0	0	0	3	108

Table B.6: Calculated metrics for PCA and LDA for BITalino + LG G Watch system.

		Gesture												
		HC	HE	WE	WF	UAF	TI	TM	UH	DH	snap	WA	UALR	Mean
Metrics	TP	110	120	142	123	111	110	135	136	133	117	123	108	
	TN	1358	1348	1326	1345	1357	1358	1333	1332	1335	1351	1345	1360	
	FP	27	61	15	6	8	45	60	36	3	7	48	12	
	FN	58	43	22	17	21	34	8	33	13	23	21	35	
	Sensitivity	65,48%	73,62%	86,59%	87,86%	84,09%	76,39%	94,41%	80,47%	91,10%	83,57%	85,42%	75,52%	82,04%
	Specificity	98,05%	95,67%	98,88%	99,56%	99,41%	96,79%	95,69%	97,37%	99,78%	99,48%	96,55%	99,13%	98,03%
	Precision	80,29%	66,30%	90,45%	95,35%	93,28%	70,97%	69,23%	79,07%	97,79%	94,35%	71,93%	90,00%	83,25%
	Negative predictive value	95,90%	96,91%	98,37%	98,75%	98,48%	97,56%	99,40%	97,58%	99,04%	98,33%	98,46%	97,49%	98,02%
	accuracy	94,53%	93,38%	97,54%	98,46%	98,06%	94,89%	95,57%	95,51%	98,92%	98,00%	95,51%	96,90%	96,44%
	F1 scope	72,13%	69,77%	88,47%	91,45%	88,45%	73,58%	79,88%	79,77%	94,33%	88,64%	78,10%	82,13%	82,22%

PCA and Naïve Bayes for BITalino + LG G Watch system

Table B.7: Confusion matrix for PCA and Naïve Bayes for BITalino + LG G Watch system

		Class predicted											
		HC	HE	WE	WF	UAF	TI	TM	UH	DH	snap	WA	UALR
Class real	HC	122	2	0	1	0	6	3	1	5	9	0	0
	HE	1	120	3	0	5	15	0	21	0	0	0	0
	WE	0	3	136	0	0	0	0	0	0	0	2	3
	WF	1	0	1	134	0	1	1	0	0	0	10	1
	UAF	1	0	1	0	120	2	0	3	0	0	0	8
	TI	12	13	0	0	0	112	8	4	0	0	4	0
	TM	28	12	0	0	0	7	129	0	0	2	1	0
	UH	2	12	1	0	3	1	1	139	0	0	0	0
	DH	1	0	0	1	0	0	0	1	139	0	0	0
	snap	0	0	0	0	0	0	0	0	0	124	0	0
	WA	0	0	20	3	0	0	1	0	2	3	124	9
	UALR	0	1	2	1	4	0	0	0	0	2	3	122

Table B.8: Calculated metrics for PCA and Naïve Bayes for BITalino + LG G Watch system.

		Gesture												
		HC	HE	WE	WF	UAF	TI	TM	UH	DH	snap	WA	UALR	Mean
Metrics	TP	122	120	136	134	120	112	129	139	139	124	124	122	
	TN	1399	1401	1385	1387	1401	1409	1392	1382	1382	1397	1397	1399	
	FP	27	45	8	15	15	41	50	20	3	0	38	13	
	FN	46	43	28	6	12	32	14	30	7	16	20	21	
	Sensitivity	72,62%	73,62%	82,93%	95,71%	90,91%	77,78%	90,21%	82,25%	95,21%	88,57%	86,11%	85,31%	85,10%
	Specificity	98,11%	96,89%	99,43%	98,93%	98,94%	97,17%	96,53%	98,57%	99,78%	100,00%	97,35%	99,08%	98,40%
	Precision	81,88%	72,73%	94,44%	89,93%	88,89%	73,20%	72,07%	87,42%	97,89%	100,00%	76,54%	90,37%	85,45%
	Negative predictive value	96,82%	97,02%	98,02%	99,57%	99,15%	97,78%	99,00%	97,88%	99,50%	98,87%	98,59%	98,52%	98,39%
	accuracy	95,42%	94,53%	97,69%	98,64%	98,26%	95,42%	95,96%	96,82%	99,35%	98,96%	96,33%	97,81%	97,10%
	F1 scope	76,97%	73,17%	88,31%	92,73%	89,89%	75,42%	80,12%	84,76%	96,53%	93,94%	81,05%	87,77%	85,05%

PCA and ANN for BITalino + LG G Watch system

Table B.9: Confusion matrix for PCA and ANN for BITalino + LG G Watch system

		Class predicted											
		HC	HE	WE	WF	UAF	TI	TM	UH	DH	snap	WA	UALR
Class real	HC	166	0	0	0	0	0	2	0	0	0	0	0
	HE	0	156	0	0	0	3	0	14	0	0	0	0
	WE	0	0	163	0	0	1	1	0	0	0	0	0
	WF	0	0	0	135	0	0	0	0	0	0	1	0
	UAF	0	0	0	0	132	0	0	1	0	0	1	0
	TI	1	4	0	0	0	130	6	1	0	0	0	0
	TM	1	0	0	0	0	7	132	0	0	1	0	0
	UH	0	3	0	0	0	3	1	153	0	0	0	0
	DH	0	0	0	1	0	0	0	0	146	1	0	0
	snap	0	0	0	1	0	0	0	0	0	138	0	0
	WA	0	0	1	2	0	0	1	0	0	0	140	1
	UALR	0	0	0	1	0	0	0	0	0	0	2	142

Table B.10: Calculated metrics for PCA and ANN for BITalino + LG G Watch system.

		Gesture												
		HC	HE	WE	WF	UAF	TI	TM	UH	DH	snap	WA	UALR	Mean
Metrics	TP	166	156	163	135	132	130	132	153	146	138	140	142	
	TN	1567	1577	1570	1598	1601	1603	1601	1580	1587	1595	1593	1591	
	FP	2	17	2	1	2	12	9	7	2	1	5	3	
	FN	2	7	1	5	0	14	11	16	0	2	4	1	
	Sensitivity	98,81%	95,71%	99,39%	96,43%	100,00%	90,28%	92,31%	90,53%	100,00%	98,57%	97,22%	99,30%	96,55%
	Specificity	99,87%	98,93%	99,87%	99,94%	99,88%	99,26%	99,44%	99,56%	99,87%	99,94%	99,69%	99,81%	99,67%
	Precision	98,81%	90,17%	98,79%	99,26%	98,51%	91,55%	93,62%	95,63%	98,65%	99,28%	96,55%	97,93%	96,56%
	Negative predictive value	99,87%	99,56%	99,94%	99,69%	100,00%	99,13%	99,32%	99,00%	100,00%	99,87%	99,75%	99,94%	99,67%
	accuracy	99,77%	98,63%	99,83%	99,65%	99,88%	98,52%	98,86%	98,69%	99,88%	99,83%	99,48%	99,77%	99,40%
	F1 scope	98,81%	92,86%	99,09%	97,83%	99,25%	90,91%	92,96%	93,01%	99,32%	98,92%	96,89%	98,61%	96,54%

SBS and Decision Tree for BITalino + LG G Watch system

Table B.11: Confusion matrix for SBS and Decision Tree for BITalino + LG G Watch system

		Class predicted											
		HC	HE	WE	WF	UAF	TI	TM	UH	DH	snap	WA	UALR
Class real	HC	158	3	0	0	0	2	1	0	3	0	0	0
	HE	2	126	0	0	1	14	2	17	0	0	1	0
	WE	0	0	161	0	0	1	1	1	0	4	111	52
	WF	0	0	0	136	0	0	0	0	0	2	14	1
	UAF	0	1	0	0	125	1	1	4	0	0	0	8
	TI	3	7	0	0	0	105	6	4	0	1	0	0
	TM	4	1	0	0	0	5	131	2	2	2	0	0
	UH	0	25	1	0	4	13	1	141	1	0	0	0
	DH	1	0	0	1	0	3	0	0	139	4	0	0
	snap	0	0	0	1	0	0	0	0	1	126	0	1
	WA	0	0	2	2	0	0	0	0	0	0	17	1
	UALR	0	0	0	0	2	0	0	0	0	1	1	80

Table B.12: Calculated metrics for SBS and Decision Tree for BITalino + LG G Watch system.

		Gesture												
		HC	HE	WE	WF	UAF	TI	TM	UH	DH	snap	WA	UALR	Mean
Metrics	TP	158	126	161	136	125	105	131	141	139	126	17	80	
	TN	1287	1319	1284	1309	1320	1340	1314	1304	1306	1319	1428	1365	
	FP	9	37	170	17	15	21	16	45	9	3	5	4	
	FN	10	37	3	4	7	39	12	28	7	14	127	63	
	Sensitivity	94,05%	77,30%	98,17%	97,14%	94,70%	72,92%	91,61%	83,43%	95,21%	90,00%	11,81%	55,94%	80,19%
	Specificity	99,31%	97,27%	88,31%	98,72%	98,88%	98,46%	98,80%	96,66%	99,32%	99,77%	99,65%	99,71%	97,90%
	Precision	94,61%	77,30%	48,64%	88,89%	89,29%	83,33%	89,12%	75,81%	93,92%	97,67%	77,27%	95,24%	84,26%
	Negative predictive value	99,23%	97,27%	99,77%	99,70%	99,47%	97,17%	99,10%	97,90%	99,47%	98,95%	91,83%	95,59%	97,95%
	accuracy	98,70%	95,13%	89,31%	98,57%	98,50%	96,01%	98,10%	95,19%	98,90%	98,84%	91,63%	95,57%	96,20%
	F1 scope	94,33%	77,30%	65,05%	92,83%	91,91%	77,78%	90,34%	79,44%	94,56%	93,68%	20,48%	70,48%	79,02%

SBS and k-NN for BITalino + LG G Watch system

Table B.13: Confusion matrix for SBS and k-NN for BITalino + LG G Watch system

		Class predicted											
		HC	HE	WE	WF	UAF	TI	TM	UH	DH	snap	WA	UALR
Class real	HC	168	0	0	0	0	0	0	0	0	0	0	0
	HE	0	157	0	0	0	2	0	0	0	0	0	0
	WE	0	0	162	0	0	0	0	0	0	0	5	0
	WF	0	0	0	139	0	0	0	0	0	1	0	0
	UAF	0	0	0	0	132	0	0	1	0	0	0	0
	TI	0	2	0	0	0	141	1	0	0	0	0	0
	TM	0	0	0	0	0	1	142	0	0	1	0	0
	UH	0	4	1	0	0	0	0	168	0	0	0	0
	DH	0	0	0	1	0	0	0	0	146	1	0	0
	snap	0	0	0	0	0	0	0	0	0	137	0	0
	WA	0	0	1	0	0	0	0	0	0	0	139	1
	UALR	0	0	0	0	0	0	0	0	0	0	0	142

Table B.14: Calculated metrics for SBS and k-NN for BITalino + LG G Watch system.

		Gesture												
		HC	HE	WE	WF	UAF	TI	TM	UH	DH	snap	WA	UALR	Mean
Metrics	TP	168	157	162	139	132	141	142	168	146	137	139	142	
	TN	1605	1616	1611	1634	1641	1632	1631	1605	1627	1636	1634	1631	
	FP	0	2	5	1	1	3	2	5	2	0	2	0	
	FN	0	6	2	1	0	3	1	1	0	3	5	1	
	Sensitivity	100,00%	96,32%	98,78%	99,29%	100,00%	97,92%	99,30%	99,41%	100,00%	97,86%	96,53%	99,30%	98,72%
	Specificity	100,00%	99,88%	99,69%	99,94%	99,94%	99,82%	99,88%	99,69%	99,88%	100,00%	99,88%	100,00%	99,88%
	Precision	100,00%	98,74%	97,01%	99,29%	99,25%	97,92%	98,61%	97,11%	98,65%	100,00%	98,58%	100,00%	98,76%
	Negative predictive value	100,00%	99,63%	99,88%	99,94%	100,00%	99,82%	99,94%	99,94%	100,00%	99,82%	99,69%	99,94%	99,88%
	accuracy	100,00%	99,55%	99,61%	99,89%	99,94%	99,66%	99,83%	99,66%	99,89%	99,83%	99,61%	99,94%	99,78%
	F1 scope	100,00%	97,52%	97,89%	99,29%	99,62%	97,92%	98,95%	98,25%	99,32%	98,92%	97,54%	99,65%	98,74%

SBS and LDA for BITalino + LG G Watch system

Table B.15: Confusion matrix for SBS and LDA for BITalino + LG G Watch system

		Class predicted											
		HC	HE	WE	WF	UAF	TI	TM	UH	DH	snap	WA	UALR
Class real	HC	94	3	0	0	0	0	0	0	1	5	0	0
	HE	9	113	5	0	20	4	7	32	0	0	2	0
	WE	0	0	145	1	0	0	0	0	0	0	5	13
	WF	0	0	0	135	0	0	1	0	0	0	14	0
	UAF	0	0	0	1	96	0	0	0	0	1	0	18
	TI	12	18	0	0	6	123	0	3	24	0	7	0
	TM	30	10	0	0	4	12	135	5	0	15	8	0
	UH	12	19	4	0	6	4	0	129	0	0	1	0
	DH	11	0	0	1	0	0	0	0	121	6	0	0
	snap	0	0	0	0	0	0	0	0	0	110	2	0
	WA	0	0	9	2	0	1	0	0	0	0	104	7
	UALR	0	0	1	0	0	0	0	0	0	3	1	105

Table B.16: Calculated metrics for SBS and LDA for BITalino + LG G Watch system.

		Gesture												
		HC	HE	WE	WF	UAF	TI	TM	UH	DH	snap	WA	UALR	Mean
Metrics	TP	94	113	145	135	96	123	135	129	121	110	104	105	
	TN	1316	1297	1265	1275	1314	1287	1275	1281	1289	1300	1306	1305	
	FP	9	79	19	15	20	70	84	46	18	2	19	5	
	FN	74	50	19	5	36	21	8	40	25	30	40	38	
	Sensitivity	55,95%	69,33%	88,41%	96,43%	72,73%	85,42%	94,41%	76,33%	82,88%	78,57%	72,22%	73,43%	78,84%
	Specificity	99,32%	94,26%	98,52%	98,84%	98,50%	94,84%	93,82%	96,53%	98,62%	99,85%	98,57%	99,62%	97,61%
	Precision	91,26%	58,85%	88,41%	90,00%	82,76%	63,73%	61,64%	73,71%	87,05%	98,21%	84,55%	95,45%	81,30%
	Negative predictive value	94,68%	96,29%	98,52%	99,61%	97,33%	98,39%	99,38%	96,97%	98,10%	97,74%	97,03%	97,17%	97,60%
	accuracy	94,44%	91,62%	97,38%	98,60%	96,18%	93,94%	93,87%	94,25%	97,04%	97,78%	95,98%	97,04%	95,68%
	F1 scope	69,37%	63,66%	88,41%	93,10%	77,42%	73,00%	74,59%	75,00%	84,91%	87,30%	77,90%	83,00%	78,97%

SBS and Naïve Bayes for BITalino + LG G Watch system

Table B.17: Confusion matrix for SBS and Naïve Bayes for BITalino + LG G Watch system

		Class predicted											
		HC	HE	WE	WF	UAF	TI	TM	UH	DH	snap	WA	UALR
Class real	HC	144	1	0	0	0	3	1	0	2	0	0	0
	HE	0	88	0	0	0	3	0	3	0	0	0	0
	WE	0	0	159	0	0	0	0	0	0	0	2	0
	WF	0	0	0	138	0	0	1	0	0	0	14	0
	UAF	0	1	1	0	123	0	0	2	0	0	0	10
	TI	16	35	0	0	0	129	19	6	0	0	0	0
	TM	5	2	0	0	0	6	118	1	0	0	0	0
	UH	0	36	0	0	2	1	0	156	0	0	1	0
	DH	3	0	0	0	0	1	3	0	143	3	0	0
	snap	0	0	0	1	0	0	0	0	1	136	4	0
	WA	0	0	1	0	0	1	1	1	0	0	116	0
	UALR	0	0	3	1	7	0	0	0	0	1	7	133

Table B.18: Calculated metrics for SBS and Naïve Bayes for BITalino + LG G Watch system.

		Gesture												
		HC	HE	WE	WF	UAF	TI	TM	UH	DH	snap	WA	UALR	Mean
Metrics	TP	144	88	159	138	123	129	118	156	143	136	116	133	
	TN	1439	1495	1424	1445	1460	1454	1465	1427	1440	1447	1467	1450	
	FP	7	6	2	15	14	76	14	40	10	6	4	19	
	FN	24	75	5	2	9	15	25	13	3	4	28	10	
	Sensitivity	85,71%	53,99%	96,95%	98,57%	93,18%	89,58%	82,52%	92,31%	97,95%	97,14%	80,56%	93,01%	88,46%
	Specificity	99,52%	99,60%	99,86%	98,97%	99,05%	95,03%	99,05%	97,27%	99,31%	99,59%	99,73%	98,71%	98,81%
	Precision	95,36%	93,62%	98,76%	90,20%	89,78%	62,93%	89,39%	79,59%	93,46%	95,77%	96,67%	87,50%	89,42%
	Negative predictive value	98,36%	95,22%	99,65%	99,86%	99,39%	98,98%	98,32%	99,10%	99,79%	99,72%	98,13%	99,32%	98,82%
	accuracy	98,08%	95,13%	99,56%	98,94%	98,57%	94,56%	97,60%	96,76%	99,19%	99,37%	98,02%	98,20%	97,83%
	F1 scope	90,28%	68,48%	97,85%	94,20%	91,45%	73,93%	85,82%	85,48%	95,65%	96,45%	87,88%	90,17%	88,14%

SBS and ANN for BITalino + LG G Watch system

Table B.19: Confusion matrix for SBS and ANN for BITalino + LG G Watch system

		Class predicted											
		HC	HE	WE	WF	UAF	TI	TM	UH	DH	snap	WA	UALR
Class real	HC	167	0	0	0	0	1	1	0	1	0	0	0
	HE	0	155	0	0	0	4	1	8	0	0	0	0
	WE	0	0	159	0	0	1	0	0	0	0	3	1
	WF	0	0	0	139	0	0	0	0	0	2	0	0
	UAF	0	0	0	0	132	0	0	1	0	0	0	1
	TI	1	2	0	0	0	126	1	0	0	0	1	0
	TM	0	0	0	0	0	10	139	0	0	3	0	0
	UH	0	6	0	0	0	1	0	160	0	0	1	0
	DH	0	0	0	1	0	0	0	0	145	1	0	0
	snap	0	0	0	0	0	0	1	0	0	132	0	0
	WA	0	0	3	0	0	1	0	0	0	2	135	2
	UALR	0	0	2	0	0	0	0	0	0	0	4	139

Table B.20: Calculated metrics for SBS and ANN for BITalino + LG G Watch system.

		Gesture												
		HC	HE	WE	WF	UAF	TI	TM	UH	DH	snap	WA	UALR	Mean
Metrics	TP	167	155	159	139	132	126	139	160	145	132	135	139	
	TN	1561	1573	1569	1589	1596	1602	1589	1568	1583	1596	1593	1589	
	FP	3	13	5	2	2	5	13	8	2	1	8	6	
	FN	1	8	5	1	0	18	4	9	1	8	9	4	
	Sensitivity	99,40%	95,09%	96,95%	99,29%	100,00%	87,50%	97,20%	94,67%	99,32%	94,29%	93,75%	97,20%	96,22%
	Specificity	99,81%	99,18%	99,68%	99,87%	99,87%	99,69%	99,19%	99,49%	99,87%	99,94%	99,50%	99,62%	99,64%
	Precision	98,24%	92,26%	96,95%	98,58%	98,51%	96,18%	91,45%	95,24%	98,64%	99,25%	94,41%	95,86%	96,30%
	Negative predictive value	99,94%	99,49%	99,68%	99,94%	100,00%	98,89%	99,75%	99,43%	99,94%	99,50%	99,44%	99,75%	99,65%
	accuracy	99,77%	98,80%	99,42%	99,83%	99,88%	98,69%	99,03%	99,03%	99,83%	99,48%	99,03%	99,42%	99,35%
	F1 scope	98,82%	93,66%	96,95%	98,93%	99,25%	91,64%	94,24%	94,96%	98,98%	96,70%	94,08%	96,53%	96,23%

PCA and Decision Tree for Myo gesture control armband

Table B.21: Confusion matrix for PCA and Decision Tree for Myo gesture control armband

		Class predicted											
		HC	HE	WE	WF	UAF	TI	TM	UH	DH	snap	WA	UALR
Class real	HC	61	54	57	35	10	38	30	60	36	20	47	6
	HE	1	0	0	0	0	0	0	0	0	1	1	0
	WE	102	91	108	75	91	68	59	98	66	47	95	35
	WF	0	0	0	7	0	0	0	0	1	0	0	0
	UAF	0	0	1	0	67	0	0	0	0	0	0	6
	TI	0	0	0	1	0	3	3	0	4	0	0	0
	TM	0	0	0	1	0	0	0	0	0	0	0	0
	UH	0	1	0	0	0	0	0	0	0	0	0	0
	DH	0	0	1	1	0	0	0	0	0	0	0	0
	snap	0	0	0	0	1	0	0	0	1	12	1	0
	WA	0	0	0	0	0	1	3	1	1	6	9	1
	UALR	1	0	0	0	0	0	0	2	2	0	2	105

Table B.22: Calculated metrics for PCA and Decision Tree for Myo gesture control armband.

		Gesture												
		HC	HE	WE	WF	UAF	TI	TM	UH	DH	snap	WA	UALR	Mean
Metrics	TP	61	0	108	7	67	3	0	0	0	12	9	105	
	TN	311	372	264	365	305	369	372	372	372	360	363	267	
	FP	393	3	827	1	7	8	1	1	2	3	13	7	
	FN	104	146	59	113	102	107	95	161	111	74	146	48	
	Sensitivity	36,97%	0,00%	64,67%	5,83%	39,64%	2,73%	0,00%	0,00%	0,00%	13,95%	5,81%	68,63%	19,85%
	Specificity	44,18%	99,20%	24,20%	99,73%	97,76%	97,88%	99,73%	99,73%	99,47%	99,17%	96,54%	97,45%	87,92%
	Precision	13,44%	0,00%	11,55%	87,50%	90,54%	27,27%	0,00%	0,00%	0,00%	80,00%	40,91%	93,75%	37,08%
	Negative predictive value	74,94%	71,81%	81,73%	76,36%	74,94%	77,52%	79,66%	69,79%	77,02%	82,95%	71,32%	84,76%	76,90%
	accuracy	42,81%	71,40%	29,57%	76,54%	77,34%	76,39%	79,49%	69,66%	76,70%	82,85%	70,06%	87,12%	69,99%
	F1 scope	19,71%	0,00%	19,60%	10,94%	55,14%	4,96%	0,00%	0,00%	0,00%	23,76%	10,17%	79,25%	18,63%

PCA and k-NN for Myo gesture control armband

Table B.23: Confusion matrix for PCA and k-NN for Myo gesture control armband

		Class predicted											
		HC	HE	WE	WF	UAF	TI	TM	UH	DH	snap	WA	UALR
Class real	HC	155	9	2	3	0	7	2	4	6	1	1	0
	HE	4	96	6	0	0	11	8	20	4	3	8	1
	WE	1	5	143	2	0	2	1	15	0	0	5	3
	WF	0	0	4	104	0	0	3	0	9	0	4	0
	UAF	0	0	0	0	168	0	0	0	0	0	0	0
	TI	3	6	1	0	0	83	29	8	3	4	3	0
	TM	0	1	0	3	0	7	47	0	4	6	2	0
	UH	2	27	11	0	1	0	1	114	0	2	6	0
	DH	0	0	0	6	0	0	1	0	83	1	1	0
	snap	0	0	0	1	0	0	2	0	1	61	1	1
	WA	0	2	0	1	0	0	1	0	1	8	124	2
	UALR	0	0	0	0	0	0	0	0	0	0	0	146

Table B.24: Calculated metrics for PCA and k-NN for Myo gesture control armband.

		Gesture												
		HC	HE	WE	WF	UAF	TI	TM	UH	DH	snap	WA	UALR	Mean
Metrics	TP	155	96	143	104	168	83	47	114	83	61	124	146	
	TN	1169	1228	1181	1220	1156	1241	1277	1210	1241	1263	1200	1178	
	FP	35	65	34	20	0	57	23	50	9	6	15	0	
	FN	10	50	24	16	1	27	48	47	28	25	31	7	
	Sensitivity	93,94%	65,75%	85,63%	86,67%	99,41%	75,45%	49,47%	70,81%	74,77%	70,93%	80,00%	95,42%	79,02%
	Specificity	97,09%	94,97%	97,20%	98,39%	100,00%	95,61%	98,23%	96,03%	99,28%	99,53%	98,77%	100,00%	97,92%
	Precision	81,58%	59,63%	80,79%	83,87%	100,00%	59,29%	67,14%	69,51%	90,22%	91,04%	89,21%	100,00%	81,02%
	Negative predictive value	99,15%	96,09%	98,01%	98,71%	99,91%	97,87%	96,38%	96,26%	97,79%	98,06%	97,48%	99,41%	97,93%
	accuracy	96,71%	92,01%	95,80%	97,35%	99,92%	94,03%	94,91%	93,17%	97,28%	97,71%	96,64%	99,47%	96,25%
	F1 scope	87,32%	62,54%	83,14%	85,25%	99,70%	66,40%	56,97%	70,15%	81,77%	79,74%	84,35%	97,66%	79,58%

PCA and LDA for Myo gesture control armband

Table B.25: Confusion matrix for PCA and LDA for Myo gesture control armband

		Class predicted											
		HC	HE	WE	WF	UAF	TI	TM	UH	DH	snap	WA	UALR
Class real	HC	141	6	0	0	1	0	2	0	8	0	0	1
	HE	7	79	24	0	1	9	3	17	2	1	18	1
	WE	1	7	105	1	3	3	2	11	0	0	4	4
	WF	2	0	0	88	0	0	2	0	14	0	0	0
	UAF	0	0	0	0	163	0	0	0	0	0	0	4
	TI	0	15	16	3	1	63	27	5	4	0	2	0
	TM	1	0	1	7	0	22	47	0	0	4	12	0
	UH	11	28	18	0	0	5	1	118	0	2	5	1
	DH	1	0	0	15	0	1	0	0	79	0	0	1
	snap	0	2	0	0	0	0	0	0	0	57	7	4
	WA	1	9	2	6	0	7	11	8	4	22	106	2
	UALR	0	0	1	0	0	0	0	2	0	0	1	135

Table B.26: Calculated metrics for PCA and LDA for Myo gesture control armband.

		Gesture												
		HC	HE	WE	WF	UAF	TI	TM	UH	DH	snap	WA	UALR	Mean
Metrics	TP	141	79	105	88	163	63	47	118	79	57	106	135	
	TN	1040	1102	1076	1093	1018	1118	1134	1063	1102	1124	1075	1046	
	FP	18	83	36	18	4	73	47	71	18	13	72	4	
	FN	24	67	62	32	6	47	48	43	32	29	49	18	
	Sensitivity	85,45%	54,11%	62,87%	73,33%	96,45%	57,27%	49,47%	73,29%	71,17%	66,28%	68,39%	88,24%	70,53%
	Specificity	98,30%	93,00%	96,76%	98,38%	99,61%	93,87%	96,02%	93,74%	98,39%	98,86%	93,72%	99,62%	96,69%
	Precision	88,68%	48,77%	74,47%	83,02%	97,60%	46,32%	50,00%	62,43%	81,44%	81,43%	59,55%	97,12%	72,57%
	Negative predictive value	97,74%	94,27%	94,55%	97,16%	99,41%	95,97%	95,94%	96,11%	97,18%	97,48%	95,64%	98,31%	96,65%
	accuracy	96,57%	88,73%	92,34%	95,94%	99,16%	90,78%	92,55%	91,20%	95,94%	96,57%	90,71%	98,17%	94,05%
	F1 scope	87,04%	51,30%	68,18%	77,88%	97,02%	51,22%	49,74%	67,43%	75,96%	73,08%	63,66%	92,47%	71,25%

PCA and Naïve Bayes for Myo gesture control armband

Table B.27: Confusion matrix for PCA and Naïve Bayes for Myo gesture control armband

		Class predicted											
		HC	HE	WE	WF	UAF	TI	TM	UH	DH	snap	WA	UALR
Class real	HC	130	9	0	0	1	1	1	1	3	1	0	0
	HE	9	76	23	1	1	4	3	23	3	0	13	0
	WE	1	10	89	2	1	4	4	6	1	0	3	2
	WF	1	0	4	81	0	0	2	0	6	2	0	1
	UAF	0	1	0	0	164	0	0	0	0	0	0	1
	TI	8	19	12	1	0	79	38	11	6	1	4	0
	TM	4	1	1	3	0	18	37	1	0	1	4	0
	UH	5	24	31	0	0	1	1	112	0	0	10	2
	DH	0	0	0	20	0	1	0	0	81	0	0	0
	snap	1	1	0	3	0	0	3	1	6	73	21	1
	WA	2	3	0	6	0	1	4	2	3	5	93	1
	UALR	4	2	7	3	2	1	2	4	2	3	7	145

Table B.28: Calculated metrics for PCA and Naïve Bayes for Myo gesture control armband.

		Gesture												
		HC	HE	WE	WF	UAF	TI	TM	UH	DH	snap	WA	UALR	Mean
Metrics	TP	130	76	89	81	164	79	37	112	81	73	93	145	
	TN	1030	1084	1071	1079	996	1081	1123	1048	1079	1087	1067	1015	
	FP	17	80	34	16	2	100	33	74	21	37	27	37	
	FN	35	70	78	39	5	31	58	49	30	13	62	8	
	Sensitivity	78,79%	52,05%	53,29%	67,50%	97,04%	71,82%	38,95%	69,57%	72,97%	84,88%	60,00%	94,77%	70,14%
	Specificity	98,38%	93,13%	96,92%	98,54%	99,80%	91,53%	97,15%	93,40%	98,09%	96,71%	97,53%	96,48%	96,47%
	Precision	88,44%	48,72%	72,36%	83,51%	98,80%	44,13%	52,86%	60,22%	79,41%	66,36%	77,50%	79,67%	71,00%
	Negative predictive value	96,71%	93,93%	93,21%	96,51%	99,50%	97,21%	95,09%	95,53%	97,29%	98,82%	94,51%	99,22%	96,46%
	accuracy	95,71%	88,55%	91,19%	95,47%	99,40%	89,85%	92,73%	90,41%	95,79%	95,87%	92,87%	96,27%	93,68%
	F1 scope	83,33%	50,33%	61,38%	74,65%	97,91%	54,67%	44,85%	64,55%	76,06%	74,49%	67,64%	86,57%	69,70%

PCA and ANN for Myo gesture control armband

Table B.29: Confusion matrix for PCA and ANN for Myo gesture control armband

		Class predicted											
		HC	HE	WE	WF	UAF	TI	TM	UH	DH	snap	WA	UALR
Class real	HC	157	4	0	0	0	0	0	0	2	2	0	0
	HE	6	124	2	0	0	5	3	4	0	2	1	0
	WE	0	1	155	0	0	1	1	4	0	0	2	0
	WF	0	0	1	112	0	0	4	0	3	0	1	1
	UAF	0	0	0	0	169	1	1	0	0	0	0	2
	TI	0	5	2	0	0	95	18	2	1	0	1	0
	TM	0	2	0	1	0	7	61	0	2	5	2	0
	UH	0	8	4	0	0	0	1	143	0	0	5	0
	DH	2	0	0	6	0	0	1	0	102	1	1	0
	snap	0	1	0	0	0	0	2	1	1	74	2	0
	WA	0	1	1	0	0	1	3	6	0	2	137	3
	UALR	0	0	2	1	0	0	0	1	0	0	3	147

Table B.30: Calculated metrics for PCA and ANN for Myo gesture control armband.

		Gesture												
		HC	HE	WE	WF	UAF	TI	TM	UH	DH	snap	WA	UALR	Mean
Metrics	TP	157	124	155	112	169	95	61	143	102	74	137	147	
	TN	1319	1352	1321	1364	1307	1381	1415	1333	1374	1402	1339	1329	
	FP	8	23	9	10	4	29	19	18	11	7	17	7	
	FN	8	22	12	8	0	15	34	18	9	12	18	6	
	Sensitivity	95,15%	84,93%	92,81%	93,33%	100,00%	86,36%	64,21%	88,82%	91,89%	86,05%	88,39%	96,08%	89,00%
	Specificity	99,40%	98,33%	99,32%	99,27%	99,69%	97,94%	98,68%	98,67%	99,21%	99,50%	98,75%	99,48%	99,02%
	Precision	95,15%	84,35%	94,51%	91,80%	97,69%	76,61%	76,25%	88,82%	90,27%	91,36%	88,96%	95,45%	89,27%
	Negative predictive value	99,40%	98,40%	99,10%	99,42%	100,00%	98,93%	97,65%	98,67%	99,35%	99,15%	98,67%	99,55%	99,02%
	accuracy	98,93%	97,04%	98,60%	98,80%	99,73%	97,11%	96,53%	97,62%	98,66%	98,73%	97,68%	99,13%	98,21%
	F1 scope	95,15%	84,64%	93,66%	92,56%	98,83%	81,20%	69,71%	88,82%	91,07%	88,62%	88,67%	95,77%	89,06%

SBS and Decision Tree for Myo gesture control armband

Table B.31: Confusion matrix for SBS and Decision Tree for Myo gesture control armband

		Class predicted											
		HC	HE	WE	WF	UAF	TI	TM	UH	DH	snap	WA	UALR
Class real	HC	160	103	2	16	0	5	14	4	24	8	0	0
	HE	1	5	1	2	0	2	3	0	0	1	1	0
	WE	1	3	98	4	0	11	7	65	2	12	57	3
	WF	1	4	3	84	0	2	2	0	15	1	2	0
	UAF	0	0	0	1	167	1	1	1	0	0	0	12
	TI	1	19	4	1	0	73	32	6	0	3	0	0
	TM	1	0	1	1	0	3	24	2	1	0	5	1
	UH	0	3	53	2	1	9	6	81	0	9	43	0
	DH	0	2	0	6	0	0	2	0	65	0	0	0
	snap	0	3	0	1	1	2	0	0	3	46	7	1
	WA	0	4	3	2	0	2	3	2	1	6	38	1
	UALR	0	0	2	0	0	0	1	0	0	0	2	135

Table B.32: Calculated metrics for SBS and Decision Tree for Myo gesture control armband.

		Gesture												
		HC	HE	WE	WF	UAF	TI	TM	UH	DH	snap	WA	UALR	Mean
Metrics	TP	160	5	98	84	167	73	24	81	65	46	38	135	
	TN	816	971	878	892	809	903	952	895	911	930	938	841	
	FP	176	11	165	30	16	66	15	126	10	18	24	5	
	FN	5	141	69	36	2	37	71	80	46	40	117	18	
	Sensitivity	96,97%	3,42%	58,68%	70,00%	98,82%	66,36%	25,26%	50,31%	58,56%	53,49%	24,52%	88,24%	57,89%
	Specificity	82,26%	98,88%	84,18%	96,75%	98,06%	93,19%	98,45%	87,66%	98,91%	98,10%	97,51%	99,41%	94,45%
	Precision	47,62%	31,25%	37,26%	73,68%	91,26%	52,52%	61,54%	39,13%	86,67%	71,88%	61,29%	96,43%	62,54%
	Negative predictive value	99,39%	87,32%	92,71%	96,12%	99,75%	96,06%	93,06%	91,79%	95,19%	95,88%	88,91%	97,90%	94,51%
	accuracy	84,36%	86,52%	80,66%	93,67%	98,19%	90,45%	91,90%	82,57%	94,57%	94,39%	87,38%	97,70%	90,20%
	F1 scope	63,87%	6,17%	45,58%	71,79%	94,89%	58,63%	35,82%	44,02%	69,89%	61,33%	35,02%	92,15%	56,60%

SBS and k-NN for Myo gesture control armband

Table B.33: Confusion matrix for SBS and k-NN for Myo gesture control armband

		Class predicted											
		HC	HE	WE	WF	UAF	TI	TM	UH	DH	snap	WA	UALR
Class real	HC	163	5	0	0	0	1	4	0	4	1	0	0
	HE	0	132	0	1	0	3	2	3	0	0	0	0
	WE	0	1	159	1	1	0	0	4	0	1	6	1
	WF	1	1	1	112	0	0	1	0	1	1	1	0
	UAF	0	0	0	1	168	1	0	0	0	0	0	0
	TI	0	4	0	1	0	101	11	2	0	4	0	0
	TM	1	0	0	2	0	3	74	1	0	3	1	0
	UH	0	2	3	0	0	1	1	147	0	0	0	0
	DH	0	0	0	2	0	0	1	0	104	3	0	0
	snap	0	0	0	0	0	0	1	0	2	73	0	0
	WA	0	1	3	0	0	0	0	4	0	0	146	2
	UALR	0	0	1	0	0	0	0	0	0	0	1	150

Table B.34: Calculated metrics for SBS and k-NN for Myo gesture control armband.

		Gesture												
		HC	HE	WE	WF	UAF	TI	TM	UH	DH	snap	WA	UALR	Mean
Metrics	TP	160	5	98	84	167	73	24	81	65	46	38	135	
	TN	816	971	878	892	809	903	952	895	911	930	938	841	
	FP	176	11	165	30	16	66	15	126	10	18	24	5	
	FN	5	141	69	36	2	37	71	80	46	40	117	18	
	Sensitivity	96,97%	3,42%	58,68%	70,00%	98,82%	66,36%	25,26%	50,31%	58,56%	53,49%	24,52%	88,24%	57,89%
	Specificity	82,26%	98,88%	84,18%	96,75%	98,06%	93,19%	98,45%	87,66%	98,91%	98,10%	97,51%	99,41%	94,45%
	Precision	47,62%	31,25%	37,26%	73,68%	91,26%	52,52%	61,54%	39,13%	86,67%	71,88%	61,29%	96,43%	62,54%
	Negative predictive value	99,39%	87,32%	92,71%	96,12%	99,75%	96,06%	93,06%	91,79%	95,19%	95,88%	88,91%	97,90%	94,51%
	accuracy	84,36%	86,52%	80,66%	93,67%	98,19%	90,45%	91,90%	82,57%	94,57%	94,39%	87,38%	97,70%	90,20%
	F1 scope	63,87%	6,17%	45,58%	71,79%	94,89%	58,63%	35,82%	44,02%	69,89%	61,33%	35,02%	92,15%	56,60%

SBS and LDA for Myo gesture control armband

Table B.35: Confusion matrix for SBS and LDA for Myo gesture control armband

		Class predicted											
		HC	HE	WE	WF	UAF	TI	TM	UH	DH	snap	WA	UALR
Class real	HC	109	12	0	2	1	0	1	0	15	0	0	0
	HE	8	62	8	0	0	12	3	7	7	0	1	0
	WE	4	4	99	4	10	10	9	10	0	0	19	2
	WF	3	10	2	63	0	0	5	0	11	0	3	3
	UAF	0	0	0	0	150	0	0	0	0	0	0	2
	TI	1	21	6	0	0	58	48	6	26	2	11	0
	TM	10	2	0	2	0	12	13	2	1	1	0	0
	UH	1	18	7	4	5	1	2	94	2	5	2	0
	DH	28	0	0	21	0	0	0	0	48	1	0	1
	snap	0	2	2	9	2	0	0	2	0	56	11	3
	WA	1	15	41	15	1	17	14	40	1	21	107	1
	UALR	0	0	2	0	0	0	0	0	0	0	1	141

Table B.36: Calculated metrics for SBS and LDA for Myo gesture control armband.

		Gesture												
		HC	HE	WE	WF	UAF	TI	TM	UH	DH	snap	WA	UALR	Mean
Metrics	TP	109	62	99	63	150	58	13	94	48	56	107	141	
	TN	891	938	901	937	850	942	987	906	952	944	893	859	
	FP	31	46	72	37	2	121	30	47	51	31	167	3	
	FN	56	84	68	57	19	52	82	67	63	30	48	12	
	Sensitivity	66,06%	42,47%	59,28%	52,50%	88,76%	52,73%	13,68%	58,39%	43,24%	65,12%	69,03%	92,16%	58,62%
	Specificity	96,64%	95,33%	92,60%	96,20%	99,77%	88,62%	97,05%	95,07%	94,92%	96,82%	84,25%	99,65%	94,74%
	Precision	77,86%	57,41%	57,89%	63,00%	98,68%	32,40%	30,23%	66,67%	48,48%	64,37%	39,05%	97,92%	61,16%
	Negative predictive value	94,09%	91,78%	92,98%	94,27%	97,81%	94,77%	92,33%	93,11%	93,79%	96,92%	94,90%	98,62%	94,61%
	accuracy	92,00%	88,50%	87,72%	91,41%	97,94%	85,25%	89,93%	89,77%	89,77%	94,25%	82,30%	98,52%	90,61%
	F1 scope	71,48%	48,82%	58,58%	57,27%	93,46%	40,14%	18,84%	62,25%	45,71%	64,74%	49,88%	94,95%	58,84%

SBS and Naïve Bayes for Myo gesture control armband

Table B.37: Confusion matrix for SBS and Naïve Bayes for Myo gesture control armband

		Class predicted											
		HC	HE	WE	WF	UAF	TI	TM	UH	DH	snap	WA	UALR
Class real	HC	138	38	2	0	0	2	7	7	6	0	1	0
	HE	4	49	1	1	0	2	0	11	1	3	0	0
	WE	0	0	73	0	0	0	0	3	0	0	6	0
	WF	2	2	0	47	0	0	2	0	11	1	0	0
	UAF	0	4	3	0	166	0	1	0	0	3	1	2
	TI	1	19	12	4	0	87	46	6	12	10	0	0
	TM	13	32	6	17	0	16	37	6	22	9	15	0
	UH	0	0	24	0	0	1	0	85	0	0	6	0
	DH	7	0	0	35	0	0	0	0	59	0	0	0
	snap	0	0	0	12	0	0	1	0	0	51	1	0
	WA	0	2	44	3	0	1	0	41	0	9	117	1
	UALR	0	0	2	1	3	1	1	2	0	0	8	150

Table B.38: Calculated metrics for SBS and Naïve Bayes for Myo gesture control armband

		Gesture												
		HC	HE	WE	WF	UAF	TI	TM	UH	DH	snap	WA	UALR	Mean
Metrics	TP	138	49	73	47	166	87	37	85	59	51	117	150	
	TN	921	1010	986	1012	893	972	1022	974	1000	1008	942	909	
	FP	63	23	9	18	14	110	136	31	42	14	101	18	
	FN	27	97	94	73	3	23	58	76	52	35	38	3	
	Sensitivity	83,64%	33,56%	43,71%	39,17%	98,22%	79,09%	38,95%	52,80%	53,15%	59,30%	75,48%	98,04%	62,93%
	Specificity	93,60%	97,77%	99,10%	98,25%	98,46%	89,83%	88,26%	96,92%	95,97%	98,63%	90,32%	98,06%	95,43%
	Precision	68,66%	68,06%	89,02%	72,31%	92,22%	44,16%	21,39%	73,28%	58,42%	78,46%	53,67%	89,29%	67,41%
	Negative predictive value	97,15%	91,24%	91,30%	93,27%	99,67%	97,69%	94,63%	92,76%	95,06%	96,64%	96,12%	99,67%	95,43%
	accuracy	92,17%	89,82%	91,14%	92,09%	98,42%	88,84%	84,52%	90,82%	91,85%	95,58%	88,40%	98,06%	91,81%
	F1 scope	75,41%	44,95%	58,63%	50,81%	95,13%	56,68%	27,61%	61,37%	55,66%	67,55%	62,73%	93,46%	62,50%

SBS and ANN for Myo gesture control armband

Table B.39: Confusion matrix for SBS and ANN for Myo gesture control armband

		Class predicted											
		HC	HE	WE	WF	UAF	TI	TM	UH	DH	snap	WA	UALR
Class real	HC	154	4	0	1	0	1	4	0	7	0	0	0
	HE	1	103	0	3	0	5	2	2	4	1	0	0
	WE	0	5	143	0	0	1	0	12	0	0	10	0
	WF	1	3	1	96	0	0	0	0	3	0	1	0
	UAF	0	2	1	0	168	0	0	0	0	0	0	0
	TI	3	17	3	7	0	70	38	4	6	5	2	0
	TM	1	3	3	1	0	21	40	0	4	2	2	0
	UH	0	5	8	0	1	11	0	125	0	2	4	0
	DH	5	2	0	6	0	0	4	0	81	4	0	0
	snap	0	2	0	3	0	0	4	7	6	70	2	0
	WA	0	0	7	1	0	0	3	11	0	2	133	3
	UALR	0	0	1	2	0	1	0	0	0	0	1	150

Table B.40: Calculated metrics for SBS and ANN for Myo gesture control armband.

		Gesture												
		HC	HE	WE	WF	UAF	TI	TM	UH	DH	snap	WA	UALR	Mean
Metrics	TP	154	103	143	96	168	70	40	125	81	70	133	150	
	TN	1179	1230	1190	1237	1165	1263	1293	1208	1252	1263	1200	1183	
	FP	17	18	28	9	3	85	37	31	21	24	27	5	
	FN	11	43	24	24	1	40	55	36	30	16	22	3	
	Sensitivity	93,33%	70,55%	85,63%	80,00%	99,41%	63,64%	42,11%	77,64%	72,97%	81,40%	85,81%	98,04%	79,21%
	Specificity	98,58%	98,56%	97,70%	99,28%	99,74%	93,69%	97,22%	97,50%	98,35%	98,14%	97,80%	99,58%	98,01%
	Precision	90,06%	85,12%	83,63%	91,43%	98,25%	45,16%	51,95%	80,13%	79,41%	74,47%	83,13%	96,77%	79,96%
	Negative predictive value	99,08%	96,62%	98,02%	98,10%	99,91%	96,93%	95,92%	97,11%	97,66%	98,75%	98,20%	99,75%	98,00%
	accuracy	97,94%	95,62%	96,25%	97,58%	99,70%	91,43%	93,54%	95,21%	96,32%	97,09%	96,45%	99,40%	96,38%
	F1 scope	91,67%	77,15%	84,62%	85,33%	98,82%	52,83%	46,51%	78,86%	76,06%	77,78%	84,44%	97,40%	79,29%